technische universität
dortmund

MAX-PLANCK-INSTITUT
FÜR MOLEKULARE PHYSIOLOGIE

Mechanistic principles of Rho GTPase patterning

Dissertation

Zur Erlangung des akademischen Grades eines
Doktors der Naturwissenschaften
(Dr. rer. nat.)

an der Fakultät für Chemie und Chemische Biologie
der Technischen Universität Dortmund

Angefertigt am Max-Planck-Institut für molekulare Physiologie, Dortmund,
vorgelegt von

Yannic Weiß

November 2024

Date of submission: 12.11.24

1st Examiner: Prof. Dr. Philippe Bastiaens
2nd Examiner: Prof. Dr. Hannes Mutschler
Supervisor: Dr. Peter Bieling

The work presented in this thesis was performed under direct supervision of Dr. Peter Bieling in the Department of Systemic Cell Biology led by Prof. Dr. Philippe Bastiaens at the Max Planck Institute of Molecular Physiology, Dortmund, Germany.

Yannic Weiß was affiliated with the International Max Planck Research School for Living Matter, Dortmund, Germany.

Declaration

Eidesstattliche Versicherung (Affidavit)

Name, Vorname
(Surname, first name)

Matrikel-Nr.
(Enrolment number)

Belehrung:

Wer vorsätzlich gegen eine die Täuschung über Prüfungsleistungen betreffende Regelung einer Hochschulprüfungsordnung verstößt, handelt ordnungswidrig. Die Ordnungswidrigkeit kann mit einer Geldbuße von bis zu 50.000,00 € geahndet werden. Zuständige Verwaltungsbehörde für die Verfolgung und Ahndung von Ordnungswidrigkeiten ist der Kanzler/die Kanzlerin der Technischen Universität Dortmund. Im Falle eines mehrfachen oder sonstigen schwerwiegenden Täuschungsversuches kann der Prüfling zudem exmatrikuliert werden, § 63 Abs. 5 Hochschulgesetz NRW.

Die Abgabe einer falschen Versicherung an Eides statt ist strafbar.

Wer vorsätzlich eine falsche Versicherung an Eides statt abgibt, kann mit einer Freiheitsstrafe bis zu drei Jahren oder mit Geldstrafe bestraft werden, § 156 StGB. Die fahrlässige Abgabe einer falschen Versicherung an Eides statt kann mit einer Freiheitsstrafe bis zu einem Jahr oder Geldstrafe bestraft werden, § 161 StGB.

Die oben stehende Belehrung habe ich zur Kenntnis genommen:

Official notification:

Any person who intentionally breaches any regulation of university examination regulations relating to deception in examination performance is acting improperly. This offence can be punished with a fine of up to EUR 50,000.00. The competent administrative authority for the pursuit and prosecution of offences of this type is the chancellor of the TU Dortmund University. In the case of multiple or other serious attempts at deception, the candidate can also be unenrolled, Section 63, paragraph 5 of the Universities Act of North Rhine-Westphalia.

The submission of a false affidavit is punishable.

Any person who intentionally submits a false affidavit can be punished with a prison sentence of up to three years or a fine, Section 156 of the Criminal Code. The negligent submission of a false affidavit can be punished with a prison sentence of up to one year or a fine, Section 161 of the Criminal Code.

I have taken note of the above official notification.

Ort, Datum
(Place, date)

Unterschrift
(Signature)

Titel der Dissertation:
(Title of the thesis):

Ich versichere hiermit an Eides statt, dass ich die vorliegende Dissertation mit dem Titel selbstständig und ohne unzulässige fremde Hilfe angefertigt habe. Ich habe keine anderen als die angegebenen Quellen und Hilfsmittel benutzt sowie wörtliche und sinngemäße Zitate kenntlich gemacht.
Die Arbeit hat in gegenwärtiger oder in einer anderen Fassung weder der TU Dortmund noch einer anderen Hochschule im Zusammenhang mit einer staatlichen oder akademischen Prüfung vorgelegen.

I hereby swear that I have completed the present dissertation independently and without inadmissible external support. I have not used any sources or tools other than those indicated and have identified literal and analogous quotations.

The thesis in its current version or another version has not been presented to the TU Dortmund University or another university in connection with a state or academic examination.*

*Please be aware that solely the German version of the affidavit ("Eidesstattliche Versicherung") for the PhD thesis is the official and legally binding version.

Ort, Datum
(Place, date)

Unterschrift
(Signature)

Abstract

Rho GTPases are regulators of morphogenesis in all eukaryotic cells. These peripheral membrane proteins spatially control actin cytoskeleton dynamics by locally concentrating at the plasma membrane in polarized activity patterns. However, the biochemical mechanisms by which Rho GTPases enrich at specific membrane sites where they are subsequently activated remain unknown. Here, I use *in vitro* reconstitution in model membrane systems to evaluate the relationship between the membrane-cytosolic shuttling of Rho GTPases and their activity state. I established a minimal system of templated Rho GTPase activity patterns that fully recapitulates the catalytic and spatial cycles of Rho GTPases. By utilizing this system, I demonstrate that effector proteins selectively stabilize active Rho GTPases on membrane surfaces. This stabilization is achieved through an avidity-driven mechanism that increases membrane retention of active Rho GTPases and decreases their diffusivity on the membrane. Together, the results show that effector proteins couple the catalytic and spatial cycles of Rho GTPases, thereby actively contributing to their spatial polarization. These findings are vital in our reconstitution of a synthetic Rho GTPase signaling network capable of spontaneous and stable polarization. To this end, I biochemically engineered and purified synthetic proteins, mediating regulatory feedback between distinct Rho GTPases based on direct recruitment. This linear feedback can promote the autonomous formation of stable Rho GTPase activity patterns, as shown by theory. I established a pipeline of biochemical assays to characterize these synthetic proteins, demonstrating their capacity to interact with active Rho GTPases and modulate their activity. Hence, I successfully created synthetic regulators of Rho GTPase activity that are directly recruited by active Rho GTPases. This paves the way for the implementation of regulatory feedback in an experimental system and is the first step toward a complete reconstitution of a minimal system that promotes the stable polarization of Rho GTPase activity.

Zusammenfassung

Rho GTPasen sind Regulatoren der Morphogenese in allen eukaryotischen Zellen. Diese peripheren Membranproteine steuern räumlich die Dynamik des Aktin-Zytoskeletts, indem sie sich lokal an der Plasmamembran in polarisierten Aktivitätsmustern anreichern. Jedoch sind die biochemischen Mechanismen, durch die Rho GTPasen an spezifischen Membranstellen, an denen sie aktiviert werden, angereichert werden, bisher unbekannt. In dieser Arbeit verwende ich *in vitro* Rekonstitutionen mit Modellmembransystemen, um die Verbindung zwischen dem Membran-Zytosol-Transport von Rho GTPasen und ihrem Aktivitätszustand zu untersuchen. Ich habe ein minimales System von templatbasierten Rho GTPase Aktivitätsmustern etabliert, das die katalytischen und räumlichen Zyklen der Rho GTPasen vollständig nachbildet. Mit Hilfe dieses Systems zeige ich, dass Effektorproteine aktivierte Rho GTPasen selektiv an Membranoberflächen stabilisieren. Diese Stabilisierung erfolgt durch einen Aviditäts-getriebenen Mechanismus, der die Membranbindung aktivierter Rho GTPasen erhöht und ihre Diffusion auf der Membran verringert. Zusammenfassend zeigen die Ergebnisse, dass Effektorproteine die katalytischen und räumlichen Zyklen der Rho GTPasen koppeln und somit aktiv zur räumlichen Polarisation von Rho GTPasen beitragen. Diese Erkenntnisse sind entscheidend für die Rekonstitution eines synthetischen Rho GTPase-Signalnetzwerks, das in der Lage ist, spontane und stabile Polarisation zu erzeugen. Zu diesem Zweck habe ich synthetische Proteine biochemisch entwickelt und aufgereinigt, die regulatorischen Feedback zwischen verschiedenen Rho GTPasen durch direkte Rekrutierung vermitteln. Dieses lineare Feedback kann gemäß theoretischen Modellen die autonome Bildung stabiler Rho GTPase-Aktivitätsmuster fördern. Ich habe eine Pipeline von biochemischen Assays zur Charakterisierung dieser synthetischen Proteine etabliert und gezeigt, dass sie in der Lage sind, mit aktiven Rho GTPasen zu interagieren und deren Aktivität zu modulieren. Damit habe ich erfolgreich synthetische Regulatoren der Rho GTPase-Aktivität erzeugt, die direkt von aktiven Rho GTPasen rekrutiert werden. Dies ebnet den Weg für die Implementierung regulatorischen Feedbacks in einem experimentellen System und ist der erste Schritt hin zu einer vollständigen Rekonstitution eines minimalen Systems, das zur stabilen Polarisation der Rho GTPase-Aktivität führt.

Table of Contents

Introduction

Pattern formation in living systems

Biological systems organize into regular structures at various length scales, ranging from the macroscopic pigmentation patterns of sea shells (Meinhardt & Klingler, 1987) to the microscopic front-back polarity of single cells during migration (Rappel & Edelstein-Keshet, 2017). The positional information transmitted by these patterns is often essential for cellular functions to arise. While biological patterns are diverse and complex, their formation can be explained by similar principles (Kondo & Miura, 2010; Mitchison & Field, 2021). Patterning may either result from external positional cues guiding the distribution of molecules (Figure 1A) or by self-organizing processes (Figure 1B), in which the pattern is created spontaneously based on local interactions between different molecules (Landge et al., 2020). Biological systems rely on both of these mechanisms. Examples for the former can be observed in *Drosophila melanogaster* embryos, where a gradient of the transcription factor Bicoid determines the embryo's anterior-posterior axis. Here, maternal mRNA encoding Bicoid is localized and translated at the anterior egg pole. Together with a limited lifetime of the protein through its time-dependent degradation or sequestration, the diffusion of the protein enables the formation of a protein gradient (Driever & Nüsslein-Volhard, 1988). However, this mode of pattern formation requires robust gradients and a precise readout to propagate the positional information reliably (Gregor et al., 2007). Otherwise, noisy input signals would heavily decrease the reproducibility of this process. Since biological noise influences numerous cellular processes (Rao et al., 2002) and an initial positional cue is not always present during patterning events in nature, it is unlikely that templated organization is the only mode of pattern formation. Furthermore, such a mechanism alone cannot explain the diversity and complexity of patterns observed *in vivo* (Kondo & Miura, 2010). Unlike systems that depend on a template for pattern formation, those based on self-organization do not require pre-existing asymmetry to establish positional information. Rather, they rely on the local amplification of fluctuations in the concentration of the system's components, which occurs through the interaction among those components (Landge et al., 2020). Self-organizing systems do not reach thermodynamic equilibrium, but they maintain a steady state (Mitchison & Field, 2021). An idealized self-organizing system based on Alan Turing's reaction-diffusion theory (Turing, 1952) was first described by Meinhardt and

Gierer, termed the activator-inhibitor system (Meinhardt & Gierer, 2000). It is a two-component system in which pattern formation depends on an autocatalytic activator that also promotes the production of its own inhibitor (Landge et al., 2020). Intuitively, if promotion and suppression of activity were equally coordinated in space and time, both processes would simply negate each other. Thus, another key requirement for this activator-inhibitor system to self-organize into regular patterns is the difference in diffusivity of both components. Generally, patterns can form spontaneously in such systems with short-range activation and long-range inhibition (Bement et al., 2024). Such a system allows for a self-amplifying activator to translate even infinitesimal fluctuations in its concentration into a localized and persistent activator peak. The activator is only confined by the increasing concentration of the fast-diffusing inhibitor. Furthermore, new activator peaks can form outside the range of the inhibitor, culminating in the emergence of a stationary pattern (Landge et al., 2020).

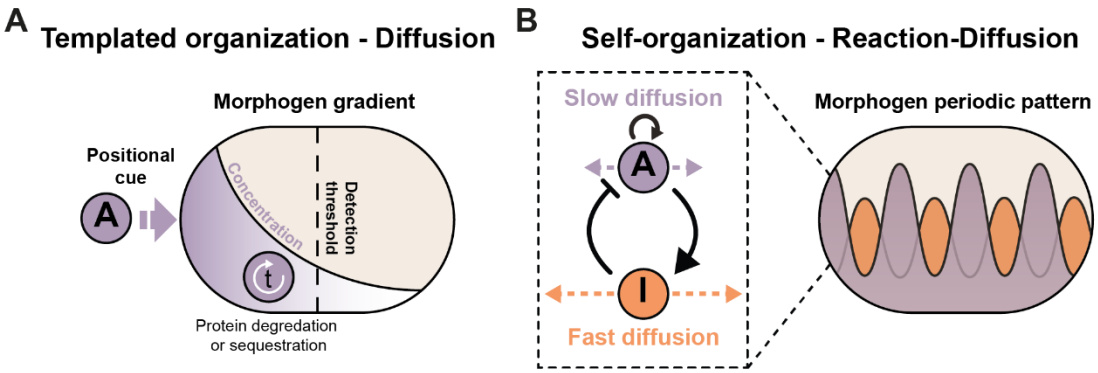

Figure 1: Comparison of different mechanisms that propagate positional information in biological systems. (**A**) Scheme of templated organization in cells where an external positional cue is translated into a morphogen (purple) gradient via diffusion and protein degradation or sequestration. Signal propagation is spatially restricted by a detection limit of morphogen concentration. (**B**) Scheme of self-organization in cells based on the activator-inhibitor system. Interaction scheme between a slow-diffusing, self-amplifying activator (purple) that positively regulates its fast-diffusing inhibitor (orange). Morphogen periodic patterns are observable, allowing for a variety of spatial patterns that regulate signal propagation (Adapted from Kondo & Miura, 2010).

Although self-organizing patterns can theoretically emerge from these minimal requirements, biological systems often display more complex dynamical behavior, with interacting constituents that are challenging to identify. However, protein patterning systems based on reaction-diffusion can be found at the core of simple organisms like *Escherichia coli*. One example is the Min system which directs the Z-Ring – a structure formed by FtsZ, a prokaryotic analog of tubulin – to the mid-zone of the bacterial cell. This structure is essential for cell division as its proper localization is required to ensure

division into two equally sized daughter cells (Lutkenhaus, 2007). Interactions between the constituents of the Min system, that regulate their membrane attachment and detachment, cause their oscillation between both cell poles. These oscillations result in the lowest effective concentration of the constituents close to the mid-zone of the bacterial cell (Raskin & De Boer, 1999; Hale et al., 2001). Since the Z-ring assembly is antagonized by the Min system, its formation occurs closest to the region of low constituent concentration. A combination of *in vivo* and *in vitro* approaches together with *in silico* approaches, uncovered the minimal requirements for these oscillatory dynamics to occur and offer an explanation for the molecular mechanism of the mid-cell assembly of the Z-ring (Vendel et al., 2019). The Min system includes three proteins, MinC, MinD and MinE (De Boer et al., 1989). Early observations *in vivo* indicated that MinC is an effector protein of MinD and antagonizes Z-ring assembly, but is not required for the oscillations of the Min system, instead it follows the oscillations of MinD (Hu & Lutkenhaus, 1999; Raskin & De Boer, 1999). Pioneering *in vitro* reconstitution of the Min system on planar supported lipid bilayers (SLBs) demonstrated that only MinD, MinE, adenosine triphosphate (ATP) and a membrane are required for complex biological patterns to emerge in this protein patterning system (Loose et al., 2008). Binding of ATP to the ATPase MinD promotes its dimerization and membrane attachment. Cooperative binding of MinE to MinD induces ATP hydrolysis, which leads to MinD's detachment from the membrane and thereby regulates the membrane-cytosolic shuttling of MinD (Vendel et al., 2019). This energy-dependent and MinE-mediated cycle of membrane attachment and detachment of MinD produces dynamic wave patterns on supported lipid bilayers from an initially homogeneous state (Loose et al., 2008). The dissection of the molecular mechanism of the Min system through the *in vitro* reconstitution enabled the systemic manipulation of the system, which revealed that the wave velocity and wavelength directly depend on the ratio of MinD and MinE concentration (Loose et al., 2008), an observation previously made for the oscillation frequency *in vivo* (Raskin & De Boer, 1999; Hale et al., 2001) and *in silico* (Meinhardt & de Boer, 2001). The reconstituted system was later expanded by additional parameters like geometrical constraints or temperature fluctuations to investigate other factors that contribute to different dynamical behaviors (Caspi & Dekker, 2016). Together these findings demonstrate the power of minimal, reconstituted systems, where input parameters are easily adjustable, allowing for a direct experimental read-out of the effects that a different parameter set might have on the system's properties.

Similar systems that rely on reaction-diffusion processes to form stable protein patterns are also found in eukaryotes. The most important examples involve Rho GTPases, which form distinct spatial patterns on the plasma membrane to direct processes involved in the morphogenesis of cells during directed cell migration, cytokinesis or membrane repair (Ridley et al., 2003; Bement et al., 2005; Benink & Bement, 2005). These protein patterning systems control actin network remodeling in distinct regions of the cell by locally recruiting downstream effector proteins. Rho GTPases exert their signaling function only when they are bound to guanosine triphosphate (GTP) and associated with the plasma membrane. As small GTPases they slowly hydrolyze GTP to guanosine diphosphate (GDP), which renders them inactive (Hodge & Ridley, 2016). Rho GTPase activity is heavily controlled by numerous regulatory proteins that are often embedded in an intricate network of multiple positive and negative feedback loops. This large network of regulators allows the distinct spatiotemporal coordination of Rho GTPase activity during numerous biological processes. While *in vivo* and *in silico* approaches have been utilized to investigate Rho GTPase pattern formation (Bement et al., 2024), an *in vitro* system that uncovers the minimal requirements for this pattern formation to occur is missing. In this thesis I will focus on the establishment of such Rho GTPase patterning systems *in vitro*.

Numerous examples of protein patterning systems have evolved in nature that either rely on spatial templates, on self-organization or a combination of both (Collinet & Lecuit, 2021). Self-organization as a mechanism is unique as it can result in spontaneous symmetry breaking and does not require external asymmetries. However, the specific underlying molecular mechanisms that enable self-organization remain elusive for many biological patterning systems. Especially since our current understanding of self-organizing patterns *in vivo* remains mostly theoretical to this date, experimental approaches are invaluable to verify and test these hypotheses. Notable exceptions are those systems that have successfully been reconstituted such as the bacterial Min system. This warrants further systematic reconstitution as a powerful approach to dissect biological pattern formation on a molecular level.

P-Loop containing NTPases

The Ras superfamily

Both, the Min system and the Rho GTPase patterning system, consist of proteins, that are part of the P-Loop containing NTPases (Leipe et al., 2002), proteins with one of the most conserved protein folds across all three domains of life – eukaryotes, prokaryotes and archaea (Koonin et al., 2000). P-Loop containing NTPases are characterized by a mononucleotide-binding fold, the P-Loop, which is capable of both, binding nucleoside triphosphates and catalyzing their hydrolysis (Saraste et al., 1990). Notably, Rho GTPases belong to the P-Loop containing NTPases of the Ras superfamily (Leipe et al., 2002), suggesting a connection between processes directing cell polarity and members of the Ras superfamily. However, this connection and, therefore, the direct involvement of Ras superfamily members in the localized organization of subcellular structures (Ridley, 2001), as well as the mechanism that leads to a polarized cell state (Goryachev & Pokhilko, 2008), are only beginning to be understood in yeast (Pruyne & Bretscher, 2000; Chiou et al., 2017) while research in metazoans remains challenging even today (Lang & Munro, 2017; Bement et al., 2024). Nevertheless, NTPases offer interesting candidates as constituents of self-organizing systems, since they undergo energy-driven cycles and therefore satisfy the prerequisite of energy dissipation essential for such systems.

Early on, studies of Ras superfamily members primarily implicated them in the transduction of proliferative signals (Hurley et al., 1984; Smith et al., 1986; Barbacid, 1987). The first discovered, and name giving, members of this family were the *HRAS*, *KRAS* and *NRAS* genes (Harvey, 1964; Kirsten & Mayer, 1967; Shimizu et al., 1983). Initial experiments identified *HRAS*, *KRAS* and *NRAS* as oncogenes due to their ability to induce tumor growth in mice and humans (Harvey, 1964; Kirsten & Mayer, 1967; Shimizu et al., 1983).

Shortly after the discovery of the first *RAS* genes, their gene product was identified as a 21 kDa large protein termed p21 (Parks & Scolnick, 1977; Shih et al., 1979). Immunoprecipitation of p21, incubated with or without guanine nucleotides, and competitive binding assays with different nucleotides as competitors revealed p21's high guanine nucleotide binding affinity and the reversibility of nucleotide binding to p21 (Scolnick et al., 1979; Shih et al., 1980). Comparison of normal human *ras* p21 and an activated version with a point mutation (G12V), found in cells with highly tumorigenic

behavior, showed a reduction in hydrolytic activity in bacterial extracts expressing the activated version (McGrath et al., 1984; Gibbs et al., 1984). This suggested that p21 can catalyze the hydrolysis of GTP to GDP, identifying p21 as a GTPase. These findings further indicated that p21's main enzymatic activity is GTP hydrolysis and that its activity state is directly correlated with the phosphorylation state of the bound nucleotide. In conclusion, the hydrolysis of GTP bound to and catalyzed by the GTPase p21 results in the inactivation of said GTPase (McGrath et al., 1984; Gibbs et al., 1984).

Simultaneously, through a combination of immunofluorescence microscopy and electron microscopy it was discovered that p21 is predominantly associated with the plasma membrane (Willingham et al., 1980). First deletion mutants of p21 harboring only a truncated C-terminus highlighted the importance of post-translational modifications (PTMs) in the C-terminal region of p21 for its plasma membrane association and the ability to exert its biological function (Willumsen et al., 1984). Prenylation of a C-terminal cysteine was found to play a central role in the correct localization of p21 (Schafer et al., 1989). The comparison with a similar C-terminal PTM, found in *Saccharomyces cerevisiae* mating hormone factor-a (Anderegg et al., 1988), suggested that both proteins could be processed similarly. It was later confirmed that prenylation is achieved by a thioether bond covalently linking the prenyl residue to the C-terminal cysteine of p21. Next, the last three C-terminal amino acids undergo proteolytic cleavage. Subsequently, the newly formed carboxy moiety distal to the cysteine is methylated (Schafer et al., 1990). The processing of the so-called CAAX-motif (C = cysteine, A = aliphatic, X = terminal amino acid) during prenylation of the p21 protein was later found to be universal among multiple members of the Ras superfamily (Choy et al., 1999; Colicelli, 2004). At the same time as the discovery of the biochemical function of the Ras GTPase p21, the epidermal growth factor (EGF)-induced signal transduction of mitotic signals was connected to the activity of the p21 protein (Kamata & Feramisco, 1984; Mulcahy et al., 1985; Malumbres & Barbacid, 2003). Extensive studies on Ras GTPases specifically investigated their functionality and their use as a direct or indirect target in drug discovery (Downward, 2003; Karnoub & Weinberg, 2008; Zimmermann et al., 2013; Lu et al., 2016). During this period, multiple other small GTPases belonging to the Ras superfamily were identified displaying similar properties while being connected to different cellular processes. Today we know five major classes of the Ras superfamily with numerous members (Figure 2) that not only have GTP hydrolysis activity but also bind to membranes through PTMs.

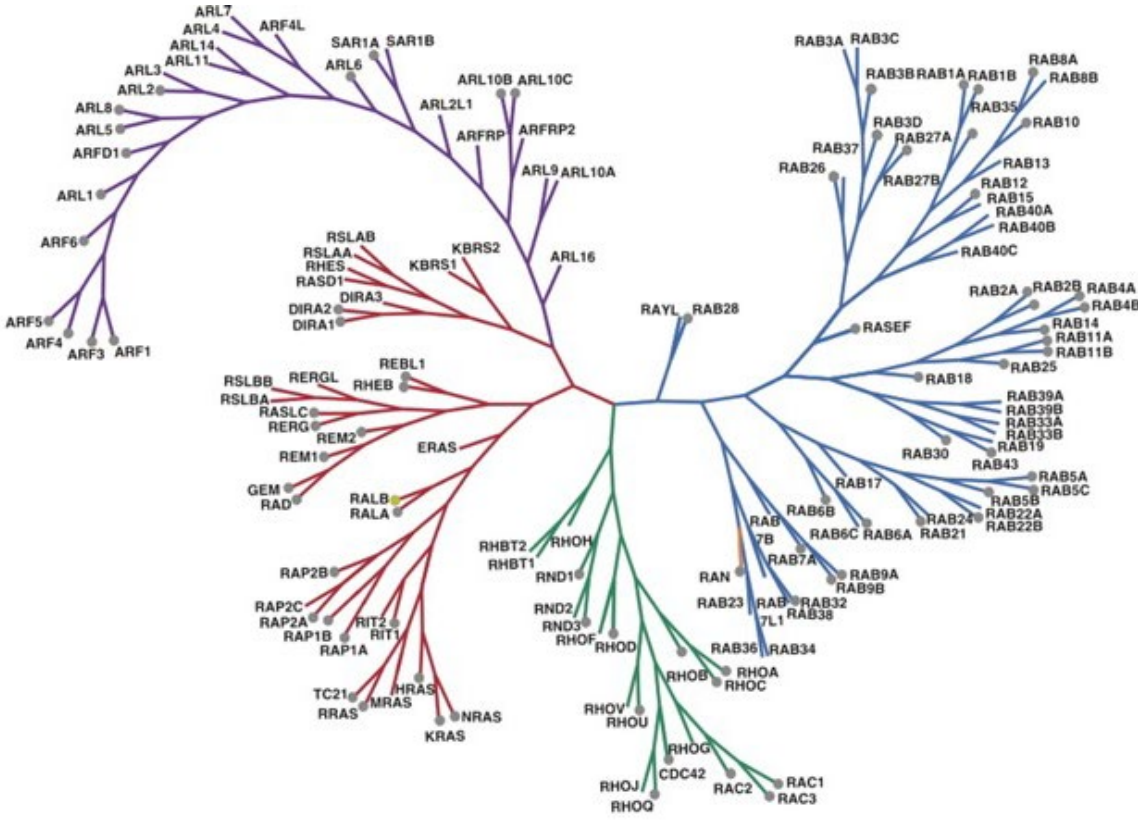

Figure 2: Phylogenetic tree of the Ras superfamily. The five major subfamilies are Arf (purple), Ras (red), Rho (green), Rab (blue) and Ran (orange) GTPases (Gray et al., 2020; modified).

Besides the aforementioned Ras GTPases, the remaining four major classes are the Rab, Arf, Ran and Rho GTPases (Colicelli, 2004; Wennerberg et al., 2005). As the largest class of the Ras superfamily, Rab GTPases act as membrane-bound signaling hubs facilitating intracellular transport of protein cargo. They regulate vesicular trafficking by recruiting effectors to different intracellular compartments that enable the docking/tethering, budding and transport of vesicles. Prenylation of the C-terminal cysteine ensures membrane association of Rab GTPases while a specific cellular membrane localization is determined by varying sequence motifs adjacent to the modified cysteine (Zerial & McBride, 2001). Like Rab GTPases, Arf GTPases are involved in the regulation of vesicular trafficking through the recruitment of various effectors to distinct cellular membranes. However, contrary to Rab GTPases, membrane binding is achieved through N-terminal myristoylation (Randazzo et al., 2000). The Ran GTPase class consists of only one member, the name giving Ran protein. Surprisingly, unlike most of the Ras superfamily members the Ran GTPase is not localized on membranes but forms an activity gradient in the cytosol/nucleosol that imposes directionality on the shuttling of macromolecules between nucleus and cytoplasm (Weis, 2003). Members of the last major class of the Ras

superfamily, the Rho GTPases, were first discovered in 1985 (Madaule & Axel, 1985). Their membrane association is predominantly enabled, similar to Ras GTPases, by the C-terminal prenylation of a CAAX-motif. Furthermore, Rho GTPases are tightly coupled to the dynamics of the actin cytoskeleton. By recruiting downstream effectors that interact with different actin networks, Rho GTPases directly influence cell morphology dependent on their activity state. Hence, Rho GTPases are master regulators of morphogenesis (Etienne-Manneville & Hall, 2002).

Relating the structure of small GTPases to their function

Insights into the structural mechanism of small GTPases emerged soon after the structure of the elongation factor EF-Tu was solved, which marks the first available crystal structure with a GTPase domain (Kabsch et al., 1977). In the following years, comparisons of several crystal structures uncovered structural similarities between GTPases. Interestingly, these shared structural motifs are not exclusive to GTPases but also conserved within certain ATPases. These enzymes, despite their vastly different functions, were later collectively categorized as P-Loop NTPases (Saraste et al., 1990; Wittinghofer & Vetter, 2011). Phylogenetic analysis suggested that some ATPases and GTPases share a common ancestor (Leipe et al., 2002). In contrast to ATPases that utilize ATP to fuel motor proteins or enzyme-driven metabolic processes, the hydrolysis of GTP through GTPases appears to be primarily related to signal transduction via the regulation of the recruitment of GTPase binding proteins (Wittinghofer & Vetter, 2011). What exactly are the structural similarities (Figure 3) that suggest common ancestry?

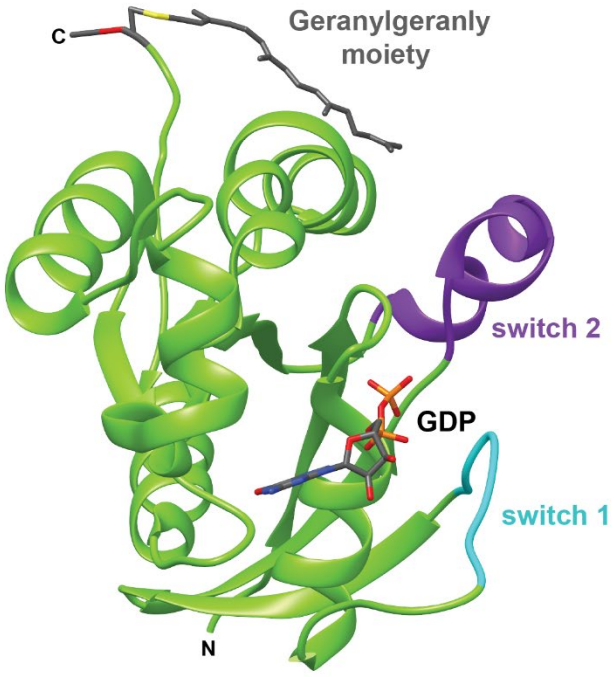

Figure 3: Structure of the Rho GTPase Cdc42. Ribbon representation of Cdc42 (green) bound to GDP. Highlighted regions and modifications are switch 1 (cyan), switch 2 (purple) and the geranylgeranyl moiety (grey). PDB: 1DOA (Hoffman et al., 2000).

While sequence homology is very low among GTPases (and ATPases) of different (sub)families, at least one domain (or parts of this domain) is found in most P-loop containing NTPases, the G-domain. This 18-20 kDa domain is the basic functional unit for GTPases. Its structure-to-function relation can be best described by dividing the G-domain into five conserved sequence motifs (Wittinghofer & Vetter, 2011). I) The P-loop, initially called the Walker A motif, facilitates phosphate binding. II) The switch 1 (sw1) has a conserved threonine (Thr), which interacts with the γ-phosphate of GTP. III) Switch 2 (sw2), initially the Walker B motif, has two functions, one being the interaction with the γ-phosphate through a glycine (Gly) and the other being a water-mediated contact with the Mg^{2+} metal ion crucial for GTP hydrolysis (Walker et al., 1982; Saraste et al., 1990; Milburn et al., 1990). IV) and V) are both motifs ensuring the guanine base-binding specificity. While the last two sequence motifs are specific to GTPases, the other three, which are mostly relevant for the mechanism of nucleotide hydrolysis, are also conserved in P-loop ATPases. Structural analysis of GTP- and GDP-bound GTPase crystal structures revealed that conformational changes are mainly restricted to the switch 1 and 2 regions. The interaction between the oxygens of the γ-phosphate of GTP with the main chain of

Thr and Gly of sw1 and sw2 respectively, are the key residues involved in the functional mechanism of GTPases. Once hydrolysis is complete, these residues no longer interact with the hydroxy group of the γ-phosphate, leading to conformational changes of the switch 1 and 2 regions. As a consequence, the GDP-bound conformation obstructs the binding interface of small GTPases for a plethora of effector proteins rendering them inactive or the "signal" as off. These conformational changes were termed the loaded-spring mechanism, universally found among members of the Ras superfamily (Vetter & Wittinghofer, 2001; Wittinghofer & Vetter, 2011). Thus, small GTPases exist in two distinct conformations: an inactive GDP-bound state with no functional output, and an active, GTP-bound state that enables the recruitment of downstream effectors to carry out biological functions. This implies a straightforward role for small GTPases in cells, where activation corresponds to signal propagation, while inactivation results in signal termination. However, the spatiotemporal coordination of Rho GTPase activity *in vivo*, for example, suggests a more complex picture (Bement et al., 2024). Hence, other regulatory processes for the activity of small GTPases must be at play to explain the emergence of intricate activity patterns.

The Rho GTPase subclasses and their spatiotemporal coordination

Among the six major Rho GTPase subclasses, the RhoA-related, Rac1-related and Cdc42-related family members are the most extensively studied. The remaining three subclasses – Rnd, RhoBTB and Miro – together with several unclassified candidates are less explored, but also show notable similarities in amino acid sequence identity and general biological function (Wennerberg & Der, 2004). The connection between Rho GTPases and the actin cytoskeleton was first demonstrated by pioneering experiments with RhoA, Rac1 and Cdc42, the three founding members of the Rho GTPase class. Microinjecting RhoA into fibroblasts induced the formation of focal adhesions and actin stress fibers, a response observed previously in fibroblasts exposed to growth factor containing serum (Ridley & Hall, 1992). Similar experiments revealed the role of Rac1 in the formation of membrane ruffles (Ridley et al., 1992). Cdc42 was first associated with budding in yeast and cell polarity (Adams et al., 1990), but was later discovered to promote actin microspikes and filopodia (Kozma et al., 1995; Nobes & Hall, 1995). Today it is known that Rho GTPases are essential for the correct localization of numerous signaling events that directly

regulate cytoskeletal remodeling (Hodge & Ridley, 2016). These processes lead to the formation of protrusive structures, such as branched actin networks in lamellipodia or dense filamentous actin bundles in filopodia, while also promoting the assembly of contractile structures like acto-myosin (Etienne-Manneville & Hall, 2002). All these structures are important for morphogenesis and the directional movement of individual cells, the latter of which is accomplished through the localization of protrusive and contractile actin structures to opposite cell ends. Since protrusion and contraction are antagonistic phenomena, driven by actin networks distinct in composition and dynamics, it is vital to separate these processes in space. Active, membrane-bound Rho GTPases guide the assembly of different actin structures by locally recruiting distinct sets of effector proteins (Ridley et al., 2003). Thus, to ensure that protrusive and contractile actin structures form at specific locations of the cell, Rho GTPases must organize into distinct activity patterns. Such patterns have been confirmed to exist *in vivo* (Figure 4) through the application of Rho GTPase activity sensors in motile cells (Machacek et al., 2009).

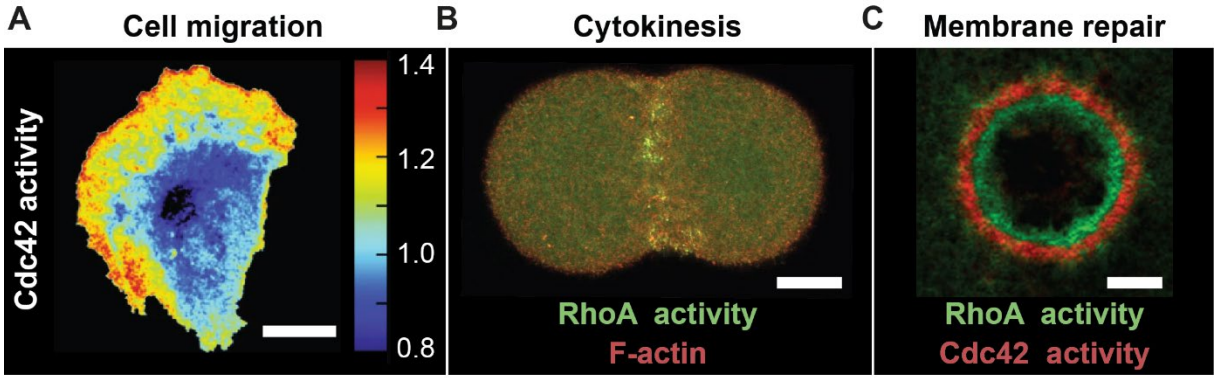

Figure 4: Rho GTPase activity patterns *in vivo*. (**A**) Cdc42 activity monitored with a fluorescence energy transfer (FRET) biosensor during migration of HeLa cells. Color scale represents FRET ratio, with high values corresponding to high Cdc42 activity. At the leading edge of the cell, Cdc42 activity spikes. Scale bar: 20 µm (De Beco et al., 2018; modified). (**B**) RhoA activity (GFP-rGBD, green) and F-actin concentration (mCherry-Utr, red) during cytokinesis in a normal starfish embryo. Active RhoA accumulates in the cytokinetic furrow. Scale bar: 20 µm (Bement et al., 2015; modified). (**C**) RhoA activity (eGFP-rGBD, green) and Cdc42 activity (mRFP-wGBD, red) during single cell wound healing in frog oocytes. Active RhoA and Cdc42 segregate into distinct activity zones around the wound. Scale Bar: 10 µm (Benink & Bement, 2005; modified).

Similar Rho GTPase activity patterns coordinating the assembly of different actin structures can be observed during cell division in budding yeast (Ozbudak et al., 2005) or during cytokinesis (Bement et al., 2005) and plasma membrane repair in mammalian cells (Benink & Bement, 2005). However, the observed dynamics of Rho GTPase activity patterns are quite distinct in these examples concerning their size and dynamics. In yeast,

the ability of cells to locate the site of bud growth depends on the oscillating localization of Cdc42 activity to a small focus at the site of bud formation (Das et al., 2012), which drastically differs from the broad distribution of RhoA and Cdc42 activity to opposing cell ends observed during cell locomotion. Both mutual exclusion and oscillations are indicative of self-organizing systems, but how exactly this spatiotemporal coordination of Rho GTPase activity is achieved remains unknown.

Regulatory cycles of Rho GTPase activity

The signaling function of Rho GTPases depends on both their cellular localization and their nucleotide state. Only membrane-bound and GTP-loaded Rho GTPases interact with effector proteins that affect actin dynamics and thereby control morphogenesis (Graziano & Weiner, 2014; Bement et al., 2024). The catalytic conversion of Rho GTPases from an active GTP-bound state to an inactive, GDP-bound state occurs via nucleotide hydrolysis, while nucleotide exchange facilitates the reverse process. Complementary to this regulation of Rho GTPase activity by catalytic cycling of their nucleotide state (Figure 5A), is the shuttling of Rho GTPases between the plasma membrane and the cytosol. This spatial cycling (Figure 5B) of Rho GTPases enables a membrane-bound state where Rho GTPases exert their signaling function and an opposing inactive state in the cytosol (Hakoshima, 2003).

Three primary classes of Rho GTPase regulators are responsible for the control of the catalytic and spatial cycle: 1) Guanine nucleotide exchange factors (GEFs) activate Rho GTPases by stimulating rapid loading of GTP (Rossman et al., 2005), 2) GTPase activating proteins (GAPs) promote Rho GTPase inactivation by accelerating GTP to GDP hydrolysis (Tcherkezian & Lamarche-Vane, 2007), 3) Rho-specific guanine nucleotide dissociation inhibitors (RhoGDIs) maintain a soluble pool of idle Rho GTPase:RhoGDI complexes in the cytosol by extracting Rho GTPases from the plasma membrane (Garcia-Mata et al., 2011). Over the past few decades, a vast number of proteins belonging to these distinct classes of proteins have been identified, providing invaluable insight into the underlying molecular mechanism of Rho GTPase regulation. The human genome alone contains 145 Rho GEFs and GAPs (Müller et al., 2020). However, despite this vast quantity of regulators, some fundamental aspects of the catalytic and spatial cycle that govern Rho GTPase activity remain unclear. The translocation of Rho GTPases in response to activating stimuli suggested early on that their activation influences their reversible membrane binding

(Philips et al., 1993; Fleming et al., 1996; Michaelson et al., 2001). This mutual dependence is further supported by RhoGDI's preferential extraction of inactive Rho GTPases from the membrane (Golding et al., 2019). These findings suggest that the catalytic and spatial cycles of Rho GTPases are linked. However, we are currently unable to define the molecular basis on which the activity of Rho GTPases is related to their general localization at cellular membranes. Establishing this connection will be essential to fully understand the formation and maintenance of Rho GTPase activity patterns *in vivo*.

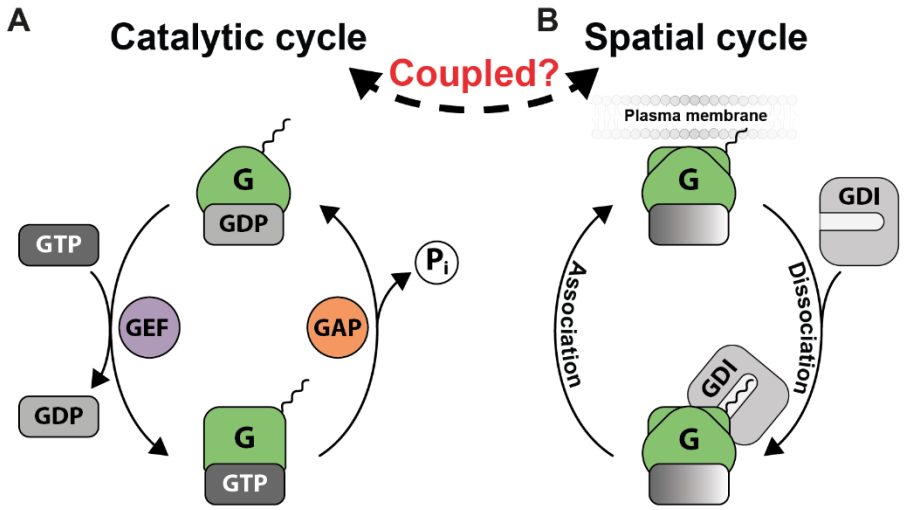

Figure 5: The regulatory cycles of Rho GTPases are potentially coupled. (**A**) Scheme of the catalytic cycle. Rho GTPases alternate between an active GTP-bound state and an inactive, GDP-bound state. The catalytic cycle controls this conversion. Activation of Rho GTPases is catalyzed by GEFs, which exchange GDP with GTP, while their inactivation is catalyzed by GAPs, which accelerate nucleotide hydrolysis. (**B**) Scheme of the spatial cycle. To exert their signaling function, Rho GTPases must be associated with the membrane. The shuttling of Rho GTPases between the plasma membrane and the cytosol is regulated by RhoGDI (Adapted from Wittinghofer & Vetter, 2011).

Guanine nucleotide exchange factors (GEFs)

The activation of Rho GTPases is directly associated with the GEF-mediated exchange of the Rho GTPase nucleotide, specifically the replacement of GDP with GTP. This reaction is confined to cellular membranes, primarily the plasma membrane, since many GEFs are localized to membranes in their active state. Spurious activation elsewhere in the cytoplasm is also potently suppressed by RhoGDI, which sterically blocks the GEF interacting regions of the Rho GTPase. Today over 70 Rho-specific GEFs are known, most of which belong to the diffuse B-cell lymphoma (Dbl) family. Members of this family are generally large, multidomain proteins. Despite their high sequence variability, members of this family share a Dbl homology (DH) domain, typically accompanied by an adjacent C-terminal Pleckstrin homology (PH) domain (Müller et al., 2020). Structural analyses of

Dbl-like GEFs provided an understanding of the mechanism underlying Rho GTPase activation (Worthylake et al., 2000). The interaction between a Rho GTPase and the DH domain stabilizes a nucleotide-free intermediate of the Rho GTPase, which is then loaded with GTP. This preferential loading with GTP is driven by mass action due to the excess of GTP over GDP in cells (Traut, 1994; Rossman et al., 2005). Binding interfaces between DH domains and Rho GTPases vary, enabling the selective interaction of Dbl-like GEFs with different Rho GTPases (Cheng et al., 2002). Although the DH domain is sufficient to confer selectivity for Rho GTPases, it is not the only factor influencing this selectivity (Müller et al., 2020). PH domains are commonly known to promote the targeting of different proteins to the membrane by associating with negatively charged lipids (Ferguson et al., 1995). However, the function of the PH domain in Dbl-like GEFs appears to be more variable. While the PH domain does contribute to the membrane-association of Dbl-like GEFs, it is not always sufficient or even required for their localization to the membrane (Stam et al., 1997; Baumeister et al., 2003). Rather, the PH domain adds another layer of complexity to the activation of Rho GTPases, as its lipid engagement positively influences the catalytic activity of Dbl-like GEFs (Rossman & Campbell, 2000; Rossman et al., 2005). Furthermore, Dbl-like GEFs are often found autoinhibited in the cytoplasm and require additional activating inputs to exert their function as a Rho GTPase activator (Schmidt & Hall, 2002). For instance, the binding of Dbs, a Dbl-like GEF, to active Rac1 increases nucleotide exchange rates for RhoA (Cheng et al., 2004). The activation of Rac1 by the Dbl-like GEF Vav1 is another example where additional factors regulate the activity of GEFs. Here, Rho GTPase activation depends on the alleviation of Vav1's autoinhibition by signaling-dependent phosphorylation of its N-terminal region (Crespo et al., 1997).

Other protein families promoting Rho GTPase nucleotide exchange have been identified, like the dedicator of cytokinesis (DOCK) protein family with 11 known members (Rossman et al., 2005). DOCK GEFs are structurally different from Dbl-like GEFs, but nucleotide exchange is facilitated by a similar mechanism involving interactions with the switch regions of Rho GTPases. However, the regulation of GEF activity in DOCK family proteins is different. Some DOCK GEFs rely on hetero-oligomerization to alleviate their autoinhibition, a process facilitated by their SH3 domain (Kukimoto-Niino et al., 2021).

Taken together, a complex framework of Rho GTPase activation emerges where multiple domains of Dbl-like GEFs and DOCK GEFs are involved in regulating both the GEF's catalytic activity and selectivity for Rho GTPases. This intricate regulation introduces

potential feedback mechanisms which may explain Rho GTPase activity pattern formation and maintenance.

GTPase activating proteins (GAPs)

Because the spontaneous hydrolysis activity intrinsic to most small GTPases is very slow, Rho GTPase signal termination is usually mediated by GAPs. Many GAPs that selectively target Rho GTPases have been identified, which are in many instances large proteins that contain a core GAP domain with a conserved fold that is flanked by regulatory domains (Tcherkezian & Lamarche-Vane, 2007; Müller et al., 2020). These proteins strongly accelerate nucleotide hydrolysis by complementing the Rho GTPase active site. This mechanism is based on an arginine residue conserved in most GAPs, termed the arginine finger. When the catalytic domain of a GAP interacts with a GTP-bound Rho GTPase, it inserts the positively charged arginine finger into the nucleotide-binding pocket, thus stabilizing the transition state that facilitates GTP hydrolysis (Fidyk & Cerione, 2002; Mosaddeghzadeh & Ahmadian, 2021). Furthermore, the insertion of the arginine finger induces subtle conformational changes in the switch regions of the Rho GTPase, which prime a water molecule for nucleophilic attack on the γ-phosphate of GTP (Fidyk & Cerione, 2002). This mechanism of GAP-mediated inactivation is conserved among RhoGAP proteins. Isolated catalytic GAP domains and full-length GAP proteins outside the cellular context are often promiscuous in their activity. However, individual GAPs are frequently implicated with distinct biological functions, suggesting that their catalytic activity and substrate selectivity is regulated by additional activating inputs. (Amin et al., 2016; Müller et al., 2020). Indeed, most GAPs are large proteins with often multiple, functionally different domains (Tcherkezian & Lamarche-Vane, 2007). For example, members of the Slit-Robo GAP (srGAP) family have an N-terminal F-BAR domain adjacent to the catalytic GAP domain (Amin et al., 2016). Membrane curvature sensing BAR domains can target proteins to regions of high curvature (Heath & Insall, 2008). In the case of srGAP family members, the F-BAR domain allows the localization to the leading edge of cellular protrusions where it can negatively regulate actin dynamics (Endris et al., 2011). In addition to the F-BAR domain, srGAP family members also have a C-terminal SH3 domain which has been shown to promote protein-protein interactions that locate the GAPs to focal adhesions (Endris et al., 2011). Besides distinct localization, lipid interactions have also been observed to directly regulate the activity of some GAPs. The

C1 domain-mediated autoinhibition of the Rac-specific GAP β2-chimaerin is alleviated upon phospholipid membrane binding through the C1 domain (Canagarajah et al., 2004). Furthermore, protein modifications like phosphorylation can either inhibit or enhance activity of RhoGAPs (Okabe et al., 2003; Ohta et al., 2006) and even change their substrate specificity (Minoshima et al., 2003).

All of these features may contribute to the selectivity of GAPs towards Rho GTPases. Thus, both GEFs and GAPs, the primary regulators of the catalytic cycle of Rho GTPases, are subject to heavy regulation. Their catalytic activity and substrate specificity depend on their localization to distinct cellular regions and various activating inputs, which is often achieved by Rho GTPases themselves (Ohta et al., 2006; Vaughan et al., 2011), suggesting complex signaling networks that rely on positive and negative feedback mechanisms.

Rho-specific guanine nucleotide dissociation inhibitor (RhoGDI)

Morphogenetic processes depend on the rapid formation and evolution of Rho GTPase activity patterns at distinct cellular compartments. Within seconds, activating stimuli must be translated into the local activation of Rho GTPases in these regions (Machacek et al., 2009; Vaughan et al., 2011). This requires a large pool of fast-diffusing inactive Rho GTPases in the cytosol. However, the hydrophobic geranylgeranyl moiety at the C-terminus of matured Rho GTPases poses a challenge for the maintenance of such a cytosolic pool. In cells this issue is alleviated by RhoGDI – the primary regulator of the spatial cycle – which solubilizes Rho GTPases by forming a sub-nanomolar affinity complex (Garcia-Mata et al., 2011; Medina Gomez et al., 2024). Upon complex formation, the geranylgeranyl moiety of the Rho GTPase is inserted into the C-terminal hydrophobic pocket of RhoGDI. This stabilizes Rho GTPases in the cytosol and shields them from proteolytic degradation, because loss of RhoGDI leads to a drastic reduction in Rho GTPase protein levels and a re-localization to cellular membranes (Boulter et al., 2010). Furthermore, an N-terminal regulatory arm of RhoGDI sterically blocks the switch regions of Rho GTPases, which inhibits nucleotide hydrolysis and dissociation (Ueda et al., 1990; Hoffman et al., 2000; Boulter et al., 2010). Besides its passive role in the catalytic cycle, RhoGDI actively contributes to the shuttling of Rho GTPases between the plasma membrane and the cytosol, by promoting their membrane extraction with a preference for the inactive state of Rho GTPases (Golding et al., 2019). This preferential extraction is

a critical ingredient for many theoretical models of Rho GTPase polarity, because it could provide a link between the GTPase activity state and its membrane binding properties (Johnson et al., 2009; Freisinger et al., 2013). I will come back to this important point in the later section of this thesis.

The sub-nanomolar affinity of the Rho GTPase:RhoGDI complex means that only a small fraction of Rho GTPases can remain free in the cytosol. While this protects the majority of Rho GTPases from degradation, it prompts the question of how enough Rho GTPases are released from RhoGDI to achieve sufficient levels within the plasma membrane to elicit a signaling response. Multiple mechanisms that may locally destabilize the interaction between RhoGDI and Rho GTPases have been proposed (Garcia-Mata et al., 2011). Lipids, like negatively charged phosphoinositides, have been postulated to destabilize the Rho GTPase:RhoGDI complex, allowing the subsequent activation of Rho GTPases on the membrane by GEFs (Fauré et al., 1999; Robbe et al., 2003). The phosphorylation of RhoGDI has been shown to decrease RhoGDIs affinity for Rho GTPases, hence kinases have been hypothesized as possible candidates that could accelerate complex dissociation (DerMardirossian et al., 2004). However, direct biochemical evidence for such RhoGDI displacement activity has been lacking. Notably, RhoGDI might not only regulate individual Rho GTPases but could also facilitate Rho GTPase crosstalk. The availability of RhoGDI is limited in cells and Rho GTPases draw from the same RhoGDI pool. This might lead to competition between Rho GTPases for this resource to prevent their degradation (Michaelson et al., 2001; Boulter et al., 2010).

In summary, all three primary regulators of the catalytic and spatial cycles of Rho GTPases – GEFs, GAPs and RhoGDI – show a complexity in their regulation, which potentially explains the diversity of Rho GTPase activity patterns observed *in vivo*.

Rho GTPase effector proteins and actin network assembly

Critical mediators of Rho GTPase signaling are a variety of effector proteins, which translate the activity of a given Rho GTPase into a specific response. For RhoA, Rac1 and Cdc42, over 70 potential effector proteins have been identified. Among those effector proteins two primary functions can be observed, they either act as kinases or as scaffolding proteins (Mosaddeghzadeh & Ahmadian, 2021). Serine/threonine kinases like the Rho-associated protein kinase (ROCK), but also lipid kinases such as the

Phosphatidylinositol 3-kinase (PI3K) are stimulated through interactions with active Rho GTPases (Bokoch et al., 1996; Riento & Ridley, 2003). Scaffolding proteins like anilin, insulin receptor substrate 53 kDa (IRSp53) and IQ motif containing GTPase activating protein (IQGAP) promote the formation of multiple protein complexes in response to active Rho GTPases (Piekny & Glotzer, 2008; Ahmed et al., 2010; White et al., 2012). These effector proteins have various functional domains that promote their localization to the plasma membrane through protein-lipid or protein-protein interactions (Bishop & Hall, 2000). For example, IRSp53 has an I-BAR domain allowing for its localization to curved membranes (Ahmed et al., 2010). In addition to functional domains that promote plasma membrane localization, many of these Rho GTPase effector proteins have coiled coil regions (Bishop & Hall, 2000). These regions have been shown to facilitate oligomerization (Kammerer, 1997). Indeed, *in vitro* experiments with the scaffolding protein IQGAP demonstrated its potential to oligomerize (Fukata et al., 1997). Thus, many Rho GTPase effector proteins are membrane associated and offer multiple Rho GTPase binding sites either through multivalency or oligomerization (Bishop & Hall, 2000). These features are essential for the signaling function of Rho GTPase effector proteins.

Rho GTPase signaling controls many morphogenetic events by controlling actin network assembly and dynamics through these effector proteins. The primary function of the actin network is to support and control cellular shape by acting as a structural scaffold and exerting forces on the plasma membrane. Additionally, it enables directed transport of cellular materials. These properties are essential in a wide variety of biological processes requiring shape changes and force generation including cytokinesis and cell locomotion (Pollard & Cooper, 2009). At the core of the actin network is the monomeric actin subunit, one of the most abundant eukaryotic proteins in the cytosol (Higgs, 2001). This globular protein functions as an ATPase that slowly hydrolyses ATP to ADP (Straub & Feuer, 1950). Through spontaneous polymerization, actin monomers can self-assemble into stable, helically arranged filaments (Korn et al., 1987). The regular head-to-tail assembly of structurally asymmetric actin monomers results in a polar filament. Over time, ATP hydrolysis leads to subtle conformational changes in the individual actin subunits within the filament, creating an “aging” effect that results in the preferential disassembly of older filaments. Together with a plethora of regulatory proteins, this effect ensures that one end of the filament (the barbed end) elongates while the other (the pointed end) disassembles (Pollard & Cooper, 2009). This constant turnover of actin, also known as treadmilling,

regulates actin monomer availability and underlies the directed force generation (Bugyi & Carlier, 2010).

At the leading edge of cells, Rho GTPases such as Rac1 and Cdc42 instruct the generation of pushing forces by the local recruitment of nucleation-promoting factors (NPFs) and formins, which promote filament nucleation and elongation. The formation of protrusive structures like lamellipodia is induced by Arp2/3-mediated branching of actin filaments. Arp2/3 complex activation requires NPFs like (N-)WASP and the WAVE regulatory complex (WRC), which are downstream effectors of Cdc42 and Rac1, respectively (Ridley et al., 2003; Gautreau et al., 2022). Initially autoinhibited through an obstructed VCA domain, these NPFs are unable to bind and activate the Arp2/3 complex. Cooperative binding of NPFs to active Rho GTPases and PIP lipids on the plasma membrane releases the VCA domain of NPFs. This domain then binds to the Arp2/3 complex and the first subunit of the new daughter filament, bringing these components into close proximity, which initiates nucleation of a branch on the pre-existing filament growing at the characteristic ~70° angle (Pollard, 2007; Fäßler et al., 2020). In conjunction with capping of the filament at the barbed end, these processes control filament length and the density of branched actin networks, all while being spatially regulated by Rho GTPases (Bieling & Rottner, 2023). Furthermore, oligomerization of NPFs, facilitated by SH3 domain-containing ligands among others, potentiates Arp2/3 activation (Padrick et al., 2008). Considering the switch-like behavior observed in the assembly of such actin structures (Sun et al., 2017), it becomes apparent that these systems are very susceptible to small changes in Rho GTPase membrane density and overall concentration.

Force generation in contractile actin structures at the rear of the cell, such as actomyosin, depends on the interaction of the motor protein myosin II with linear actin filaments. Classically, this interaction and therefore an increase in contractility is spatially coordinated by RhoA (Ridley et al., 2003). Here, the phosphorylation of the myosin light chain (MLC) induces the interaction of myosin II with the actin filaments. This phosphorylation is achieved by the serine/threonine kinase ROCK, which is directly regulated by RhoA activity (Leung et al., 1996; Riento & Ridley, 2003).

Given the relevance of the actin network in morphogenesis, the spatiotemporal coordination of all regulatory processes involved must be essential. This is accomplished by Rho GTPases that can organize into spatial activity patterns and direct the formation of force-generating actin structures *in vivo*. However, the formation of distinct actin

structures feeds back onto Rho GTPases and thus is an integral part in the regulation of Rho GTPase activity patterns (Castro-Castro et al., 2011; Segal et al., 2018). To identify the underlying molecular mechanism behind cell polarization based on Rho GTPases it is important to uncover the intricate feedback loops regulating Rho GTPase activity and determine the minimal requirements for such activity patterns to occur.

Feedback loops organize Rho GTPase activity in time and space

While initially Rho GTPases were believed to operate as simple molecular switches, the evidence accumulated over the years suggests otherwise. The visualization of Rho GTPase activity *in vivo* revealed its intricate spatiotemporal coordination, which supports the idea of a complex regulatory network (Benink & Bement, 2005; Machacek et al., 2009; Das et al., 2012; Michaux et al., 2018). This is further supported by the plethora of complex biological processes controlled by only a few Rho GTPases (Heasman & Ridley, 2008). Spatio-temporal Rho GTPase activity patterns emerge from activity-dependent feedback and crosstalk between Rho GTPases. This regulation takes place at the level of Rho GTPase regulators and includes a variety of positive and negative feedback mechanisms (Bement et al., 2024). To account for the diverse dynamics of Rho GTPase activity observed in these processes, a highly plastic regulatory framework is required. Positive and negative feedback in the regulation of Rho GTPase activity is primarily achieved by the Rho GTPase-dependent recruitment of GEFs and GAPs. Three types of feedback mechanisms are conceivable for the regulation of Rho GTPase activity and have been demonstrated by a combination of various *in vivo* approaches. They mainly differ in the number and types of components that establish a link between the active Rho GTPase and the recruited GEF or GAP. The simplest scenario is direct feedback (Figure 6A), where an active Rho GTPase recruits the regulator directly. This will naturally enhance the regulator's activity due to dimensionality reduction. In addition, recruitment could also allosterically enhance regulator activity. However, only a few GEFs and no GAPs are known to allosterically interact with active Rho GTPases (Bement et al., 2024). One such example is activated Cdc42-associated GEF (ACG), a member of the DOCK180 protein family, which functions as a GEF for Cdc42. An interaction of the GEFs ACB domain with active Cdc42 mediates an increase in its activity. Thus, demonstrating non-linear positive feedback in the regulation of Cdc42 activity (Lin et al., 2006). Another means of regulator recruitment is effector-

based feedback (Figure 6B), which involves an intermediary step where an effector is recruited that facilitates the regulator's recruitment. Prominently, in yeast Cdc42 recruits the scaffolding protein Bem1, which then facilitates recruitment of Cdc24, a GEF of Cdc42 (Butty, 2002). Finally, effector target-based feedback (Figure 6C) refers to a mode of recruitment in which the regulator associates to downstream targets of Rho GTPase effector proteins. Specifically actin networks have been shown to translocate GEFs and GAPs to regions of active Rho GTPases (Castro-Castro et al., 2011; Segal et al., 2018) and a large number of Rho GEFs and GAPs can localize to actin networks (Müller et al., 2020). This indirect feedback mechanism can result in different degrees of temporal delay, which increases the versatility in dynamics of Rho GTPase activity patterns (Bement et al., 2024).

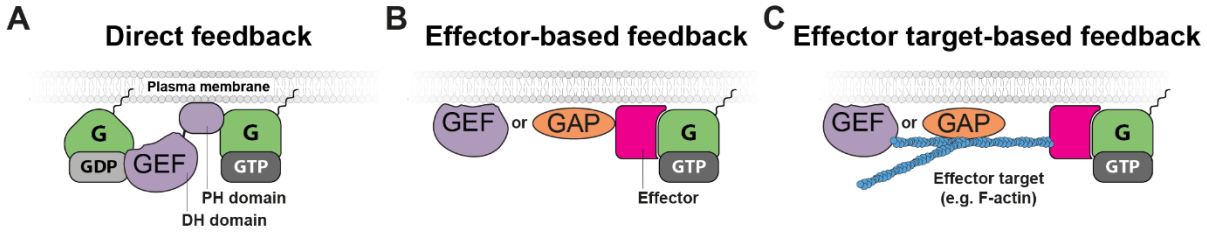

Figure 6: Feedback mechanisms in the regulation of Rho GTPase activity mediated by GEFs and GAPs. (**A**) Scheme of direct feedback where a GEF is recruited by an active Rho GTPase via its PH domain. (**B**) Scheme of effector-based feedback. Here, GEFs or GAPs are recruited to the membrane by an effector of Rho GTPases. (**C**) Scheme of effector target-based feedback. Processes downstream of Rho GTPase effectors, like F-actin assembly, may translocate or stabilize GEFs and GAPs on membranes (Adapted from Bement et al., 2024).

The number of Rho GTPase signaling systems that rely on self-organizing Rho GTPase activity patterns suggests that self-organization is a core aspect of Rho GTPase regulation and function. To understand these systems at the molecular level, it is necessary to establish feedback mechanisms. Specifically in the formation of Rho GTPase activity patterns, numerous key regulatory feedback mechanisms have been identified (Bement et al., 2024). However, due to the complexity of Rho GTPase regulation on the genetic level, no single patterning system has ever been reconstituted. Such a reconstitution would be instrumental to identify the exact molecular mechanism governing Rho GTPase activity pattern formation.

Objectives

In this project I aimed to identify biochemical mechanisms that allow Rho GTPase signaling systems to form patterns by *in vitro* reconstitution. The main objectives of this thesis can be divided into five main points:

1) Study the relationship between Rho GTPase activation and membrane turnover

In a collaboration with Lila Hoachlander-Hobby from the Bement Lab, we investigated the activity-dependent accumulation of Rho GTPases on membranes *in vivo*. We were able to quantify this accumulation during single cell wound healing, demonstrating the coupling of the catalytic and spatial cycle of Rho GTPases.

2) Reconstitute a templated Rho GTPase pattern

To investigate Rho GTPase activity patterns and untangle them from the complex environment they are observed in, I turned to *in vitro* reconstitutions on supported lipid bilayers (SLBs). As a starting point I set out to reconstitute Rho GTPase activity patterns based on a lipid template. By utilizing a self-organizing lipid system discovered by the Hansen Lab (Hansen et al., 2019), I successfully established a system capable of local activation of Rho GTPases, specifically Cdc42. However, the enrichment of Rho GTPases in these areas of activity, as expected from *in vivo* observations, could not be observed.

3) Identify factors allowing for Rho GTPase membrane enrichment

In order to recapitulate Rho GTPase enrichment as observed *in vivo* I expanded my reconstitution by implementing RhoGDI1 and effector proteins which are as previously described two classes of proteins directly coupled to the regulation and signaling output of Rho GTPases. The latter class indeed facilitated the enrichment at sites of Rho GTPase activity.

4) Investigate the mechanism of Rho GTPase membrane enrichment

Single molecule approaches and flow-out experiments allowed me to identify an increase in membrane stability of active Rho GTPases facilitated by effector proteins as a mechanism behind the enrichment at sites of their activity. Can we utilize these findings to reconstitute a synthetic polarizing Rho GTPase system?

5) Design and characterize a self-organizing, synthetic Rho GTPase signaling system

In a final part, I designed and biochemically characterized components of a system theoretically capable of pattern formation based on direct feedback between different Rho GTPases facilitated by their regulators. This network topology together with the previous

findings allowed me to design and purify proteins that may facilitate the feedback links required for spontaneous symmetry-breaking of Rho GTPase activity. This sets the stage for the *in vitro* reconstitution of a full system of self-organizing Rho GTPase patterns.

Results

Coupling of the regulatory cycles of Rho GTPases

Cdc42 enriches at membrane sites where it is activated *in vivo*

The cycling of Rho GTPases between an active and an inactive state as well as their shuttling between plasma membrane and cytosol are integral parts in the regulation of Rho GTPase signaling. Unsurprisingly, the coupling of both cycles, catalytic and spatial, has been hypothesized and, in fact, is often a requirement in theoretical approaches investigating Rho GTPase pattern formation (Jilkine et al., 2007; Goryachev & Pokhilko, 2008). To understand this relationship, we collaborated with Lila Hoachlander-Hobby and Prof. William Bement at the University of Wisconsin-Madison, who utilized single cell wound healing experiments in *Xenopus laevis* oocytes, to quantify and correlate active and total Cdc42 around cell wounds. Accumulation of active Cdc42 around the wound has been reported previously and was found to direct the actin network crucial for cell repair (Benink & Bement, 2005). This system is therefore appropriate to compare the accumulation of active Cdc42 relative to its total amounts *in vivo*.

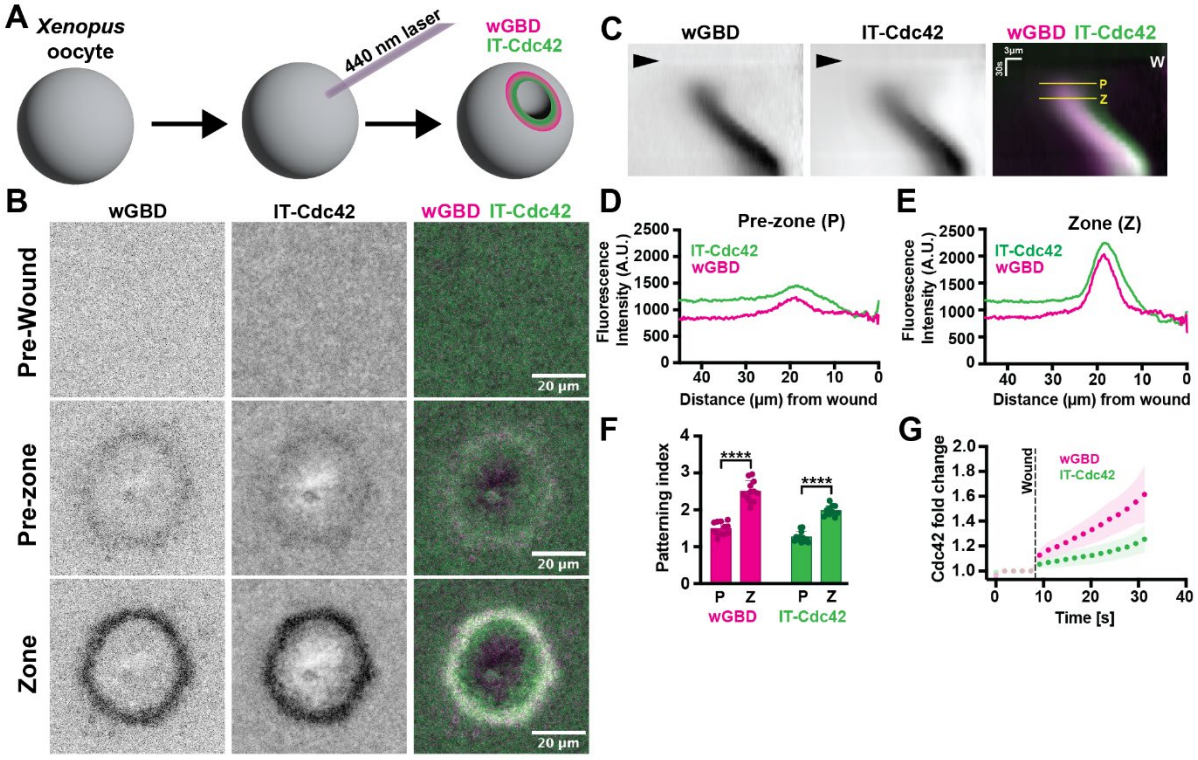

Figure 7: Enrichment of active Cdc42 around single cell wounds *in vivo*. (**A**) Scheme of a *Xenopus laevis* oocyte with a laser-induced wound and the resulting concentric rings of enriched wGBD and IT-Cdc42 around the wound. (**B**) Dual color confocal microscopy images of wGBD (mCherry-wGBD) and IT-Cdc42 (IT-GFP-Cdc42) at the plasma membrane before wounding (top, Pre-wound), after wounding prior to the complete formation of a zone (middle, Pre-zone), and after wounding when the zones are fully formed (bottom, Zone). (**C**) Kymographs of the confocal images from (B) generated by radially averaging signal intensity around the wound over time (Moe et al., 2021). Time of wounding is denoted by the black arrow, while the position of the wound is shown by a "W". Zone time points are indicated by yellow lines together with the letters P for Pre-zone (40 s after wounding) and Z for Zone (60 s after wounding). (**D**) Pre-zone or (**E**) zone time point line scans generated from the kymograph in (C) showing IT-Cdc42 (green) and wGBD (magenta) fluorescence intensity as a function of distance from the wound center. (**F**) Patterning indices of IT-Cdc42 (green) and wGBD (magenta) at the Pre-zone time point compared to the Zone time point. Two-sample t-tests were used to determine statistical significance between Pre-zone and Zone time points; ****$p < 0.0001$; $n = 12$. (**G**) Patterning indices of IT-Cdc42 (green) and wGBD (magenta) around the wound as a function of time. All experiments were performed by Lila Hoachlander-Hobby in the laboratory of Prof. William Bement.

Laser-induced wounds in *Xenopus laevis* oocytes lead to the formation of concentric rings of plasma membrane-bound and active Cdc42 (Figure 7A). By introducing mRNA of the Rho GTPase binding domain (GBD) of WASP flanked by mCherry as a fluorescent label (mCherry-wGBD) together with the mRNA of internally labeled Cdc42 via microinjection to the oocyte system, we were able to follow both active and total Cdc42 over time (Figure 7B). While an increase in both can be observed around the wound, activity of Cdc42 and total amounts do not completely overlap, with the overall amounts accumulating closer to the wound edge (Figure 7C-E). The degree of accumulation, and therefore Rho GTPase

patterning, was quantified by the patterning index (PI), the ratio within the Cdc42 enriched zone vs the zone 30 μm away from the wound. We found that upon wounding the patterning index for both active and total Cdc42 increased above 1, with a PI of 1 indicating equal partitioning and thus the absence of patterning. The enrichment zone (Z) was fully established 60 s after wounding with a PI around 2 for both active and total Cdc42 (Figure 7F), suggesting a near doubling of total Cdc42 close to the wound. Interestingly, we observed that the accumulation of total Cdc42 around the wound is generally slower relative to the increase in Cdc42 activity (Figure 7G).

These experiments conducted by our collaborators uncovered that the accumulation of Rho GTPases at sites of their activity occurs during their spatiotemporal coordination around single cell wounds, suggesting coupling of their catalytic and spatial cycles. They are also suggestive of a chronological order of the underlying molecular processes involved, in which Rho GTPase enrichment occurs after their activation.

Generating a template for localized activation of Rho GTPases on model membrane systems

The previous experiments show that Rho GTPases not only organize into activity patterns but also enrich on the membrane at sites of their activity. However, the molecular mechanism by which the enrichment of active Rho GTPases is facilitated remains unknown. Top-down approaches trying to dissect the molecular processes involved are often challenging because of the sheer number of interacting proteins and reacting molecules present in the system. Hence, I turned to an *in vitro* reconstitution approach with a limited set of molecules. Throughout this section of the thesis, I will use TIRF microscopy in combination with supported lipid bilayers (SLBs) to reconstitute templated Rho GTPase activity patterns and investigate Rho GTPase enrichment at sites of their activity. TIRF microscopy is ideal to study processes on flat surfaces because of its high axial resolution, which ensures a high signal-to-noise ratio (Fish, 2009).

SLBs are commonly used in reconstitutions and can mimic specific lipid environments of the cell (Golding et al., 2019). To faithfully recapitulate a system displaying Rho GTPase activity patterns, I generated SLBs (see Methods: Preparation of supported lipid bilayers (SLBs)) encompassing the key components (Table 1) of the inner leaflet of the plasma membrane (Van Meer et al., 2008; Lorent et al., 2020).

Table 1: Lipid composition of the plasma membrane-Mix (PM-Mix) as molar fractions used for SLB generation.

Component	Molar fraction
DOPC	26.5
DOPE	26.5
DOPS	22.5
PI(4)P	2
$PI(4,5)P_2$	2
Cholesterol	0.5
PE-PEG5000	20

Matching these levels of the individual lipid species in the reconstitution is important to ensure a fluid and continuous lipid bilayer. Furthermore, the fraction of negatively charged lipids directly influences recruitment of Rho GTPases and their regulators. This lipid compartment in the reconstitution not only allows the implementation of the spatial cycle of Rho GTPases, but also enables their localized activation. However, to achieve the latter a spatial input, mimicking the sub-regions on the membrane in which Rho GTPases are activated by GEFs, is required. Hence, I utilized a recently developed self-organizing phosphatidylinositol phosphate (PIP) lipid system which is based on competing reactions between a kinase and a phosphatase (Hansen et al., 2019). Together, the phosphatidylinositol-4-phosphate 5-kinase (PIP5K) and the competing 5'-phosphatase, fused to a lipid binding domain specific for the product of the phosphatase PI(4)P (DrrA-OCRL), generate regions on SLBs enriched for either PI(4)P or $PI(4,5)P_2$ lipids. The basic features for such large-scale lipid patterns to form on SLBs in this kinase-phosphatase system include competing enzymatic reactions exhibiting positive feedback to varying degrees through product recognition, asymmetric binding kinetics of the enzymes to the product and the lipid diffusion within the membrane. Based on these features, the system shows an asymmetric response to stochastic fluctuations in the molecular density of membrane-bound enzymes. In combination with reaction-diffusion processes, this results in the formation of mutually exclusive PI(4)P or $PI(4,5)P_2$ lipid-zones on SLBs (Hansen et al., 2019).

To harness this self-organizing system, I included both PIP species (2 % each) in the plasma membrane-like composition used for SLB generation (PM-Mix) and tested the fluidity of the lipid bilayer.

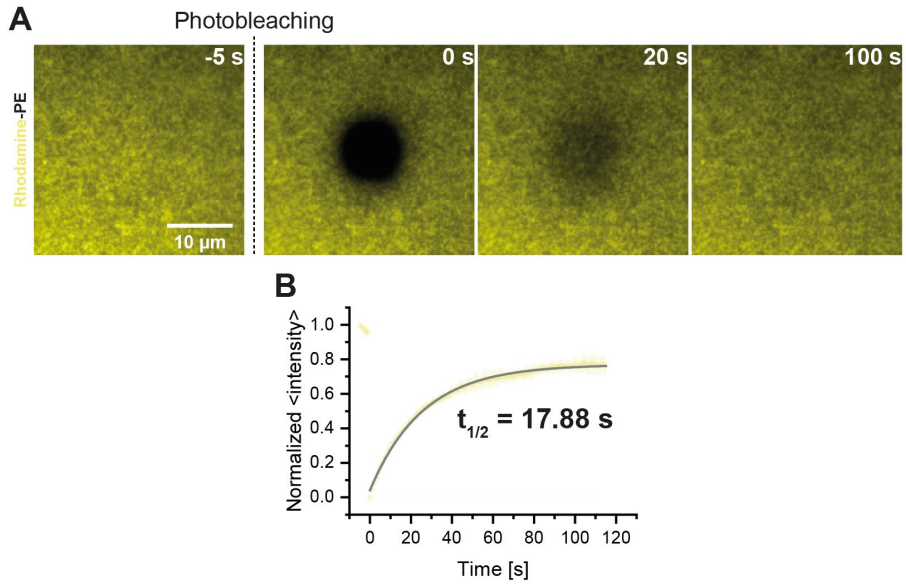

Figure 8: Fluidity of SLBs made with a plasma membrane mimicking lipid composition, containing PI(4)P and PI(4,5)P_2 (PM-Mix), determined by fluorescence recovery after photobleaching (FRAP). (**A**) Time-lapse TIRFM images of rhodamine-PE (0.01% in the PM-Mix, yellow) at indicated times before or after photobleaching at t = 0 s. (**B**) Normalized fluorescence intensity in FRAP regions plotted over time and fitted with a mono exponential function to obtain $t_{1/2}$. All numeric data represent the mean from five independent experiments (symbols) ± SD (shaded areas) (N=5). All scale bars are 10 µm as indicated.

Fluorescence recovery after photobleaching (FRAP) experiments with the plasma membrane-like lipid bilayer, additionally including rhodamine-PE (0.01%), revealed rapid recovery of the fluorescence signal within seconds after photobleaching, confirming membrane fluidity (Figure 8).

To validate lipid pattern formation on PM-Mix SLBs with an initially homogeneous distribution of lipids, I exposed the lipid bilayer to PIP5K (20 nM) and DrrA-OCRL (4-6 nM). Shortly after, PI(4)P and PI(4,5)P_2 organized into mutually exclusive regions, visualized by a fluorescently labeled PI(4,5)P_2 lipid binding domain of PLCδ (A647-PH). The highly dynamic lipid pattern stabilized after 10 to 15 minutes and remained relatively stable throughout the experiment (Figure 9A, B).

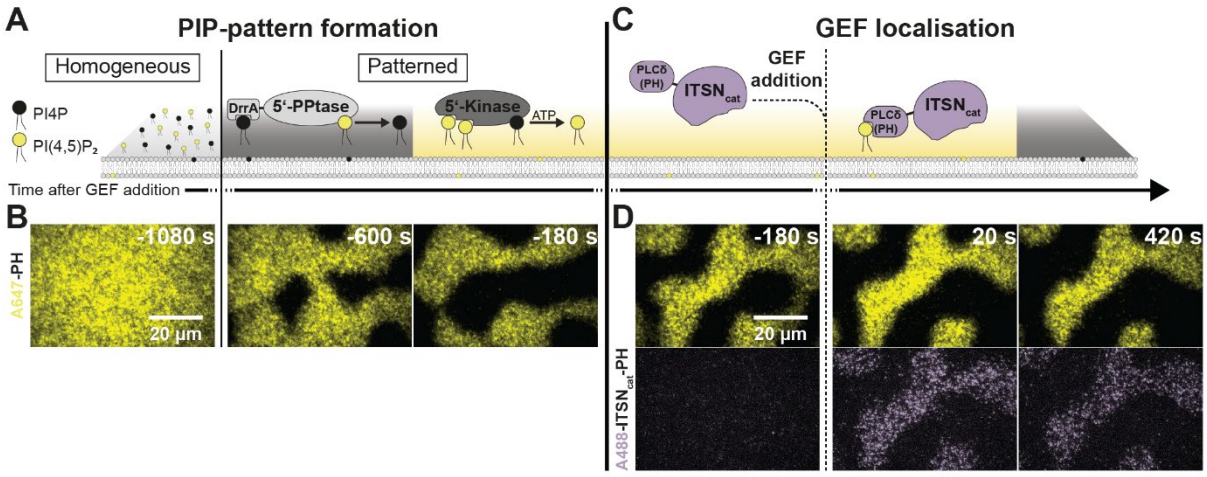

Figure 9: Lipid pattern formation and localization of ITSN$_{cat}$-PH to specific membrane compartments. (**A**) Scheme of PI(4)P and PI(4,5)P_2 lipid pattern formation by PIP5K and DrrA-OCRL on PM SLBs. (**B**) Time-lapse TIRFM images of pattern formation on PM SLBs (initially containing 2% PI(4)P and PI(4,5)P_2 each) by PIP5K (20 nM) and DrrA-OCRL (here 4 nM, for all following experiments 6 nM were used) visualized by A647-PH (2 nM, yellow) at indicated times before GEF addition. (**C**) Schematic representation or (**D**) time-lapse multi-color TIRFM images of PIP lipid patterns on PM SLBs visualized by A647-PH (2 nM, yellow) at indicated times before or after addition of A488-ITSN$_{cat}$-PH (1 nM, purple) at t = 0 s.

To utilize this self-organizing system as a spatial input and simultaneously implement parts of the catalytic cycle in the reconstitution of Rho GTPase patterning, I added the catalytic domain of intersectin, a Cdc42 specific GEF, fused to the PI(4,5)P_2 lipid binding domain of PLCδ (ITSN$_{cat}$-PH), after the lipid pattern stabilized. Localization of ITSN$_{cat}$-PH was visualized by a fluorescently labeled version of the synthetic protein (A488-ITSN$_{cat}$-PH). Furthermore, to later prevent extensive activation of Rho GTPases in solution, the concentration of ITSN$_{cat}$-PH was kept to a minimum (1 nM). As anticipated, despite only using low concentrations, the GEF associated with the lipid bilayer and did so exclusively in areas of enriched PI(4,5)P_2 (Figure 9C, D).

Single molecule experiments revealed an ITSN$_{cat}$-PH density in these regions of 0.2 molecules per µm^2 (Figure 10). Nevertheless, because of the high catalytic activity of intersectin toward Cdc42 (Hussain et al., 2001), it is plausible to expect activation of Cdc42 in these regions.

Hence, I reconstituted the localized recruitment of a Cdc42-specific GEF to distinct lipid regions of a dynamic and self-organizing lipid pattern. This system should hypothetically be able to activate Cdc42 locally based on the "activation template" it provides.

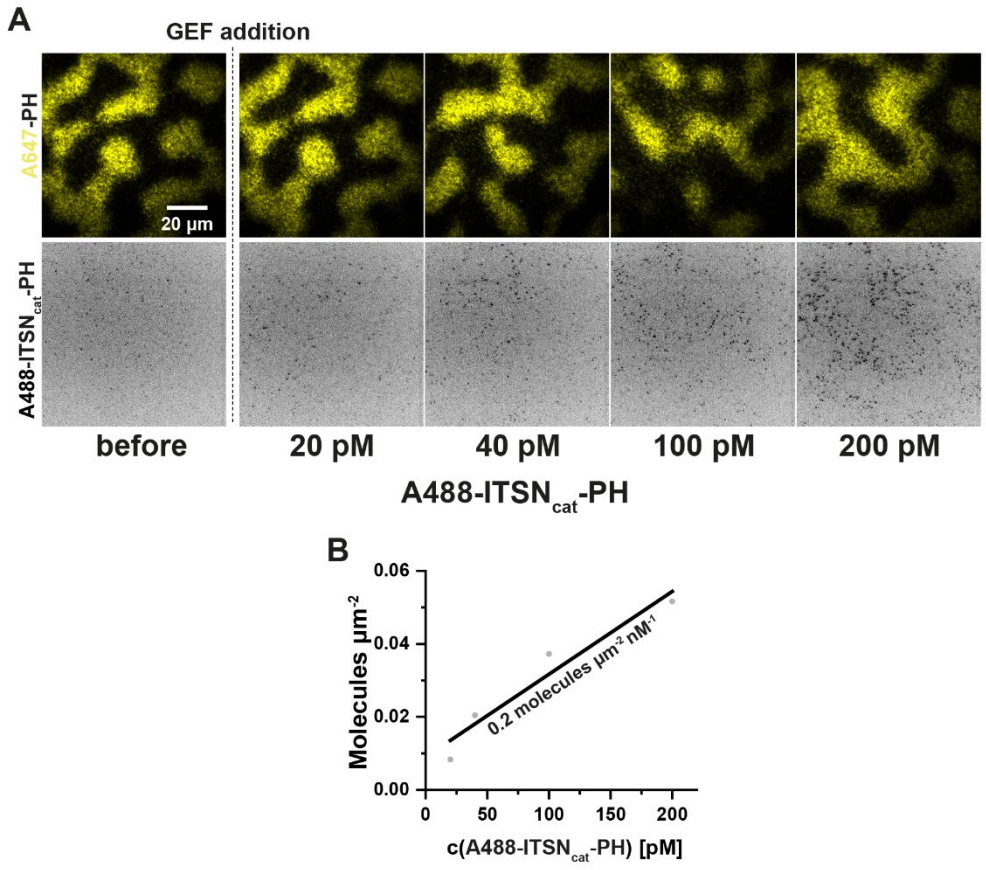

Figure 10: Density of ITSN$_{cat}$-PH in PI(4,5)P$_2$ areas. (**A**) TIRFM images of A647-PH (2 nM, top) and single molecules of A488-ITSN$_{cat}$-PH (varying concentration, bottom) at indicated times before and after addition of (A488)-ITSN$_{cat}$-PH (Total concentration: 1 nM) at t = 0 s. (**B**) Number of molecules per µm^2 in regions of high PI(4,5)P$_2$ plotted against the corresponding concentration of labelled GEF and fitted with a linear function to obtain the density of GEFs inside regions of high PI(4,5)P$_2$.

Membrane-templated Rho GTPase activation

To assess whether Cdc42 can indeed be activated in subregions of the SLB with the current system and to ultimately probe the processes involved in Rho GTPase patterning, Cdc42 had to be implemented in a way that allows for the visualization of its amounts on the membrane and its activity state. This was achieved by using fluorescently labeled and prenylated Cdc42 (A647-Cdc42) in combination with a recruitment-based activity sensor, a fluorescently labeled binding domain of Cdc42 (A488-wCRIB). With these additional components I tested if local activation of Cdc42 can be achieved in the form of a spatial input through the PI(4,5)P$_2$ pattern to which ITSN$_{cat}$-PH selectively localizes (Figure 11A).

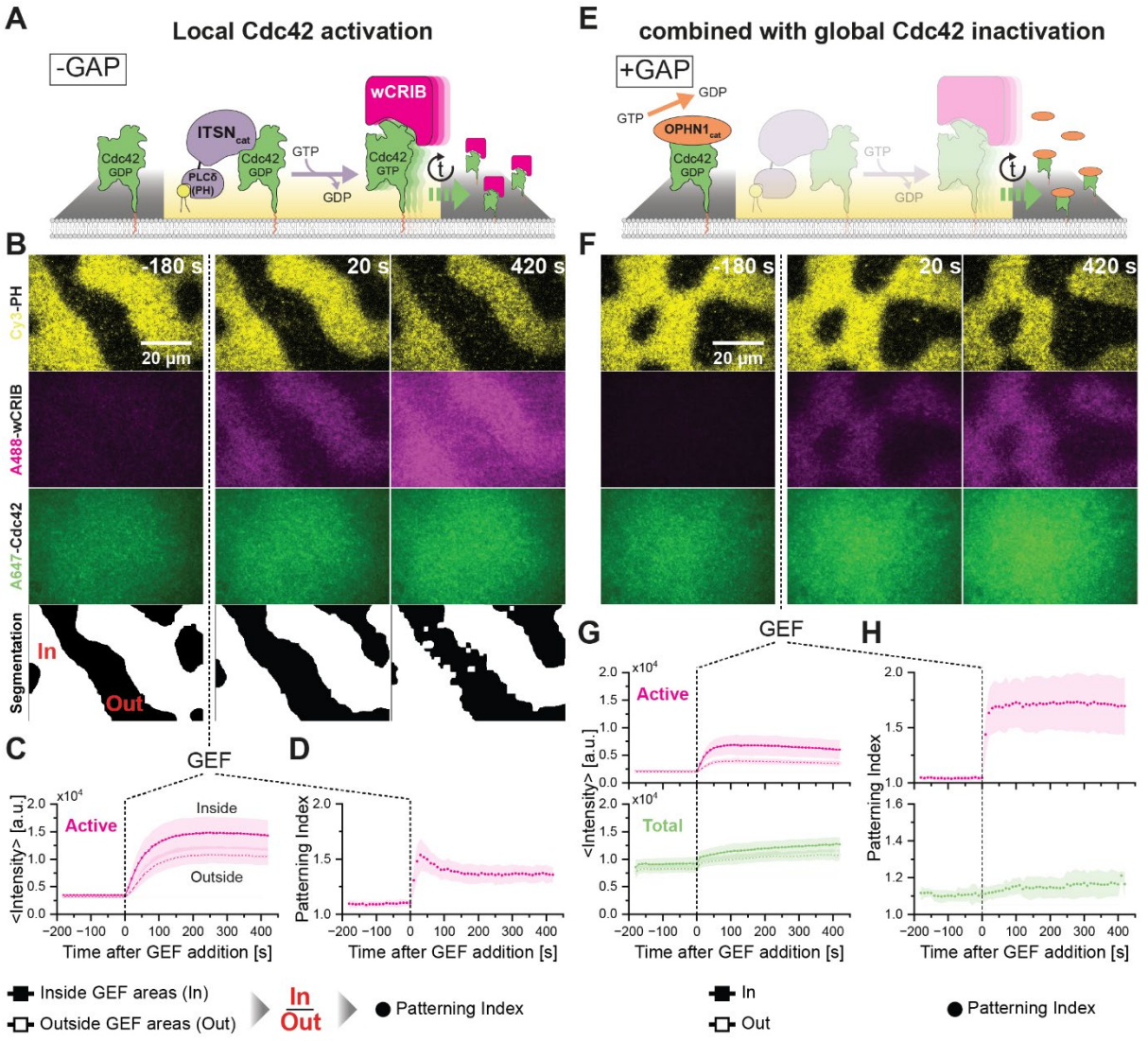

Figure 11: Reconstitution of membrane-templated Rho GTPase activity patterns *in vitro*. (**A**) Scheme of the local activation of Cdc42 by ITSN$_{cat}$-PH in the PI(4,5)P$_2$-rich areas of PM SLBs, the resulting binding of the activity probe wCRIB and the diffusion of active Cdc42 into GEF-lacking areas over time. (**B**) Time-lapse multi-color TIRFM images of Cy3-PH (2 nM, yellow), A488-wCRIB (40 nM, magenta) and A647-Cdc42 (5.5 nM, green) on PIP patterns at indicated times before or after addition of ITSN$_{cat}$-PH (1 nM) at t = 0 s. Bottom row shows segmentation based on the lipid pattern. (**C**) Average intensities inside (filled squares, $<I_{In}>$) and outside (hollow squares, $<I_{0ut}>$) of the GEF-containing membrane areas or (**D**) patterning index (full circle, $PI = <I_{In}> / <I_{0ut>}$) of A488-wCRIB (magenta) over time. (**E**) to (**H**) correspond to (A) to (D), with the additional presence of OPHN1$_{cat}$ (20 nM). However, the segmentation is not shown in (**F**). Additionally, in (**G**) are the average intensities inside and outside of the GEF-containing membrane areas and in (**H**) the patterning index of A647-Cdc42 (green) over time. All numeric data represent the mean from three independent experiments (symbols) ± SD (shaded areas) (N=3). All scale bars are 20 µm as indicated.

The presence of the lipid sensor Cy3-PH (2 nM), the activity sensor A488-wCRIB (40 nM) and the labeled Rho GTPase A647-Cdc42 (5.5 nM) did not noticeably change the dynamics of lipid pattern formation induced by the kinase-phosphatase system (Figure 11B). Lipid patterns formed, as previously described, within 10-15 minutes and remained stable

throughout the 10-minute imaging period with only minor fluctuations in the overall area of enriched PI(4)P or PI(4,5)P_2 regions (Figure 11B). Despite the presence of a lipid pattern, prenylated A647-Cdc42 bound homogenously to the lipid bilayer (Figure 11B). This shows that the minor imbalance in negative membrane charge is insufficient in significantly changing the distribution of Rho GTPases across the bilayer. Upon addition of $ITSN_{cat}$-PH (1 nM), shortly after acquiring a baseline signal, activation of Cdc42 was followed by monitoring the activity sensor signal. As anticipated, the addition of even such low concentrations of GEF resulted in a rapid rise in the amount of surface-recruited A488-wCRIB. This initial rise was predominantly observed in regions of enriched PI(4,5)P_2 lipids, indicated by the increasing signal in the activity channel. However, this was quickly followed by an increase in activity throughout the lipid bilayer, also in regions not bound by $ITSN_{cat}$-PH (Figure 11B, C). This gradual increase in activity outside of the GEF-containing membrane regions is likely the result of active Rho GTPases quickly equilibrating across the membrane via diffusion. Interestingly, however, the addition of $ITSN_{cat}$-PH affected total levels of Cdc42 associated with the membrane only slightly, with an overall increase of bound A647-Cdc42 independent of the membrane region (Figure 11B). To quantify the degree of patterning of active Cdc42, similarly to the previously described *in vivo* experiments, I quantified their partitioning across the two distinct PIP membrane regions by the patterning index as a ratiometric measure. Segmenting enriched PI(4,5)P_2 or PI(4)P regions based on the lipid channel (see Methods: Data analysis) allowed the comparison of Cdc42 activity in regions recruiting or lacking $ITSN_{cat}$-PH. The resulting ratio, the PI, is a measure of patterning strength and can be followed over time to infer patterning stability.

Already in the absence of $ITSN_{cat}$-PH, the patterning index of the activity channel indicated slight patterning (PI > 1), albeit at a constant level. We interpret this minor deviation from the expected equipartitioning as a result of the random positioning of the large PIP domains in the uneven TIRF field, which can result in minor apparent enrichment for low numbers of experiments such as in this case. Because of the excess GTP in the reaction buffer (see Methods: Membrane-templated Rho GTPase patterns (single molecule and bulk)), some Rho GTPases are likely in their active GTP-bound form, leading to the detection of residual activity by A488-wCRIB prior to GEF addition. Upon $ITSN_{cat}$-PH addition, the patterning index rapidly increased (PI ≈ 1.54). However, after the sudden increase, the PI did not stabilize, but over time returned to levels (PI ≈ 1.35) closer to

baseline (Figure 11D). This transient nature of the activity pattern is likely caused by the diffusion of Cdc42 that was activated in regions recruiting $ITSN_{cat}$-PH into regions lacking $ITSN_{cat}$-PH. Consequently, the system is dominated by the activation of Cdc42 because it is only opposed by the slow intrinsic hydrolysis rate of Rho GTPases. We therefore concluded that, while the system allows the local activation of Cdc42, it can only do so ineffectively and transiently.

To reconstitute a stable Rho GTPase activity pattern, the activation of Cdc42 had to be restricted and counteracted by an opposing activity. To this end, I introduced a soluble GAP, the catalytic domain of oligophrenin-1 ($OPHN1_{cat}$), to the system, while keeping all previous components constant as before (Figure 11E). By fully implementing the catalytic cycle of Rho GTPases through the addition of $OPHN1_{cat}$ (20 nM), I achieved nearly complete inactivation of Cdc42 in the absence of $ITSN_{cat}$-PH, suggested by reduced binding of A488-wCRIB (Figure 11F, G). However, localized activation of Cdc42 was maintained upon $ITSN_{cat}$-PH addition, indicated by a rapid increase in activity sensor signal, albeit with a smaller amplitude (~40%) relative to previous experiments in the absence of the GAP (Figure 11F, G). Noticeably, upon $ITSN_{cat}$-PH addition, the patterning index of active Cdc42 saturated (PI ≈ 1.7) and now remained stable (Figure 11H). Hence, I successfully established a system displaying stable Rho GTPase activity patterns for prolonged periods of time. However, membrane-bound A647-Cdc42 showed an even distribution across the bilayer as indicated by a stable patterning index close to 1.0 before and after $ITSN_{cat}$-PH addition. While the value of the patterning index (PI ≈ 1.1) suggests slight patterning, this most likely results from two reasons: 1) a slight preference of Rho GTPases for negatively charged lipids, in this case $PI(4,5)P_2$ over PI(4)P and 2) the aforementioned uneven illumination during TIRF microscopy leading to deviations from equipartitioning in the segmentation maps. Therefore, the system still lacks the strong accumulation of Rho GTPases in GEF-containing regions as observed *in vivo*.

In conclusion, by introducing both catalytic regulators and thereby closing the catalytic cycle, I successfully reconstituted a system of templated Rho GTPase activity patterning. However, with the current set of components I was unable to detect activity-dependent enrichment of Rho GTPases in specific subregions of the bilayer. Thus, other factors present *in vivo* must be responsible for the enrichment of Rho GTPases at sites of their activity.

Local enrichment of Rho GTPases on membranes is induced by effectors

Given that the complete implementation of the catalytic cycle was not sufficient to recapitulate the observed properties of Rho GTPase activity patterns *in vivo*, I decided to incorporate the solubilization factor, RhoGDI1, in the reconstitution. RhoGDI serves as the primary regulator of cellular Rho GTPase distribution, maintaining an inactive pool of Rho GTPases in the cytosol and ensuring fast membrane-cytosol shuttling through the extraction of inactive Rho GTPases from the membrane (Johnson et al., 2009; Freisinger et al., 2013). Previous work has shown that RhoGDI1 only has a slight preference (~2x-3x) for extracting the inactive species of Rho GTPases (Golding et al., 2019). Based on this preference, I hypothesized that concentration patterns of Cdc42 might develop in the presence of RhoGDI1. To test this, I modified the reconstituted system to include RhoGDI1 at concentrations equal to those of the Rho GTPase. Specifically, I substituted the free, prenylated Cdc42 by RhoGDI1:Cdc42 complexes with a 1:1 binding stoichiometry. Given that RhoGDI potently reduces the concentration of free, prenylated Cdc42 in solution by sequestration, I first set out to determine the concentration of RhoGDI1:Cdc42 complexes allowing for significant membrane binding of Cdc42. The required complex concentration to achieve comparable membrane binding was empirically determined to be approximately 100-fold higher than the previously used concentration of free, prenylated Cdc42 (Figure 12). This empirically determined concentration matched mass action calculations, which estimate at equilibrium a free concentration of ~ 7 nM for both free, prenylated Cdc42 and RhoGDI1 at 600 nM of RhoGDI1:Cdc42 complexes and a K_D of 90 pM (Medina Gomez et al., 2024).

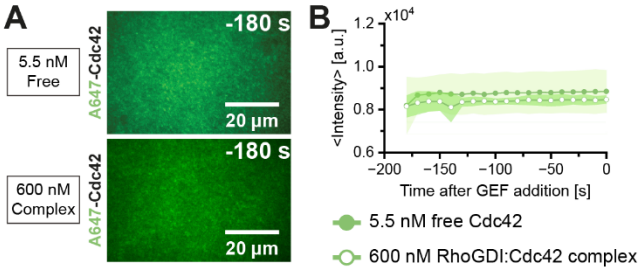

Figure 12: Matching membrane loading of free Cdc42 and in complex with RhoGDI1. (**A**) TIRFM images of A647-Cdc42 (5.5 nM, top) and A647-Cdc42:RhoGDI1 complexes (600 nM, bottom) on PIP patterns before addition of $ITSN_{cat}$-PH at t = 0 s. (**B**) Average intensities of A647-Cdc42 (filled circles) and A647-Cdc42:RhoGDI1 complexes (hollow circles) on the membrane over time. All numeric data represent the mean from three independent experiments (symbols) ± SD (shaded areas) (N=3). All scale bars are 20 µm as indicated.

The inclusion of RhoGDI1 in the otherwise unchanged reconstituted system, allowed the assessment of possible effects on Rho GTPase patterning by RhoGDI1 (Figure 13A).

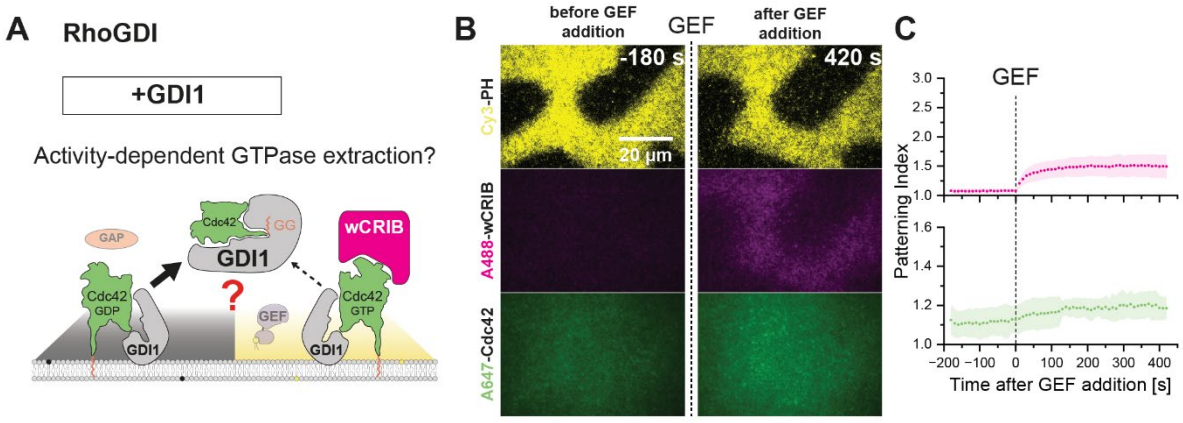

Figure 13: RhoGDI1 alone cannot enrich Rho GTPases at membrane sites of their activity. (**A**) Scheme or (**B**) time-lapse multi-color TIRFM images of the effects of RhoGDI1 on templated Rho GTPase activity patterns. Images of Cy3-PH (2 nM, yellow), A488-wCRIB (40 nM, magenta) and A647-Cdc42:RhoGDI1 complexes (600 nM, green) on PIP patterns at indicated times before or after addition of $ITSN_{cat}$-PH (1 nM) at t = 0 s in the presence of $OPHN1_{cat}$ (20 nM). (**C**) Patterning indices ($PI = \langle I_{In} \rangle / \langle I_{Out} \rangle$) of A488-wCRIB (magenta) or A647-Cdc42 (green) under conditions as in (B) over time.

Lipid pattern formation was not affected by the additional presence of RhoGDI1. Upon $ITSN_{cat}$-PH addition, activation of Cdc42 occurred in GEF-containing regions, again indicated by increased A488-wCRIB binding. The system showed a sustained activity pattern as observed in previous experiments, albeit at reduced (PI < 1.5) patterning strength (Figure 13B, C). More importantly, however, the distribution of Cdc42 on the lipid bilayer remained homogenous and no enrichment of Cdc42 in GEF-containing regions was observed (Figure 13B, C). This could be partially because of the low concentrations of free RhoGDI1 in the system under these conditions (estimated to be ~ 7 nM as stated above), which might not be sufficient to selectively destabilize the inactive form of Cdc42 by extraction. We were unable to explore higher amounts of free RhoGDI1 or work at significant RhoGDI1 excess, since this prevented the membrane binding of Cdc42 due to potent sequestration. Together, these results suggest that the main regulators of Rho GTPase activity – namely, GEFs, GAPs and RhoGDI – are not sufficient to facilitate enrichment of Cdc42 active sites, and thus, cannot recapitulate patterning observed *in vivo*.

To further assess the effects of RhoGDI1, I took a step back and tested the behavior of the system, including RhoGDI1, in the absence of the soluble GAP, $OPHN1_{cat}$ (Figure 14A). Remarkably, even prior to the addition of $ITSN_{cat}$-PH, high levels of A488-wCRIB binding

could be observed across the lipid bilayer with a slight preference for regions of enriched $PI(4,5)P_2$ (Figure 14A-C). Similar to previous experiments without $OPHN1_{cat}$, excess GTP in buffer inevitably leads to some active, GTP-bound Cdc42. However, in the presence of RhoGDI1 the inactive, GDP-bound form of Cdc42 is additionally sequestered in solution, favoring the preferential release of the spuriously activated GTP-bound Cdc42 from RhoGDI1 and its association with the membrane. Despite this increase in pre-activation, the addition of $ITSN_{cat}$-PH still led to an increase in the patterning index, but only slightly above levels before GEF addition (Figure 14C). Interestingly, the direct comparison of the RhoGDI1-including system with and without $OPHN1_{cat}$, shows that Cdc42 activity levels in the presence of the GAP never exceed those observed in its absence, even when compared to the activity levels before $ITSN_{cat}$-PH addition in the absence of $OPHN1_{cat}$ (Figure 14B and E).

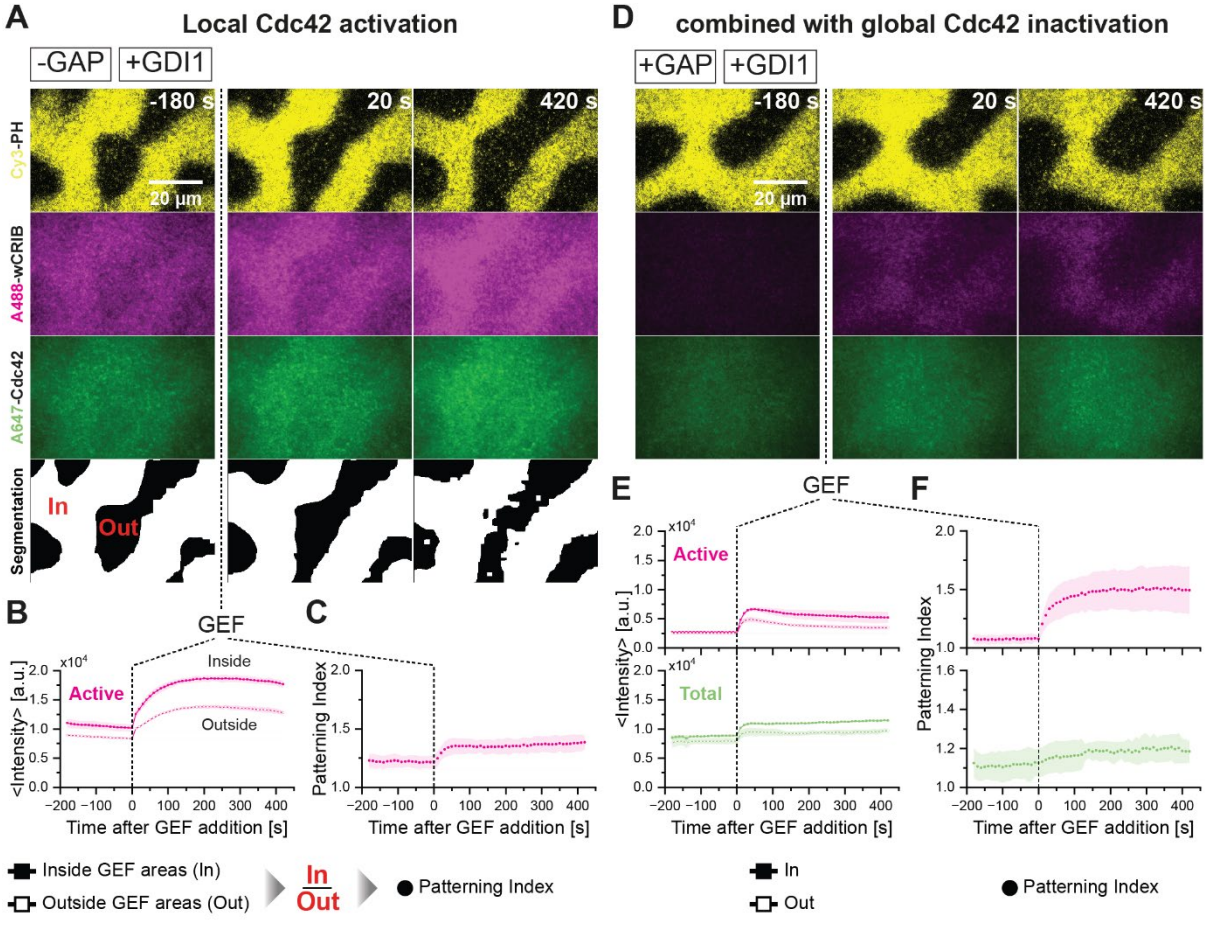

Figure 14: RhoGDI1 negligibly affects the reconstitution of membrane-templated Rho GTPase activity patterns *in vitro*. (**A**) Time-lapse multi-color TIRFM images of Cy3-PH (2 nM, yellow), A488-wCRIB (40 nM, magenta) and A647-Cdc42:RhoGDI1 complexes (600 nM, green) on PIP patterns at indicated times before or after addition of $ITSN_{cat}$-PH (1 nM) at t = 0 s. Bottom row shows segmentation based on the lipid pattern. *(Continued on the following page.)*

Figure 14: (**B**) Average intensities inside (filled squares, $<I_{In}>$) and outside (hollow squares, $<I_{Out}>$) of the GEF-containing membrane areas or (**C**) patterning index (full circle, $PI = <I_{In}> / <I_{Out}>$) of A488-wCRIB (magenta) over time. (**D**) to (**F**) correspond to (A) to (C), with the additional presence of $OPHN1_{cat}$ (20 nM). However, the segmentation is not shown in (**D**). Additionally, in (**E**) are the average intensities inside and outside of the GEF-containing membrane areas and in (**F**) the patterning index of A647-Cdc42 (green) over time.

Hence, I reconstituted a minimal system that includes the main regulatory players of the catalytic and spatial cycles of Cdc42, yet it failed to accurately reproduce Rho GTPase patterning observed *in vivo*. To identify the missing factor in the reconstitution that might promote coupling of both cycles, I focused on Rho GTPase effectors. Within the cellular context, Rho GTPases are embedded in a complex and extensive signaling network, composed of numerous effectors, which discriminate between the active and inactive states of Rho GTPases (Mosaddeghzadeh & Ahmadian, 2021). Besides this defining primary functionality, many Rho GTPase effectors frequently associate either directly or indirectly with other components of the plasma membrane (Bishop & Hall, 2000). Additionally, they often interact with more than one active Rho GTPase through multiple binding sites or by oligomerization (Meca et al., 2019). Hence, I hypothesized that these avidity-increasing properties might potentially facilitate preferential stabilization of active Rho GTPases on the membrane. To investigate this, I substituted the previously used activity sensor A488-wCRIB with a native but labeled version of the full-length protein, which has a polybasic stretch flanking the Cdc42-binding CRIB domain that is known to bind $PI(4,5)P_2$ lipids (Figure 15A). Full length N-WASP in contrast to wCRIB, is therefore endowed with one of the aforementioned membrane avidity-increasing features.

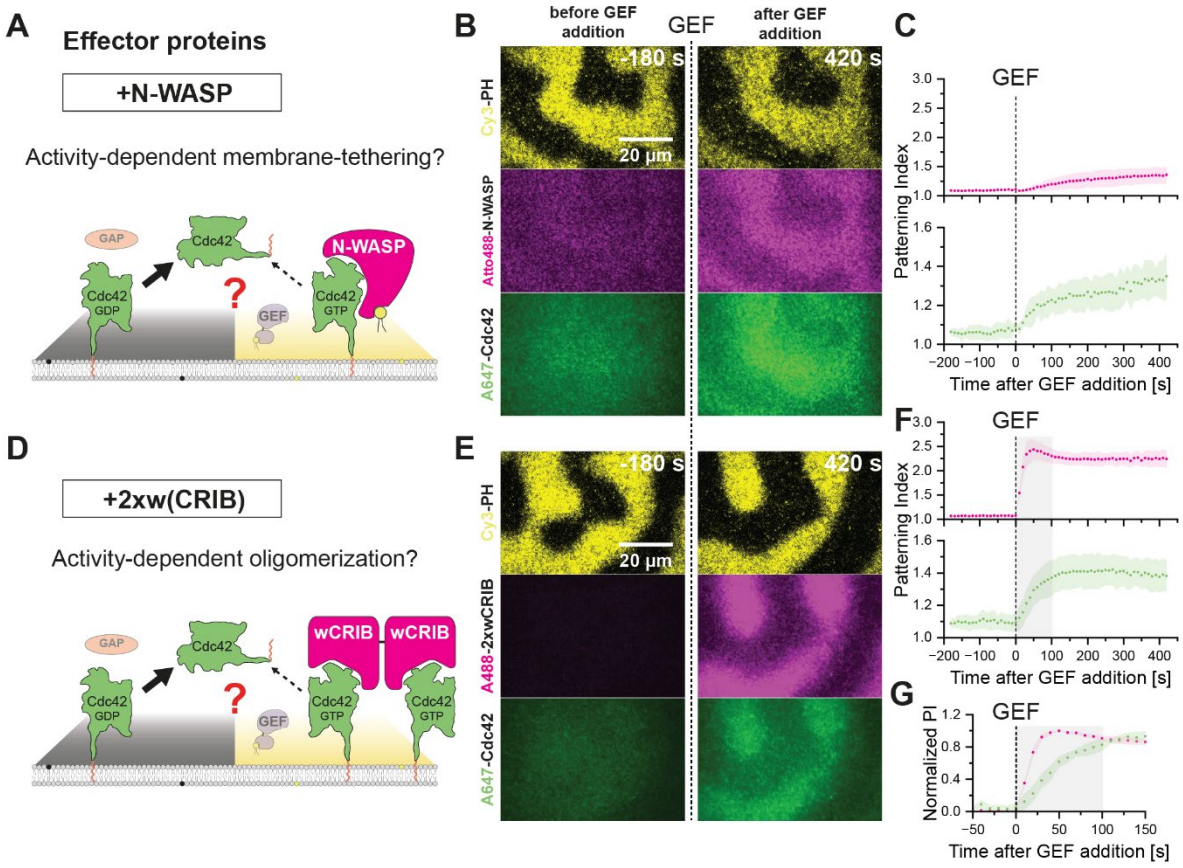

Figure 15: Effector proteins can enrich Rho GTPases at membrane sites of their activity. (**A**) Scheme or (**B**) time-lapse multi-color TIRFM images of the effects of full-length N-WASP on templated Rho GTPase activity patterns. Images of Cy3-PH (2 nM, yellow), Atto488-N-WASP (40 nM, magenta) and A647-Cdc42 (5.5 nM, green) on PIP patterns at indicated times before or after addition of ITSN$_{cat}$-PH (1 nM) at t = 0 s in the presence of OPHN1$_{cat}$ (20 nM). (**C**) Patterning indices (PI = <I_{In}> / <I_{Out}>) of Atto488-N-WASP (magenta) or A647-Cdc42 (green) under conditions as in (B) over time. (**D**) Scheme or (**E**) time-lapse multi-color TIRFM images of the effects of the synthetic dimerization mimic 2xwCRIB on templated Rho GTPase activity patterns. Conditions as in (A) with Atto488-N-WASP replaced by A488-2xwCRIB (20 nM, magenta). (**F**) corresponds to (C) under conditions as in (E). Additionally, the grey shaded box highlights the first 100 seconds after the addition of ITSN$_{cat}$-PH. (**G**) Normalized patterning indices of A488-2xwCRIB (magenta) or A647-Cdc42 (green) under conditions as in (E) over time with the grey shaded box highlighting the first 100 seconds after the addition of ITSN$_{cat}$-PH. All numeric data represent the mean from three independent experiments (symbols) ± SD (shaded areas) (N=3). All scale bars are 20 µm as indicated.

By introducing Atto488-N-WASP (20 nM), I was able to directly test the influence of a membrane-binding effector on the system. The new "activity" read-out Atto488-N-WASP does not only report the activity of Cdc42 because it also binds to negatively charged lipids. Hence, compared to previous experiments with wCRIB, both active and total Cdc42 levels on the membrane were increased prior to ITSN$_{cat}$-PH addition (Figure 15B). However, the increased total Cdc42 levels show the accumulation of Cdc42 on the membrane in the presence of a membrane-bound effector, albeit across the lipid bilayer (Figure 15B). As expected, the addition of ITSN$_{cat}$-PH induced activation of Cdc42 in GEF-

containing regions, indicated by an increase of the patterning index of N-WASP (Figure 15C). Strikingly, however, not only N-WASP but also Cdc42 concentrated in regions of its activation (PI ≈ 1.35, Figure 15C). Thus, membrane-bound effectors like N-WASP can locally concentrate active Rho GTPases on the membrane, likely by tethering them to the membrane. In summary, these findings indicate a potential role of Rho GTPase effectors in the enrichment of Rho GTPases at sites of their activity, ultimately enabling the coupling of the catalytic and spatial cycle essential for Rho GTPase patterning.

To test if the availability of multiple Rho GTPase binding sites is sufficient to elicit similar effects, I mimicked effector dimerization by covalently linking two CRIB domains of the Cdc42 effector WASP (2xwCRIB) with a flexible peptide of 19 amino acids. I used A488-2xwCRIB, a fluorescently labeled version, as an activity sensor instead of A488-wCRIB, but at a reduced concentration (20 nM), which retains the molarity of the binding domain (Figure 15D). Substitution of wCRIB by 2xwCRIB significantly improved the contrast of the activity signal (Figure 15E), which is in line with previous observations *in vivo* (Mahlandt et al., 2021). Consequently, the patterning index reached higher peak values (PI ≈ 2.4) compared to experiments in the presence of only monovalent A488-wCRIB (Figure 15F). More importantly, introduction of the dimeric effector resulted in a strong enrichment of Cdc42 in GEF-containing regions (PI ≈ 1.4, Figure 15F). Hence, multivalency of Rho GTPase effectors sufficiently increases the avidity of active Cdc42 toward membranes to induce enrichment at sites of their activity. Interestingly, as observed during single cell wounding experiments, the accumulation of total Cdc42 was slightly slower relative to Cdc42 activation in GEF-containing regions (Figure 15G).

To test if the combination of RhoGDI1 and Rho GTPase effectors potentially further enhance the accumulation of Rho GTPases on the membrane, I performed experiments in presence of both (Figure 16A). While Cdc42 enriched to similar levels as before (PI ≈ 1.4), the patterning index of the activity signal was slightly lower (PI ≈ 1.9) compared to equivalent experiments conducted in the absence of RhoGDI1 (Figure 16B).

Together, these results demonstrate the ability of effector proteins to enrich Rho GTPases like Cdc42 on the membrane at sites of their activity. Both membrane association and the presence of multiple binding sites contribute to the enrichment. Thus, the catalytic and spatial cycles of Rho GTPases can be linked by effector proteins displaying membrane avidity-increasing properties.

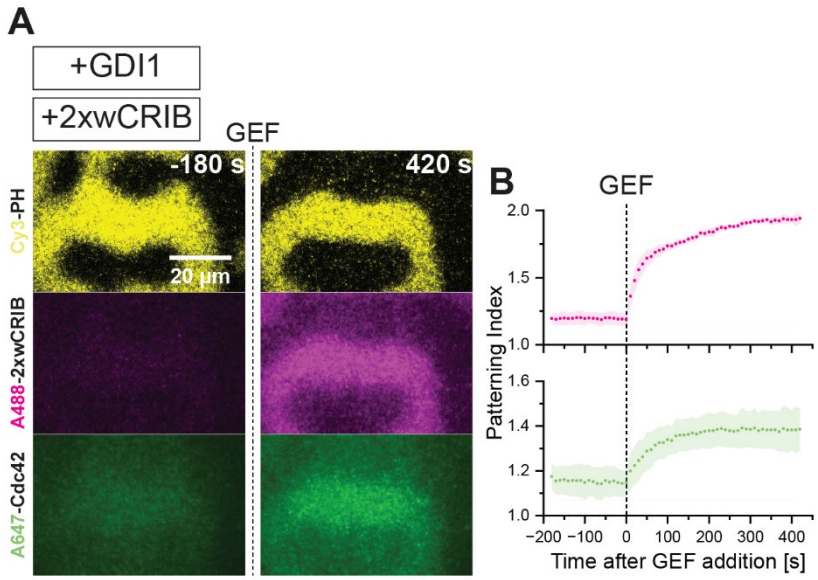

Figure 16: Dimerization mimic also enriches Rho GTPases at membrane sites of their activity in the presence of RhoGDI1. (**A**) Time-lapse multi-color TIRFM images of Cy3-PH (2 nM, yellow), A488-2xwCRIB (20 nM, magenta) and A647-Cdc42:RhoGDI1 complexes (600 nM, green) on PIP patterns at indicated times before or after addition of $ITSN_{cat}$-PH (1 nM) at t = 0 s. (**B**) Patterning index (full circle, $PI = \langle I_{In} \rangle / \langle I_{Out} \rangle$) of A488-2xwCRIB (magenta) and A647-Cdc42 over time. All numeric data represent the mean from three independent experiments (symbols) ± SD (shaded areas) (N=3). All scale bars are 20 µm as indicated.

The mechanism of Rho GTPase enrichment at sites of their activity

Because of the observation that Rho GTPase effectors concentrate active Rho GTPases on the membrane, I set out to obtain deeper insights into the underlying molecular mechanism. Specifically, I considered two mechanisms by which the accumulation could be achieved that were explored experimentally in the following sections: 1) The increase in the number of interactions of active Rho GTPases with the membrane mediated by Rho GTPase effectors could result in a decrease of their diffusion on the membrane. This would effectively trap them at sites of their activity (Figure 17A). 2) Alternatively, the additional interactions with the membrane might simply increase the dwell time of the active species, leading to their stabilization in GEF-rich regions (Figure 17B). These hypotheses are not mutually exclusive, and their effect could be synergistic.

To test the first hypothesis, I utilized single molecule TIRFM experiments enabling the direct measurement of the diffusion speed of Rho GTPases in GEF-containing and GEF-lacking areas. Visualization of single A647-Cdc42 molecules required a 100-fold decrease in the labeled fraction of Cdc42, while keeping overall concentrations identical (Figure 17C). Diffusion of Cdc42 was studied in the presence of labeled wCRIB, 2xwCRIB or N-WASP. According to my expectations, no difference in diffusion of Cdc42 in GEF-containing

and GEF-lacking regions of the membrane could be detected with only the simple wCRIB present (Figure 17D, E). Interestingly, both in the presence of 2xwCRIB and N-WASP, single molecules of Cdc42 moved slower in GEF-containing regions relative to GEF-lacking regions, as demonstrated by stepsize and MSD analysis (Figure 17D, E). N-WASP reduced overall diffusion also in regions devoid of GEF activity, which was in line with N-WASP weakly binding to membranes regardless of the PIP state in previous experiments. In conclusion, these results demonstrate that the diffusional trapping of active Rho GTPases contributes to their accumulation on the membrane.

To test the second hypothesis, I turned to microfluidic flow-out experiments allowing the study of effector-mediated membrane stabilization of Rho GTPases. Dissociation kinetics of A647-Cdc42 were studied inside and outside GEF-containing regions in the presence of either wCRIB or 2xwCRIB. Flow-out studies in the presence of N-WASP were not performed because of the prohibitively large quantities of protein required for these experiments. Extraction of Cdc42 was initiated with a flow-out buffer mix containing all the components present prior to flow onset, except A647-Cdc42 (see Methods: Cdc42 dwell time measurements). To accelerate dissociation of Cdc42, RhoGDI1 (22 nM) was included in the flow-out buffer mix. Both wCRIB and 2xwCRIB behaved similarly compared to previous patterning experiments, the former did not induce the accumulation of Cdc42 at sites of its activation while the latter did (Figure 17F). Interestingly, in the case of wCRIB, no differences in membrane retention of Cdc42 inside and outside GEF-containing regions were observed. In the presence of 2xwCRIB, membrane dwell times of Cdc42 were generally longer compared to when wCRIB was present. Strikingly, dwell times inside GEF-containing regions were significantly higher (~1.4x) relative to outside these regions (Figure 17G). Hence, the effector-mediated stabilization of Rho GTPases can contribute to the accumulation of Rho GTPases during pattern formation. I therefore concluded that both the reduction in diffusion as well as the increase in membrane stability of active Rho GTPases induced by Rho GTPase effectors likely contribute to the overall accumulation of Rho GTPases at sites of their activity.

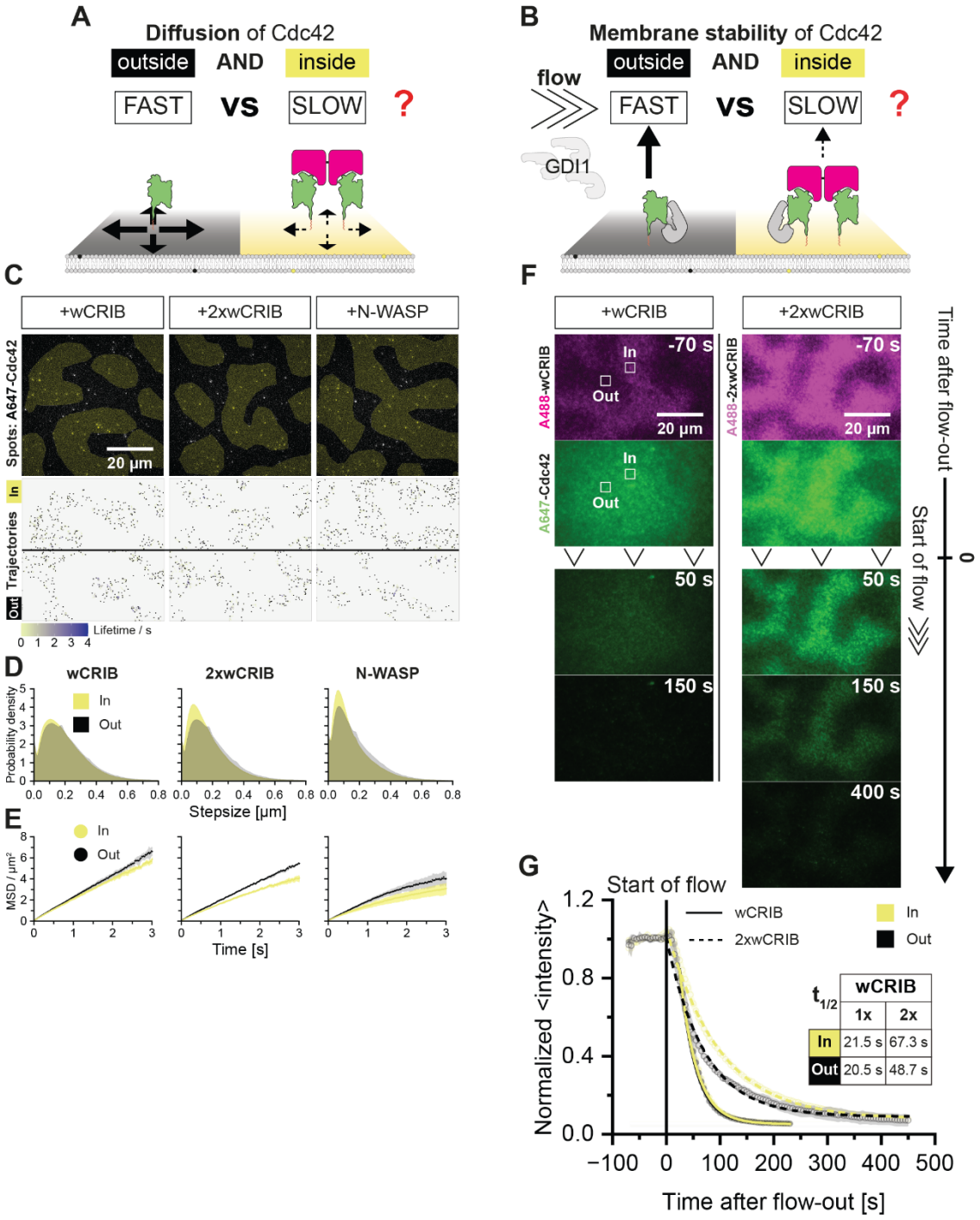

Figure 17: The mechanism of effector-driven Rho GTPase enrichment at membranes *in vitro*. (**A**) Scheme of effector-mediated changes in diffusivity or (**B**) membrane stability of Cdc42 as possible mechanisms of active Rho GTPase membrane enrichment. (**C**) Still images (top) and trajectories (bottom) of single A647-Cdc42 molecules (5.5 nM total, 55 pM labeled) on PIP-templated activity patterns either inside (yellow) or outside (black) of GEF-containing regions in the presence of either wCRIB, 2xwCRIB or N-WASP as indicated. (**D**) Stepsize distribution or (**E**) MSD over time of Cdc42 trajectories inside (yellow) and outside (black) GEF areas at conditions as indicated. (**F**) Time-lapse multi-color TIRFM images of PIP-templated Cdc42 activity patterns in the presence of A488-wCRIB or A488-2xwCRIB at indicated times before or after buffer flow-out at t = 0 s. *(Continued on the following page.)*

Figure 17: Flow-out buffer contained all proteins at the same concentrations before flow onset, except for A647-Cdc42 that was omitted, and additional free RhoGDI1 (22 nM) to accelerate Cdc42 membrane dissociation. White boxes (4.1 µm x 4.1 µm) indicating ROIs used for analysis. (**G**) Normalized average intensities of A647-Cdc42 inside (yellow) or outside (black) GEF-containing areas as a function of time after buffer wash-out in the presence of either A488-wCRIB (solid lines) or A488-2xwCRIB (dashed lines). Half-times were obtained by mono-exponential fits to the data. All numeric data represent the mean from three independent experiments (symbols) ± SD (shaded areas) (N=3). All scale bars are 20 µm as indicated.

While I have shown the effector-mediated accumulation of Rho GTPases at sites of their activity which is based on an increase in membrane retention of active Rho GTPases, all these experiments uncovering this mechanism were performed *in vitro*. To test whether the activation of Rho GTPases also increases their membrane retention *in vivo*, our collaborators introduced Cdc42, internally tagged with photoactivatable GFP (IT-PA-GFP-Cdc42)(Patterson & Lippincott-Schwartz, 2002), to the single cell wound healing experiments in *Xenopus laevis* oocytes. By determining the half-time to disappearance of IT-PA-GFP-Cdc42 after photoactivation at different times and in different regions during wounding, the retention of Cdc42 can be evaluated (Figure 18A). Membrane retention of Cdc42 increased in regions around the wound compared to regions outside the wound or prior to wounding, as indicated by an increased half-time to disappearance (Figure 18B-K). Furthermore, the membrane retention of active Cdc42 at the wound edge progressively increased over time (Figure 18L).

However, the observed increase in membrane retention of active Cdc42 near the wound edge could be caused by other cellular processes initiated at the onset of wounding, such as the *de novo* synthesis of phosphoinositide lipids around the wound (Vaughan et al., 2014). To directly correlate GEF-mediated activation of Rho GTPases to an increase in their membrane retention, a chimeric construct consisting of the C2 domain of protein kinase Cβ fused to the catalytic domain of intersectin (C2-Itsn-CAT-BFP) was generated. C2-fusions have been shown to accumulate around wounds (Moe et al., 2021). At the onset of wounding, both the activity sensor wCRIB and the GEF fusion protein rapidly accumulated around the wound to levels greater than the levels observed in the control (compare Figure 18M and Figure 18P). The recruitment of the GEF fusion protein drastically increased membrane retention of Cdc42 around the wound as indicated by the increased half-time to disappearance (Figure 18M-T), thus confirming that the GEF-mediated activation of Cdc42 affects their membrane retention *in vivo*.

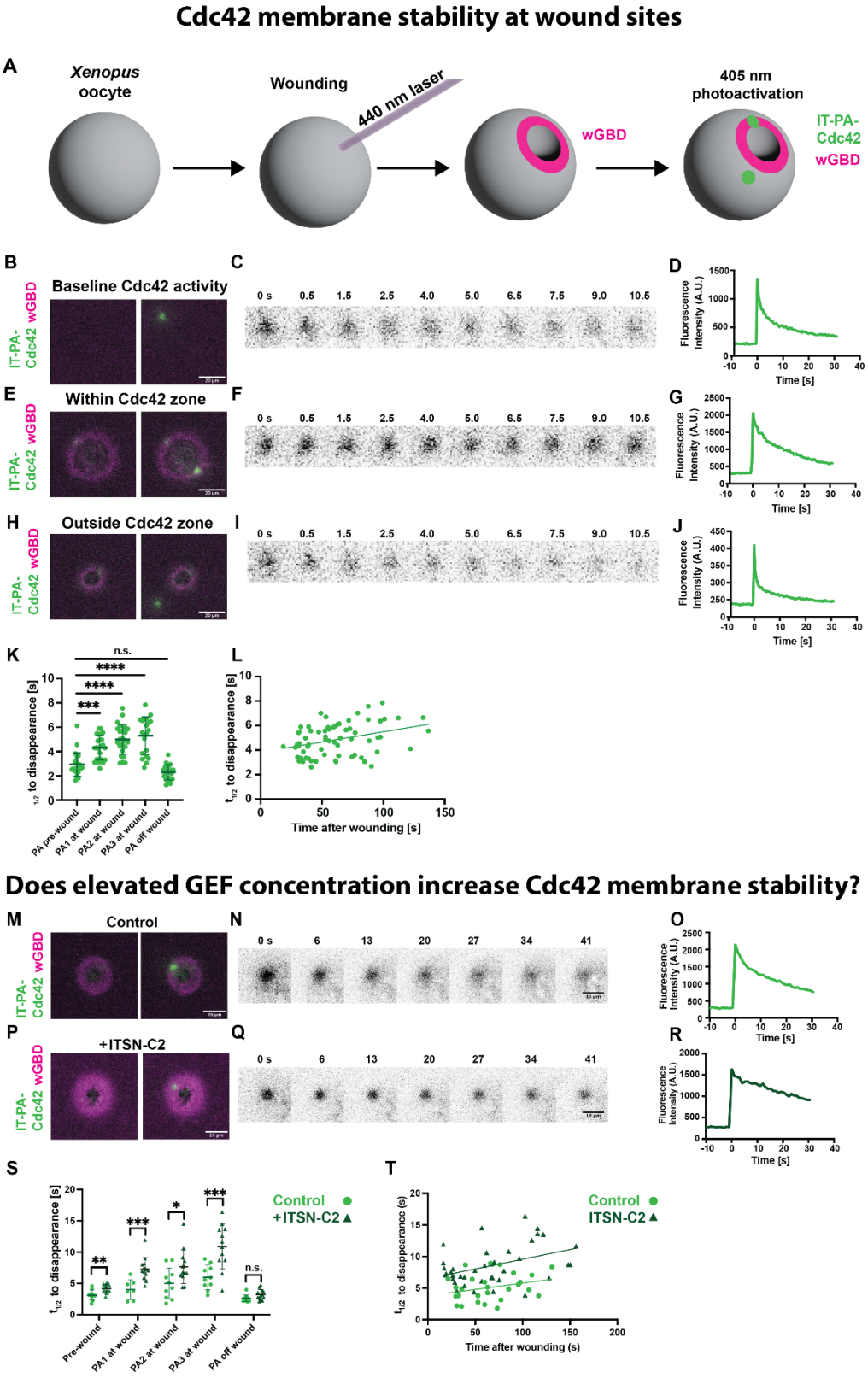

Figure 18: Cdc42 activation increases membrane dwell time *in vivo*. (**A**) Scheme showing photoactivation of IT-PA-Cdc42 inside and outside of increased Cdc42 activity around a wound. (**B**) Representative image of baseline Cdc42 activity (wGBD) before (left) and immediately after (right) photoactivation of IT-PA-Cdc42. *(Continued on the following page.)*

Figure 18: (**C**) Montage of IT-PA-Cdc42 from (B) showing disappearance over time. (**D**) IT-PA-Cdc42 fluorescence intensity from (B) over time after photoactivation. (**E-G**) Micrograph, montage, and plot of IT-PA-Cdc42 photoactivation within the Cdc42 activity zone around a wound. (**H-J**) Micrograph, montage, and plot of IT-PA-Cdc42 photoactivation outside the Cdc42 activity zone around a wound. (**K**) Plot of the t1/2 to disappearance of IT-PA-Cdc42 prior to wounding (PA pre-wound) within the Cdc42 zone for the earliest photoactivation (PA1), within the Cdc42 zone for a later photoactivation (PA2), within the Cdc42 zone for the latest photoactivation (PA3), and outside the Cdc42 zone (PA off wound). One way ANOVA with Dunnett comparison was used to determine significance; ***p<0.001, ****p<0.0001. (**L**) Positive correlation between t1/2 to disappearance of photoactivation within the Cdc42 zone and time after wounding (p = 0.0043). (**M-O**) Micrograph, montage, and plot of IT-PA-Cdc42 photoactivation within the Cdc42 activity zone around a wound. (**P-R**) Micrograph, montage, and plot of IT-PA-Cdc42 photoactivation within the Cdc42 activity zone with ITSN-C2 mediated increased Cdc42 activity. (**S**) Plot comparing the t1/2 to disappearance of IT-PA-Cdc42 in control and ITSN-C2 conditions prior to wounding (Pre-wound) within the Cdc42 zone for the earliest photoactivation (PA1), within the Cdc42 zone for a later photoactivation (PA2), within the Cdc42 zone for the latest photoactivation (PA3), and outside the Cdc42 zone in wounded cells (PA off wound). Two-sample t-tests were used to determine significance; *p<0.05, **p<0.01, ***p<0.001. (**T**) Correlations between t1/2 to disappearance of photoactivation within the Cdc42 zone and time after wounding for control (p = 0.1523) and ITSN-C2 (p = 0.0106) conditions. All experiments were performed by Lila Hoachlander-Hobby in the laboratory of Prof. William Bement.

In this first part of my thesis, I demonstrated that Rho GTPases concentrate at sites where they are activated *in vivo*. Reconstitution uncovered the relevance of Rho GTPase effectors during Rho GTPase patterning. I specifically found that membrane avidity-increasing properties, like membrane association and multivalency, of Rho GTPase effectors facilitate Rho GTPase retention through a combination of diffusional trapping and an increase in membrane stability.

Self-organization of Rho GTPase activity based on linear feedback

A synthetic polarizing Rho GTPase system – Network topology

The reconstitution in the previous section of my thesis was based on templated Rho GTPase activity patterns. Relying on such a spatial template allowed for the identification of biochemical factors responsible for the coupling of the catalytic and spatial cycle of Rho GTPases. However, polarization of Rho GTPase activity in various processes *in vivo* appears to not always require a template (Bement et al., 2024). Although Rho GTPases are often thought of as simple switches, where the active state propagates a signal and the inactive state causes signal termination, the regulation of their activity in both space and time is quite complex. Based on activity-dependent feedback, symmetry of Rho GTPase activity can spontaneously be broken on membranes. This is most prominently observed and best studied during budding in yeast (Howell et al., 2009; Chiou et al., 2017) but also found during cellular processes like cytokinesis (Bischof et al., 2017). This activity-dependent feedback is often facilitated by catalytic regulators themselves, namely GEFs and GAPs (Bement et al., 2024). Despite being extensively investigated, the vast and complex regulatory network of Rho GTPases poses a challenge in identifying a precise molecular mechanism for Rho GTPase polarization. Thus, I pursued the realization of a minimal synthetic Rho GTPase signaling system that can achieve autonomous polarization of Rho GTPase activities. My preliminary work on this subject is summarized in the following section of my thesis.

To achieve the segregation of Rho GTPase activities based on feedback, multiple requirements for the network topology had to be met for a biochemically feasible reconstitution *in vitro*. There are numerous feedback schemes of dynamical systems, which have been proposed to allow for spontaneous symmetry breaking. For example, a bistable system which has two stable steady states could have a state of high RhoA/low Cdc42 activity and vice versa (Jilkine et al., 2007). However, a system of this nature would require non-linear, cooperative feedback terms. While this can in principle be achieved biochemically through allosteric regulation, the engineering of such allosteric regulation would be challenging. Additionally, over time a bistable system would settle in one of its two stable steady states, leading again to a homogenous distribution of Rho GTPase activity. At the beginning of this project, our collaborator (A. Koseska, MPI Bonn) proposed

a topology based on linear feedback alone, which should circumvent these problems in theory. This specific topology consists of two main modules, on the one side a positive feedback circuit between Rac1 and Cdc42 and on the other side a toggle-switch topology between RhoA and Rac1. The latter module is extended by the negative regulation of Cdc42 through RhoA, allowing the introduction of asymmetry in the negative feedback, which is required for a stable polarized state of Rho GTPase activity (Figure 19). Since linear feedback can be realized by biochemical approaches based on simple direct recruitment, I decided to use this topology as a basis for the *in vitro* reconstitution of synthetic self-organizing Rho GTPase activity patterns.

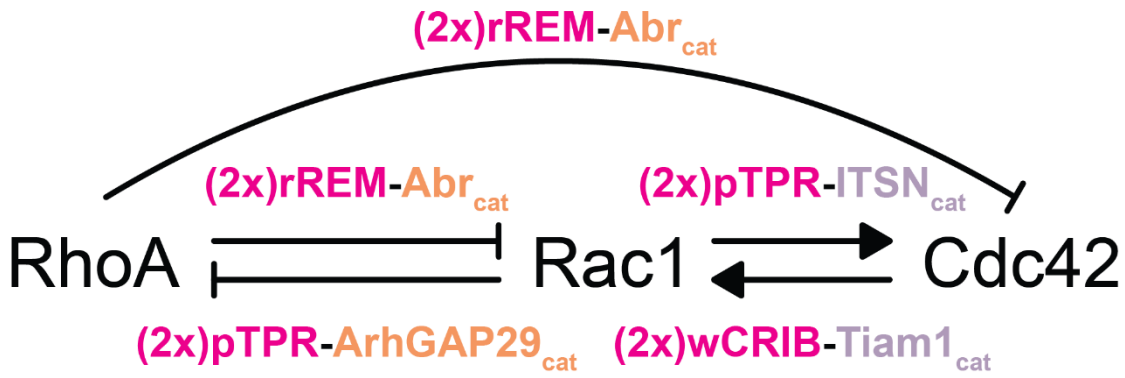

Figure 19: Network topology of a synthetic polarizing Rho GTPase system. A system based on this network topology is theoretically able to spontaneously break symmetry of Rho GTPase activity based on linear feedback between active RhoA, Rac1 and Cdc42. Chimeras consisting of a Rho GTPase binding domain (GBD, magenta) and either the catalytically active domain of a GAP (orange) or a GEF (purple) that facilitate the respective feedback links are shown.

For the biochemical implementation of linear feedback in our system, I required molecules endowed with two main features, 1) the ability to be recruited by specific active Rho GTPases, and 2) once recruited, the ability to modulate activity of other Rho GTPases. While the former can be achieved by Rho GTPase binding domains, the latter requires the catalytic domain of either a GAP for inactivation (negative feedback) or a GEF for activation (positive feedback). Hence, I designed artificial chimeric proteins of a Rho GTPase binding domain linked to the catalytic domain of either a GAP or a GEF, which I called GBD-GAP or GBD-GEF chimeras respectively.

Besides these feedback links the system relies on greatly different diffusion speeds of active and inactive Rho GTPases. While the usage of a supported lipid bilayer as a platform for the reconstitution theoretically provides compartments with varying diffusion speeds, it does not inherently result in activity-dependent partitioning of Rho GTPases between solution and membrane. To achieve this, a third feature was required for the chimeras,

3) the ability to couple the catalytic and spatial cycle of Rho GTPases. Based on the findings from the first part of my thesis, this can be achieved by using Rho GTPase binding domains of increased valency. Because of this, I fused a second binding domain to each chimera resulting in the 2xGBD-GAP/GEF chimera variants later on in the project.

Each chimera had to be specific for certain Rho GTPases to be able to facilitate the exact feedback links of the proposed network topology (Figure 19). Recruitment to specific active Rho GTPases was facilitated by the respective Rho GTPase binding domains of Rhotekin (rREM), known to be specific for RhoA (Blumenstein & Ahmadian, 2004), p67phox (pTPR), which is specific for Rac1 (Lapouge et al., 2000) and WASP (wCRIB) that specifically binds to Cdc42 (Rudolph et al., 1998). For the biochemical implementation of the Rho GTPase inactivation, I focused on the catalytic domain of GAPs, which have been proposed to be specific for either RhoA or Cdc42/Rac1, namely, ArhGAP29$_{cat}$ (Saras et al., 1997) or Abr$_{cat}$ (Amin et al., 2016) respectively. For GEF-mediated activation, I utilized the catalytic domain of GEFs known to be specific for either Rac1 or Cdc42, namely, Tiam1$_{cat}$ (Müller et al., 2020) or ITSN$_{cat}$ (Hussain et al., 2001) respectively. Importantly, feedback strength scales with the chimera concentration, allowing for simple adjustments in the reconstitution. However, the asymmetry in negative feedback is not scalable since it is achieved by only one chimera.

In conclusion, the four 2xGBD-GAP/GEF chimeras, namely, 2xrREM-Abr$_{cat}$, 2xpTPR-ArhGAP29$_{cat}$, 2xpTPR-ITSN$_{cat}$ and 2xwCRIB-Tiam1$_{cat}$ should in theory be sufficient to facilitate all feedback links of the proposed network topology. Together with an activity-dependent slowdown and retention of active Rho GTPases on the membrane, these chimeras should be able to induce stable self-organizing Rho GTPase activity patterns

Characterization of chimeras facilitating feedback

To validate whether each chimera possesses the desired properties, their binding domains as well as catalytic domains were first tested biochemically. While the 2x variants of the chimeras are ultimately required to couple the catalytic and spatial cycle of Rho GTPases, the monovalent versions should behave similarly concerning the specificity of both binding and catalytic activity. Because I generated the monovalent chimeras first, most of the characterization was performed with them.

Negative feedback

For the double negative feedback circuit, I required 2xrREM-Abr$_{cat}$ and 2xpTPR-ArhGAP29$_{cat}$. It is essential that the former chimera binds to active RhoA and not Cdc42/Rac1, while being able to inactivate Cdc42 and Rac1, but not RhoA. Furthermore, the GAP kinetics for Cdc42 and Rac1 should be different, to introduce kinetic asymmetry in inactivation. To assess the binding of the rREM-containing chimeras, I coated thiol beads with RhoAQ63L, a constitutively active variant of the Rho GTPase. Using a fluorescently labeled chimera (A488-rREM-Abr$_{cat}$) allowed for the visualization of chimera binding to RhoAQ63L-coated beads (Figure 20A). Beads coated with dCherry as a mock protein served as a control (see Methods: Bead assays). Widefield microscopy revealed a strong association of A488-rREM-Abr$_{cat}$ with RhoAQ63L-coated beads compared to control beads, indicated by an increase in fluorescence intensity (Figure 20B). This observation was confirmed by the quantification of the average fluorescence intensity per bead (Figure 20C). Hence, (2x)rREM-Abr$_{cat}$ chimeras can bind active RhoA.
To evaluate the catalytic activity of Abr$_{cat}$ chimeras, I utilized the previously established GTP hydrolysis sensors, Cy3- and TAMRA-GTP (Eberth et al., 2005; Amin et al., 2016). These fluorescent nucleotide analogs are sensitive toward changes in their local environment, resulting in altered photophysical properties upon, for example, hydrolysis-induced conformational changes of Rho GTPases. Hence, Rho GTPase-bound Cy3-GTP (RhoA) or TAMRA-GTP (Cdc42 and Rac1) allow monitoring of GTP hydrolysis kinetics, by following loss of fluorescence over time. While Rho GTPases possess an intrinsic hydrolysis rate (Supplementary figure 1, reanalyzed raw data from Weiß, Master thesis, TU Dortmund, 2021), the presence of Abr$_{cat}$ chimeras should significantly accelerate their hydrolysis rates, if the chimera is catalytically active for the specific Rho GTPase (Figure 20D). Thus, I performed titration experiments of rREM-Abr$_{cat}$ to identify its catalytic efficiencies for RhoA, Rac1 and Cdc42 (reanalyzed raw data from Weiß, Master thesis, TU Dortmund, 2021). Both the hydrolysis rates of Cdc42 and Rac1 rose with increasing amounts of rREM-Abr$_{cat}$, while GTP hydrolysis by RhoA was only slightly affected by the chimera (Figure 20E-G). To determine catalytic efficiencies of rREM-Abr$_{cat}$, I plotted the observed rates, acquired through a mono-exponential fit of the data from the titration experiments, vs the chimera concentration and fitted the data with a linear function (Figure 20H). Remarkably, comparison of the catalytic efficiencies of rREM-Abr$_{cat}$ revealed

a 2.2-fold higher catalytic efficiency for Rac1 relative to Cdc42, while being negligible for RhoA (Figure 20I).

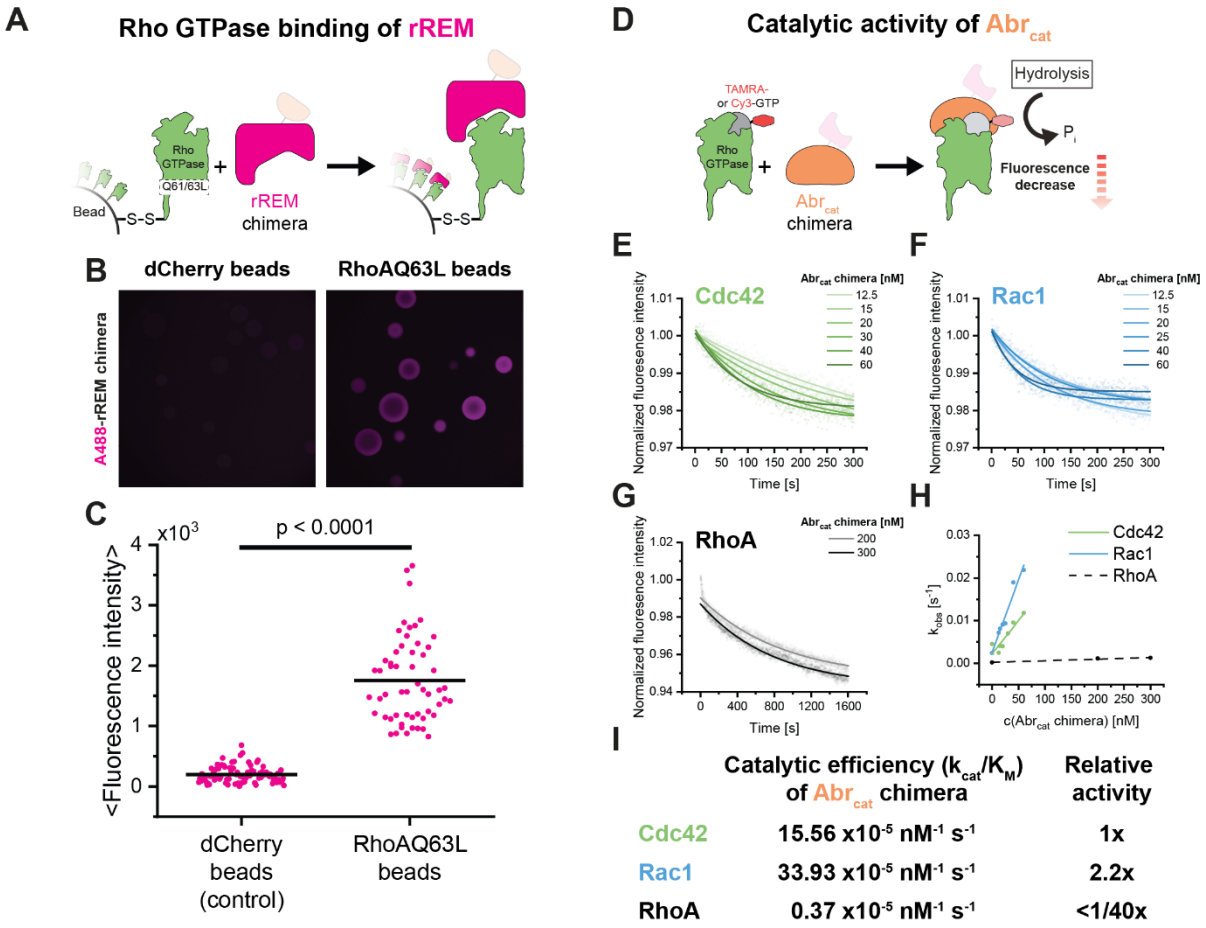

Figure 20: Characterization of the domains of the GBD-GAP chimera rREM-Abr$_{cat}$. (**A**) Scheme of the chimera rREM-Abr$_{cat}$ binding to thiol beads coated with an active variant (point mutation: Q61/63L) of a Rho GTPase. (**B**) Widefield images of thiol beads coated with dCherry (left, control) or RhoAQ63L (right) and incubated with 800 nM of A488-rREM-Abr$_{cat}$ (magenta). (**C**) Quantification of the average fluorescence intensity per bead (dCherry beads: n = 86, RhoAQ63L beads: n = 56). A Mann-Whitney-U-test was used to determine statistical significance; $p < 0.0001$. (**D**) Scheme of Rho GTPase activity assays in the presence of the chimera rREM-Abr$_{cat}$. Rho GTPases were loaded with either TAMRA-GTP (Cdc42, Rac1) or Cy3-GTP (RhoA). Normalized fluorescence intensities of (**E**) TAMRA-GTP:Cdc42 (green, 100 nM), (**F**) TAMRA-GTP:Rac1 (blue, 100 nM) or (**G**) Cy3-GTP:RhoA (black, 100 nM) as a function of time in the presence of varying amounts of the chimera rREM-Abr$_{cat}$. Observed rate constants were obtained by mono-exponential fits of the data and (**H**) plotted as a function of rREM-Abr$_{cat}$ concentration with the intrinsic hydrolysis rate of each Rho GTPase used at c(Chimera) = 0 nM. (**I**) Catalytic efficiencies of rREM-Abr$_{cat}$ for each Rho GTPase were determined by linear fits of the data. Raw data for the characterization of the catalytic domain (Weiß, Master thesis, TU Dortmund, 2021) was reanalyzed.

In conclusion, while binding was only confirmed for active RhoA, requiring further evaluation of the binding specificity of (2x)rREM-Abr$_{cat}$, its catalytic activity showed the necessary specificity, including asymmetry in the inactivation of Rac1 and Cdc42. Thus,

preliminary characterization of (2x)rREM-Abr$_{cat}$ indicated the suitability of this chimera to facilitate its desired feedback links.

The second negative feedback link of the toggle switch will be carried out by a second chimera, 2xpTPR-ArhGAP29$_{cat}$, that can bind to active Rac1 and inactivate RhoA. To assess the binding of pTPR chimeras, I performed microscale thermophoresis (MST) experiments with the isolated binding domain pTPR. Specifically, I used a fluorescently labeled and constitutively active version of Rac1 (A647-Rac1Q61L) together with varying amounts of pTPR to set up multiple ligand-binding reactions. The formation of a pTPR:A647-Rac1Q61L complex slows the movement of the Rho GTPase along a temperature gradient and thus, fluorescence is retained for a longer period of time in the detection area with increasing amounts of the ligand (Figure 21A).

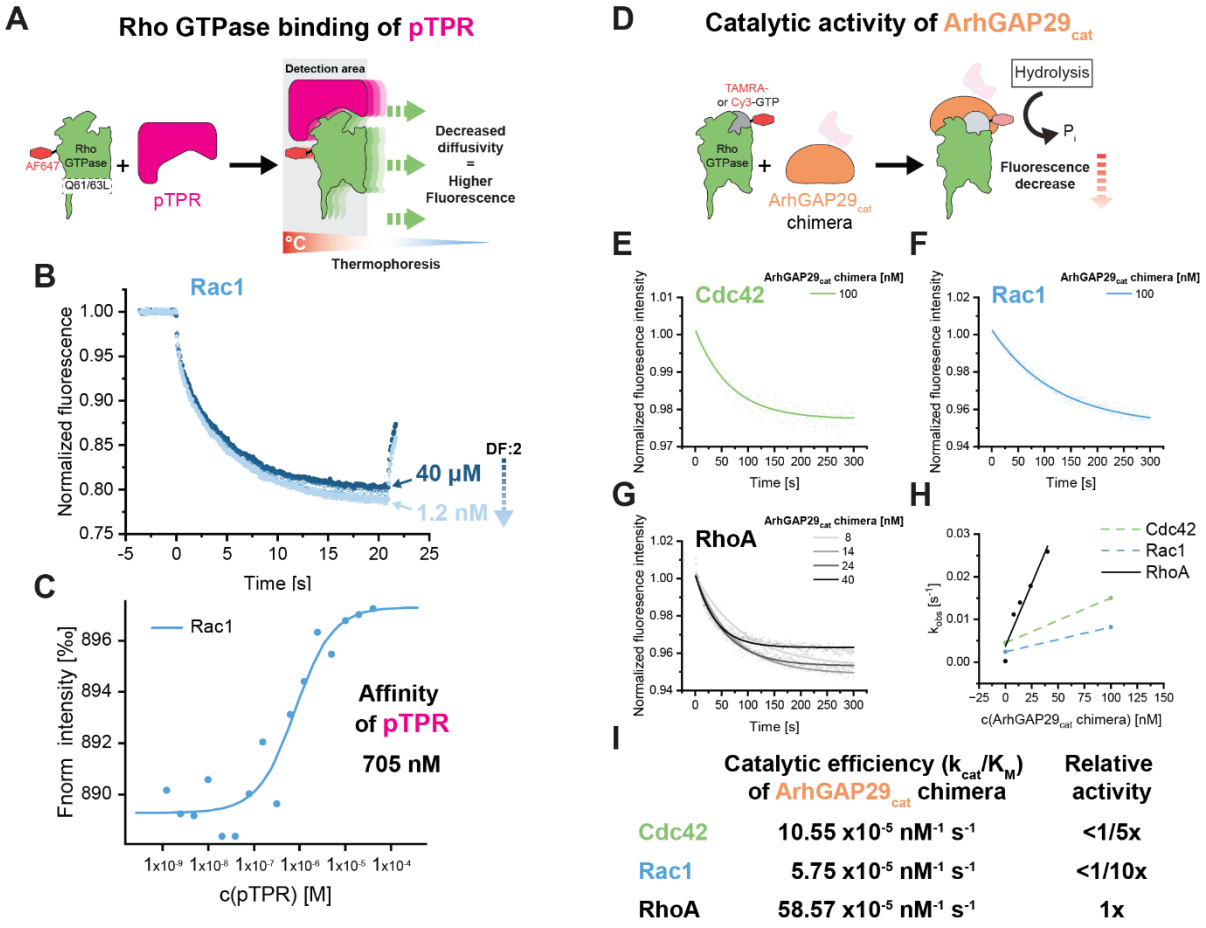

Figure 21: Characterization of the domains of the GBD-GAP chimera pTPR-ArhGAP29$_{cat}$. (**A**) Scheme of the binding domain pTPR binding to an active variant (point mutation: Q61/63L) of a Rho GTPase resulting in slower diffusion along a temperature gradient. The decrease in diffusivity can be utilized in microscale thermophoresis experiments by measuring fluorescence in a specific detection area which is simultaneously heated. (**B**) Normalized fluorescence of AF647-Rac1Q61L (blue) as a function of time in the presence of varying amounts of the binding domain pTPR (serial dilution: 40 µM to ~1.2 nM, dilution factor = 2). *(Continued on the following page.)*

Figure 21: (**C**) MST data analysis was performed with the NT Analysis software from NanoTemper yielding the affinity of pTPR for Rac1Q61L using a K_d fit for the titration data. (**D**) Scheme of Rho GTPase activity assays in the presence of an ArhGAP29$_{cat}$ chimera (p2CRIB-ArhGAP29$_{cat}$). Rho GTPases were loaded with either TAMRA-GTP (Cdc42, Rac1) or Cy3-GTP (RhoA). Normalized fluorescence intensities of (**E**) TAMRA-GTP:Cdc42 (green, 100 nM), (**F**) TAMRA-GTP:Rac1 (blue, 100 nM) or (**G**) Cy3-GTP:RhoA (black, 100 nM) as a function of time in the presence of varying amounts of an ArhGAP29$_{cat}$ chimera (p2CRIB-ArhGAP29$_{cat}$). Observed rate constants were obtained by mono-exponential fits of the data and (**H**) plotted as a function of the concentration of an ArhGAP29$_{cat}$ chimera (ArhGAP29$_{cat}$ -p2CRIB) with the intrinsic hydrolysis rate of each Rho GTPase used at c(Chimera) = 0 nM. (**I**) Catalytic efficiencies of an ArhGAP29$_{cat}$ chimera (p2CRIB-ArhGAP29$_{cat}$) for each Rho GTPase were determined by linear fits of the data.

As anticipated, increasing amounts of pTPR led to a decelerated loss in fluorescence intensity (Figure 21B). To determine the binding affinity of pTPR for active Rac1, I analyzed the MST curves with the NT Analysis software from NanoTemper (Figure 21C). The Rho GTPase binding domain pTPR binds active Rac1 with sub-micromolar affinity (K_D = 705 nM). Although only performed with the isolated pTPR, these results suggest that (2x)pTPR-ArhGAP29$_{cat}$ chimeras are likely to bind active Rac1.

To evaluate the catalytic activity of ArhGAP29$_{cat}$ chimeras, I performed similar GTP hydrolysis assays as I did for Abr$_{cat}$ chimeras (Figure 21D). While GTP hydrolysis accelerated for RhoA already at low concentrations of the ArhGAP29$_{cat}$ chimera (p2CRIB-ArhGAP29$_{cat}$), an increase in the hydrolysis rate of Cdc42 and Rac1, compared to their intrinsic rates, occurred only at moderate chimera concentrations (Figure 21E-G). Comparison of the catalytic efficiencies of the ArhGAP29$_{cat}$ chimera showed a strong preference for RhoA inactivation (Figure 21I).

In summary, the domains of 2xrREM-Abr$_{cat}$ and 2xpTPR-ArhGAP29$_{cat}$ generally show the features necessary to biochemically realize the double negative feedback circuit. However, further evaluation of the catalytic efficiencies of (2x)pTPR-ArhGAP29$_{cat}$ is required.

Positive feedback

The positive feedback circuit of the proposed network topology consists of 2xpTPR-ITSN$_{cat}$ and 2xwCRIB-Tiam1$_{cat}$. The former chimera needs to bind active Rac1 and activate Cdc42. Since the binding domain of pTPR chimeras was already confirmed to bind active Rac1 (Figure 22A), only the catalytic activity of ITSN$_{cat}$ chimeras had to be studied. To that end, I turned to GEF activity assays relying on Cdc42 complexed with mant-GDP. The emission intensity of mant-GDP is significantly higher (~2x) when it interacts with GTPases (John et al., 1990). Thus, in the presence of excess unlabeled GTP and ITSN$_{cat}$ chimeras, nucleotide exchange can be monitored over time by a loss in fluorescence (Figure 22B). Increasing the concentration of pTPR-ITSN$_{cat}$ led to a monotonic increase in the nucleotide exchange rates for Cdc42, which were determined by mono-exponential fits to the time courses (Figure 22C). The ITSN$_{cat}$ chimera displayed strong GEF activity for Cdc42, indicated by the high catalytic efficiency (Figure 22D).

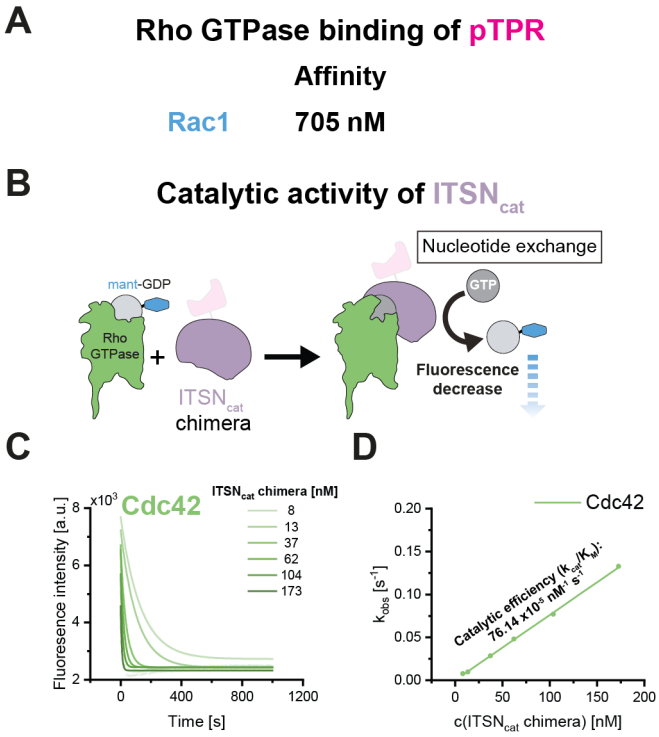

Figure 22: Characterization of the domains of the GBD-GEF chimera pTPR-ITSN$_{cat}$. (**A**) Binding affinity for Rac1 as previously determined for the binding domain pTPR. (**B**) Scheme of nucleotide exchange assays from mant-GDP:Rho GTPase complexes in the presence of the chimera pTPR-ITSN$_{cat}$. (**C**) Fluorescence intensities of mant-GDP:Cdc42 (green, 100 nM) as a function of time in the presence of varying amounts of the chimera pTPR-ITSN$_{cat}$ and excess unlabeled GTP (200 µM). Observed rate constants were obtained by mono-exponential fits of the data and (**D**) plotted as a function of pTPR-ITSN$_{cat}$ concentration to determine its catalytic efficiency for Cdc42 by a linear fit of the data.

These preliminary results suggest that (2x)pTPR-ITSN$_{cat}$ is equipped with the required features to facilitate one part of the positive feedback circuit in the network topology.

The final chimeric protein required for the complete biochemical network, is 2xwCRIB-Tiam1$_{cat}$. This chimera must bind active Cdc42 and activate Rac1. To assess the binding of wCRIB chimeras to Rho GTPases, I again utilized nucleotides labeled with mant and took advantage of the fact that effector binding inhibits nucleotide dissociation (Herrmann et al., 1995). However, I had to ensure that the Rho GTPase is continuously in its active conformation to allow the formation of an effector:Rho GTPase complex. Thus, I loaded Cdc42 with mant-GppNHp, the non-hydrolyzable variant of mant-GTP. Together with excess unlabeled GppNHp and varying amounts of wCRIB-Tiam1$_{cat}$, the effector domain-induced inhibition of spontaneous nucleotide exchange can be observed over time (Figure 23A). Since the spontaneous exchange of nucleotides in Rho GTPases is rather slow, experiments were conducted over several hours. With increasing amounts of the wCRIB chimera, nucleotide exchange rates drastically decreased, indicated by the mono exponential fits of the data (Figure 23B). To obtain the affinity, observed exchange rates were plotted vs the chimera concentration and fitted with a hyperbolic function (see Methods: Data analysis). Despite a dissociation constant that was lower than expected (K_D = 10.6 µM), binding of wCRIB chimera to Cdc42 was clearly detected (Figure 23C). Hence, binding of (2x)wCRIB-Tiam1$_{cat}$ to active Cdc42 is attainable.

To evaluate the catalytic activity of Tiam1$_{cat}$ chimeras, I conducted similar GEF assays as previously done for ITSN$_{cat}$ chimeras (Figure 23D). In the presence of wCRIB-Tiam1$_{cat}$, nucleotide exchange of GDP-mant in complex with Rac1 is accelerated (Figure 23E). The catalytic efficiency of Tiam1$_{cat}$ chimeras for Rac1 is significantly lower (27-fold) than the catalytic efficiency of ITSN$_{cat}$ chimeras for Cdc42 (compare Figure 23F and 22D). While the catalytic strength directly translates into the feedback strength, it is not much of concern since the feedback strength can be simply modulated by chimera concentration. Thus, (2x)wCRIB-Tiam1$_{cat}$ is endowed with the features that allow the realization of its corresponding feedback link.

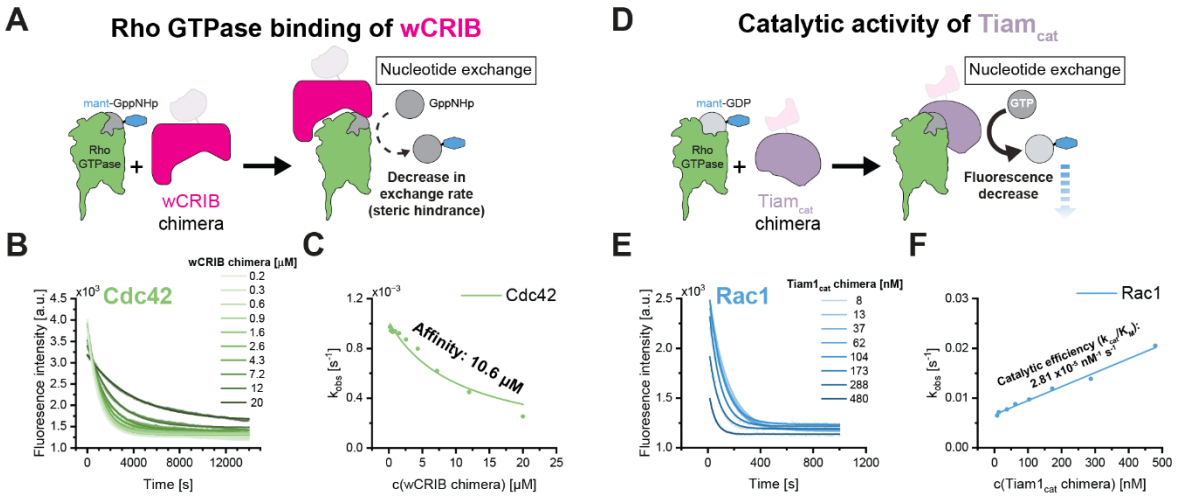

Figure 23: Characterization of the domains of the GBD-GEF chimera wCRIB-Tiam$_{cat}$. (**A**) Scheme of nucleotide exchange assays from mant-GppNHp:Rho GTPase complexes in the presence of the chimera wCRIB-Tiam1$_{cat}$. Binding of the wCRIB domain to the Rho GTPase sterically hinders the spontaneous nucleotide exchange leading to a slower loss of fluorescence. (**B**) Fluorescence intensities of mant-GppNHp:Cdc42 (green, 100 nM) as a function of time in the presence of varying amounts of the chimera wCRIB-Tiam1$_{cat}$ and excess unlabeled GppNHp (200 µM). Observed rate constants were obtained by mono-exponential fits of the data and (**C**) plotted as a function of wCRIB-Tiam1$_{cat}$ concentration to determine its catalytic efficiency for Rac1 by a hyperbolic K_d fit of the data. (**D**) Scheme of nucleotide exchange assays from mant-GDP:Rho GTPase complexes in the presence of the chimera wCRIB-Tiam1$_{cat}$. (**E**) Fluorescence intensities of mant-GDP:Rac1 (blue, 100 nM) as a function of time in the presence of varying amounts of the chimera wCRIB-Tiam1$_{cat}$ and excess unlabeled GTP (200 µM). Observed rate constants were obtained by mono-exponential fits of the data and (**F**) plotted as a function of wCRIB-Tiam1$_{cat}$ concentration to determine its catalytic efficiency for Rac1 by a linear fit of the data.

Together the initial results presented in this section of my thesis show the feasibility of the biochemical realization of Rho GTPase feedback through rationally designed GBD-GAP/GEF chimeras. In conclusion, these findings suggest that 2xrREM-Abr$_{cat}$, 2xpTPR-ArhGAP29$_{cat}$, 2xpTPR-ITSN$_{cat}$ and 2xwCRIB-Tiam1$_{cat}$ display the desired properties required to biochemically carry out the feedback links of the initially designed network topology, which should be capable of inducing spontaneous and stable polarization of Rho GTPase activity. This work can therefore be used as a starting point for further characterizations of the chimeras based on the assays introduced here and for their full implementation in the minimal synthetic Rho GTPase signaling system.

Discussion and Conclusion

The catalytic and spatial cycles of Rho GTPases can be coupled by effector proteins

Despite the essential role of Rho GTPase activity patterns in numerous biological processes, a comprehensive understanding of the underlying molecular processes that drive their formation has remained elusive. The findings outlined in the first section of my thesis have uncovered some of the main biochemical principles by which the catalytic and spatial cycles of Rho GTPases are coupled and, in doing so, revealed how these proteins concentrate at sites where they are being activated. This coupling is achieved through the effector-mediated stabilization of active Rho GTPases on the membrane, which relies on an increased avidity in membrane binding. This stabilization manifests in both an increase in dwell time of Rho GTPases and a decrease of their diffusional movement on the membrane.

At the same time, the results indicate that the primary regulators of the spatial cycle, RhoGDI, and the catalytic cycle, GEFs and GAPs, are insufficient to accumulate Rho GTPases at sites of their activity. While the observations regarding RhoGDI are more puzzling and will be discussed in greater detail later, the results of the *in vitro* reconstitution do suggest that coupling of both cycles is not achieved through a GEF-mediated increase in Rho GTPase membrane recruitment. This directly contrasts models proposed in literature postulating that GEFs can induce the dissociation of Rho GTPase:RhoGDI complexes (Worthylake et al., 2000; Ugolev et al., 2008). Such a mechanism would lead to increased recruitment and subsequent accumulation of Rho GTPases in GEF-enriched membrane regions in the *in vitro* reconstitutions even in the absence of effector proteins, which I did not observe. The inability of GEFs to increase recruitment of Rho GTPases is further supported by the apparent temporal sequence of events observed in experiments in the presence of effectors. That is, the delayed accumulation of Rho GTPases relative to their activation. This suggests that GEFs act on inactive Rho GTPases already present at the membrane. Contrary to traditional models of the Rho GTPase regulatory cycles in which Rho GTPase inactivation by GAPs is inevitably followed by membrane extraction through RhoGDI (Cho et al., 2019), it potentially allows membrane-bound Rho GTPases to repeatedly undergo their catalytic cycle before being

extracted. These prolonged membrane-bound phases of Rho GTPases highlight the requirement of GAPs counteracting the lateral diffusion of constantly (re-)activated Rho GTPases along the membrane to enable stable Rho GTPase activity patterns, which is consistent with the results presented here and has been hypothesized before (Bement et al., 2006).

By simple fusion of two Rho GTPase effector binding domains, I successfully generated an artificial protein (2xwCRIB) that mimics effector dimers. Remarkably, dimerization is sufficient to enrich active Cdc42 on the membrane. However, this enrichment was only moderate in my *in vitro* reconstitution (~1.4x, Figure 15) and somewhat more pronounced *in vivo* (~2x, Figure 7). This small disparity is likely the result of the strong difference in the biochemical complexity of the cellular environment. Nonetheless, the moderate degree of the enrichment detected in both systems prompts the question of whether this phenomenon has biological relevance. While moderate in effect, the region-specific retention of active Rho GTPases on the membrane enables the maintenance of robust Rho GTPase activity patterns. Hence, in these regions biological noise is less likely to terminate Rho GTPase signaling output. Crucially, many systems of effector signaling behave in a switch-like manner (Sun et al., 2017; De Seze et al., 2023). That is, if a certain threshold in the apparent concentration of Rho GTPase effectors on the membrane is reached, activation of downstream processes follows. Thus, in the correct parameter regime these systems can be anticipated to be very sensitive to small fluctuations in Rho GTPase density on the membrane. Furthermore, in the context of Rho GTPase activity pattern formation, the stabilization of active Rho GTPases on the membrane through effectors offers a straightforward mechanism enabling coupling of their catalytic and spatial cycles. This coupling has been identified as a crucial mechanistic ingredient in theoretical approaches used to study the formation of Rho GTPase activity patterns. Many of these models assume that Rho GTPases dissociate from the membrane only when in their inactive state (Jilkine et al., 2007; Goryachev & Pokhilko, 2008). The findings of the *in vitro* reconstitution indicate that, although the spatial and catalytic cycles of Rho GTPases are coupled, it is not achieved by an enhanced extraction of inactive Rho GTPases. It nevertheless remains to be tested, theoretically and experimentally, if this moderate degree of coupling is sufficient for the formation of Rho GTPase activity patterns.

Interestingly, the results presented in the first section of my thesis demonstrate the inability of RhoGDI to induce enrichment of Cdc42, why is that? Previous studies suggested preferential extraction of inactive Rho GTPases over their active form from the membrane, facilitated by RhoGDI (Johnson et al., 2009; Freisinger et al., 2013; Golding et al., 2019). Intuitively such a mechanism should elicit the accumulation of Rho GTPases at sites of their activity, even though only a marginal difference in RhoGDI's preference for inactive over active Rho GTPases (2-3x) has been reported (Golding et al., 2019). The concentration of free RhoGDI1 in the system, generated by using a 1:1 stoichiometric Rho GTPase:RhoGDI complex in the *in vitro* reconstitution, might simply not be sufficient to exert a strong effect. The preferential extraction of inactive Rho GTPases from the membrane was investigated under conditions with excess RhoGDI (Golding et al., 2019). So what do we know about the relative concentrations of RhoGDI and its client GTPases in mammalian cells? Based on previous studies, the amount of RhoGDI in cells is almost equal (1.1:1) to the sum of the concentrations of its main clients RhoA, Rac1 and Cdc42 (Michaelson et al., 2001), suggesting near stoichiometric levels *in vivo*. Importantly, loss-of-function experiments show that knockdown of RhoGDI results in the massive degradation of Rho GTPases (Boulter et al., 2010). This points toward a simple but elegant homeostatic mechanism by which the protein levels of many Rho GTPases can be matched to the availability of RhoGDI, which would be difficult to achieve by genetic means alone. This mechanism can also be expected to prevent the accumulation of excess free RhoGDI, at least over long periods of time. Such strong excess of free RhoGDI would not be compatible with Rho GTPase signaling, as experimentally demonstrated by chronic RhoGDI overexpression experiments (Moissoglu et al., 2006), because it would prevent significant membrane binding of its GTPase clients due to potent sequestration. Nonetheless, stimulation of Rho GTPase activity can be expected to result in a transient build-up of free RhoGDI in solution as a result of the increased membrane stability of active GTPases on the membrane as shown here. Such activity-dependent accumulation of RhoGDI has been previously observed via biosensors of the RhoGDI-Cdc42 interactions (Hodgson et al., 2016). These conditions, which are very difficult to mimic in our reconstitutions due to the vastly lower membrane-to-solution ratios, might still contribute to the enrichment of active Rho GTPases *in vivo*.

Because stoichiometric amounts of RhoGDI were insufficient to facilitate this enrichment, I reasoned that several other factors present in cells must be able to contribute to the enrichment. These additional factors might also be responsible for the observed difference in the patterning index between the *in vivo* and *in vitro* systems (compare Figure 7 and Figure 15). Besides the overall larger number of multivalent effectors *in vivo*, processes downstream of these effectors might enhance Rho GTPase accumulation at sites of their activity as well. Actin dynamics are inherently connected to Rho GTPase activity through effectors of the WASP and formin families (Alekhina et al., 2017). These effectors must be associated with the membrane while also interacting with Rho GTPases to initiate either the WASP-family dependent branching of the actin network via the Arp2/3 complex (Rottner et al., 2021) or the formin-dependent generation of actomyosin (Tojkander et al., 2015). This indirect interaction of active Rho GTPases with supramolecular structures like actin networks might stabilize them on the membrane. Furthermore, another factor that might contribute to the accumulation of Rho GTPases at sites of their activity are the lipids of the plasma membrane. While the *in vitro* reconstitution was built on an SLB that mimics the composition of the plasma membrane and even includes the dynamic conversion of PI(4)P and PI(4,5)P_2, it cannot fully recapitulate the complex organization of the plasma membrane. Rho GTPases associate preferentially with anionic lipids because of their C-terminal polybasic motif (Finkielstein et al., 2006). Thus, recruitment to lipid regions of anionic nature is favored. *In vivo*, Rho GTPase nanoclusters have been observed to form through interactions with anionic phosphoinositide lipids (Remorino et al., 2017). These nanoscale domains may function as scaffolds by promoting Rho GTPase effector protein interactions potentially facilitating Rho GTPase enrichment (Budnar et al., 2019). However, formation and maintenance of these nanoclusters likely depends on the actin cytoskeleton (Garcia-Parajo & Mayor, 2024), which is absent in the *in vitro* reconstitution. In conclusion, it is most likely that all these phenomena together contribute to the accumulation of active Rho GTPases at sites of their activity *in vivo*, leading to the observed difference between both systems investigated in the first section of my thesis.

The *in vitro* reconstitutions uncovered the molecular mechanism behind the effector-mediated stabilization of active Rho GTPases on the membrane. That is, the avidity-driven increase in membrane dwell time and diffusion of active Rho GTPases. These results alone do not allow the exclusion of either mechanism, but rather indicate that both contribute

to the enrichment of active Cdc42 on the membrane. Furthermore, the activity-dependent increase in the retention of Cdc42 on membranes is confirmed by our *in vivo* studies, which show a correlation between GEF-mediated activation of Cdc42 around the edge of the wound and an increase in the retention of Cdc42 at activation sites.

Remarkably, the multivalent 2xwCRIB also significantly increased the signal intensity that indicates the level of Rho GTPase activity. Multivalent Rho GTPase activity sensors have been described as improved reporters for Rho GTPase activity before (Mahlandt et al., 2021). However, the use of a multivalent Rho GTPase effector binding domain in the *in vitro* reconstitution demonstrated its capability to enrich active Cdc42 on the membrane. Therefore, the application of Rho GTPase activity sensors based on multivalent effector binding domains must be approached carefully, and results should be interpreted with caution regarding the potential risk of artificially influencing the system.

Lastly, while the work presented in the first section of my thesis was done with Cdc42, the mechanism revealed for the coupling of the catalytic and spatial cycles of Rho GTPases is most likely relevant for and transferable to other GTPases of the Ras superfamily as well. For example, Rab GTPases follow a similar spatial and catalytic regulatory paradigm, with RabGDI, GEFs and GAPs as key players (Bezeljak et al., 2020). This similarity together with recruitment of effector proteins involved in vesicular trafficking increases the likelihood that effector-mediated stabilization also drives the enrichment of active Rab GTPases at certain membrane regions.

Together, the findings outlined in the first section of my thesis contribute to the understanding of Rho GTPase pattern formation by revealing effector-mediated stabilization of active Rho GTPases as the process that couples their catalytic and spatial cycles. By utilizing the *in vitro* reconstituted system of templated Rho GTPase activity patterns, I was able to demonstrate a simple way to introduce this coupling. This is a starting point for the investigation and *in vitro* reconstitution of self-organizing Rho GTPase activity patterns.

A synthetic polarizer of Rho GTPase activity

Crosstalk between Rho GTPases through their catalytic regulators, such as GEFs and GAPs, has been hypothesized to be essential for spatially organizing Rho GTPase activity (Bement et al., 2024). The direct coupling of Rho GTPase activation or inactivation to their activity creates feedback circuits that allow the self-organized polarization of their activities (Bement et al., 2024), and has been observed *in vivo* (Vaughan et al., 2011; Das et al., 2012; Graessl et al., 2017). In addition to polarization, Rho GTPase signaling systems *in vivo* are known to quickly adapt to the changing environment they are embedded in (Diez et al., 2005; Weiner et al., 2007). While many network topologies have been suggested for a plethora of different dynamic systems in cells (Bement et al., 2024), experimental confirmation of the exact players involved is often missing. Thus, in the second part of my thesis I focused on a network topology that should guide the *in vitro* reconstitution of a minimal synthetic Rho GTPase signaling system. I designed suitable artificial molecules supposed to facilitate Rho GTPase crosstalk in the form of GBD-GAP/GEF chimeras and started characterizing their catalytic activities and binding affinities. These results establish a foundation of assays that can be used for the reconstitution of the full synthetic network.

The proposed network topology that allows stable polarization of Rho GTPase activities includes feedback between the three most abundant Rho GTPases, RhoA, Rac1 and Cdc42. With higher numbers of Rho GTPases used, complexity of the *in vitro* reconstitution automatically increases, since it requires additional feedback, so why not decrease their number? The system was designed to mimic front-back polarity observed in motile cells. Directional migration of cells requires functionally diverse actin networks to establish a protruding front and a contractile back. At the cell front, protruding structures depend on actin polymerization to induce a forward motion while the formation of actomyosin is required at the back of the cell to promote contractions. These processes are directed by spatially segregated RhoA activity at the back and Cdc42/Rac1 activity at the front of the cell. Thus, mimicking such behavior in the *in vitro* reconstitution requires mutual antagonism between RhoA and Cdc42/Rac1 activity (Nobes & Hall, 1995, 1999; Ridley et al., 2003). Furthermore, a system that includes RhoA, Rac1 and Cdc42 is still less difficult to realize *in vitro* than alternatives. The reason for this is that the use of all three Rho

GTPases together with the implementation of some asymmetry in feedback strength omits the necessity of non-linearities in the feedback itself. Other systems, specifically the ones based on fewer Rho GTPases, require non-linear feedback and therefore cannot rely on simple linear feedback through direct recruitment of the regulators (Lo et al., 2014). But why is the biochemical implementation of non-linearities in the *in vitro* reconstitution challenging? This type of feedback in an *in vitro* reconstitution could be directly achieved by using regulators of Rho GTPases that bind cooperatively to their ligands. While studies have identified such GEFs, e. g. for RhoA (Chen et al., 2010; Medina et al., 2013), options for these regulators are limited to a few (Bement et al., 2024). Hence, engineering a new regulator harboring this feature based on these few examples would be difficult. Still, there are other possibilities that theoretically introduce non-linear feedback. Enzymes that are partially saturated or inhibited by stoichiometric amounts of an inhibitor may introduce non-linearities (Ferrell, 1996; Jilkine et al., 2007). However, experimental observations thus far primarily suggest that the introduction of non-linear feedback *in vivo* is mainly achieved through the cooperative binding of Rho GTPase regulators to their ligands (Goryachev & Leda, 2017; Bement et al., 2024). Ultimately, even if such non-linear feedback were successfully engineered, the complexity of an *in vitro* system utilizing this approach would be comparable to, if not greater than, that of one based on the previously proposed network topology. This is the main reason why we chose a network topology that is solely based on linear feedback.

The use of GBD-GAP/GEF chimeras as feedback mediators comes with another important benefit, which directly relates to the results in the first part of my thesis. By simply using multivalent GBDs, we can couple the catalytic and spatial cycles of Rho GTPases in a straightforward manner. Designing this feature by other means would have been very difficult as it would require dedicated biochemical players differentially regulating the membrane stability of Rho GTPases depending on their activation state. We have no evidence that any such molecules other than effector proteins exist *in vivo*, which is why we opted for this specific strategy.

The general design of these chimeras enables linear feedback in the *in vitro* reconstitution through direct recruitment of catalytic domains to active Rho GTPases. However, the use of isolated catalytic domains as independent modules can also have pitfalls. Especially

Rho GAPs are notorious for their promiscuity concerning their GTPase substrates and often require adjacent domains present in the full length enzyme for specificity (Amin et al., 2016). This general theme of promiscuity was confirmed by the results presented, which demonstrate at least some activity of Abr_{cat} and $ArhGAP29_{cat}$ towards all Rho GTPases tested (RhoA, Rac1 and Cdc42). However, both GAP domains chosen still exhibit pronounced preferences for the desired substrate. Nonetheless, it remains to be tested experimentally whether this specificity is sufficient for these chimeras to facilitate the required feedback in the *in vitro* reconstitution. Ultimately, it might be necessary to increase the specificity of the chimeras' catalytic activity by potentially changing the design of the chimeric protein or by mutagenesis.

The preliminary results for the characterization of the chimeras demonstrate that the fusion of isolated binding and catalytic domains retains the activity of the individual functional elements. Fusion did not impair their ability to bind Rho GTPases nor abolished their catalytic activity. However, the specificity for the binding and catalytic activity of GBD-GAP/GEF chimeras deserves more rigorous testing in the future. While binding of the chimeras to their respective active Rho GTPases could be confirmed, binding specificity was not. Hence, further analysis of the binding specificity is required, for example through binding assays of the chimeras, including RhoA, Rac1 and Cdc42, for instance by visual bead-based assays as established here.

In addition to binding, some of the catalytic activities of the chimeras, specifically GBD-GAP chimeras, should be re-evaluated because the activity readouts used to determine GAP activity, Cy3-GTP and TAMRA-GTP, are highly sensitive to changes in the environment (Eberth et al., 2005; Amin et al., 2016) and might be affected by the association of an effector binding domain with a Rho GTPase. However, alternative means of GAP assays exist (Self & Hall, 1995). Nevertheless, I successfully established a pipeline that includes multiple assays to characterize GBD-GAP/GEF chimeras, which serves as a foundation for further characterization of the final 2x variants of the chimeras.

While theory shows that our network topology should be able to drive autonomous Rho GTPase polarization, experimental validation is still missing. Final proof would require the integration of the full system, which poses a challenge in itself given the large parameter

space in which every concentration of each protein becomes a key variable. However, some approaches might allow to first test the function of specific modules in isolation. For instance, by utilizing the *in vitro* reconstituted system of templated Cdc42 activity patterns described in the first section, the ability of chimeras to introduce feedback can be tested. The addition of the feedback chimeras to this templated Cdc42 activity system should be able to generate either overlapping or mutually exclusive domains of either Rac1 or RhoA activity. Visualizing and following Rho GTPase activity in these systems would therefore constitute an intermediate goal and allow the experimental confirmation of feedback.

A complete *in vitro* reconstitution of a minimal synthetic system displaying self-organizing Rho GTPase activity patterns, based on simple linear feedback through direct recruitment of GBD-GAP/GEF chimeras, would be the first of its kind. Such an experimental system, that can induce a stably polarized state of Rho GTPase activity, would be orthogonal to theoretical approaches investigating protein patterning systems generically. Thus, it would allow a direct comparison of changes in the dynamical behavior of the *in vitro* system, based on initial parameters, with results obtained through theory.

While the focus of my work was on the biochemical mechanisms of Rho GTPase signaling, one crucial outcome of this signaling is the control of actin assembly. Actin network dynamics are directly affected by Rho GTPase activity (Alekhina et al., 2017), but experimental and theoretical evidence suggests that the actin network in turn also influences Rho GTPase activity through, for example, F-actin dependent recruitment of different GAPs (Bement et al., 2015; Michaux et al., 2018). While challenging due to the increased complexity of such reconstitutions, the coupling of the actin machinery to the *in vitro* system of self-organizing Rho GTPase signaling would be the next logical step toward systems integration. This would be interesting for multiple reasons. First, it would pave the way for understanding how functionally distinct actin networks are assembled from a common cytoplasmic environment in response to signaling at membranes. Second, it would provide invaluable insight into the coupling between these two molecular systems, which are strongly intertwined at all levels in living cells. Finally, such systems would be naturally endowed with advanced properties such as delayed and mechanosensitive feedback, which would be essential ingredients for more complex dynamic behaviors such as oscillations and wave propagation.

Conclusion

The results presented throughout this thesis contribute toward the complete *in vitro* reconstitution of a synthetic polarizing Rho GTPase signaling system. The results demonstrated how coupling of the catalytic and spatial cycles of Rho GTPases is achieved through effector-mediated stabilization. While this aids in the general understanding of Rho GTPase activity pattern formation, it is also essential for the *in vitro* reconstitution of a complete system displaying polarization of Rho GTPase activity. Thus, I utilized this knowledge in the second part of my research and generated artificial constructs, namely 2xGBD-GAP/GEF chimeras, that can biochemically facilitate the feedback links of a network topology equipped with the features necessary for stable polarization. Moreover, I laid the groundwork for the characterization of these 2xGBD-GAP/GEF chimeras and by doing so solidified the feasibility of such an approach to successfully create crosstalk between Rho GTPases.

Materials and Methods

Materials

Commercial chemicals and proteins

Table 2: Commercial chemicals and proteins.

Chemicals/Proteins	Manufacturer
18:1 (Δ9-Cis) DOPE	Avanti Polar lipids
18:1 DOPS	Avanti Polar lipids
18:1 PEG5000 PE	Avanti Polar lipids
2-log ladder	New England Biolabs
Activated Thiol Sepharose 4B	GE Healthcare/Cytiva
AF488-NHS ester	Lumiprobe
AF647-NHS ester	Lumiprobe
ATP	Sigma-Aldrich
Atto488-Maleimide (Atto488)	ATTO-TEC
Benzamidine	Thermo Fischer Scientific
Blocker Casein (b-Casein)	Thermo Fisher Scientific
Catalase	Sigma-Aldrich
Chemicals (general)	Sigma-Aldrich, Merck, AppliChem
Chloroform	Sigma-Aldrich
Cholesterol (ovine)	Avanti Polar lipids
DMSO	Invitrogen
DNaseI	Sigma Aldrich
EDA-GTP-5/6-TAMRA	Jena Bioscience
EDA-GTP-Cy3	Jena Bioscience
EDTA	Gerbu
EDTA-Free cOmpleteTM protease inhibitor tablets	Roche
Fetal bovine serum (FBS)	PAN Bitech GmbH
Geranylgeranyl pyrophosphate ammonium salt	Sigma-Aldrich
Glucose oxidase	Serva
GppNHp	Jena Bioscience
GTP	Sigma Aldrich
Hellmanex III	Hellma GmbH
Hydrogen peroxide	Roth
Mant-GDP	Jena Bioscience
Mant-GppNHp	Jena Bioscience
PBS	Corning

Peptides (general)	GenScript
Precision Plus Protein standards	Bio-Rad Laboratories
Q5 HF DNA polymerase	New England Biolabs
RedSafe, DNA Stain	Chembio Ltd
Soy PC	Avanti Polar lipids
Sulpho-Cy3-NHS	Lumiprobe
Sulphuric acid	Sigma-Aldrich
synthetic PI(4.5)P_2	Avanti Polar lipids
synthetic PI(4)P	Avanti Polar lipids
TCEP	Sigma-Aldrich
Triethylamine	Sigma-Aldrich
Triton X-100	Sigma-Aldrich

Commercial kits

Table 3: Commercial kits.

Kit	Manufacturer
NucleoBond Xtra Midi Plus EF	Macherey-Nagel
NucleoSpin plasmid kit	Macherey-Nagel
Zymoclean Gel DNA Recovery Kit	Zymo Research

Material and equipment

Table 4: Material and equipment.

Material/Equipment	Manufacturer
ÄKTA pure system	GE Healthcare/Cytiva
ÄKTA purifier system	GE Healthcare/Cytiva
centrifugal concentrator (Vivaspin)	Sartorius
Detergent removal columns	Pierce
HiPrep 26/10 column	GE Healthcare/Cytiva
HiTrap chelating column	GE Healthcare/Cytiva
HisTrap excel column	GE Healthcare/Cytiva
Mastercycler Pro	Eppendorf
Microfluidizer	Hyland Scientific
Monolith Nt. 115 (blue/red)	Nanotemper
Monolith Nt. 115 Premium Capillary	Nanotemper
MonoQ 5/50 GL	GE Healthcare/Cytiva
MonoS 5/50 GL	GE Healthcare/Cytiva
NaonoDrop Spectrophotometer ND-1000	Thermo Fisher

Plasma cleaner	Plasma technology
QuantaMaster Fluorometer	Photon Technology International (PTI)
Rotary evaporator	KNF
Superdex 200 XK 16/60	GE Healthcare/Cytiva
Superdex 200 XK 26/60	GE Healthcare/Cytiva
Superdex 75 10/300 GL increase	GE Healthcare/Cytiva
Superdex 75 XK 16/60	GE Healthcare/Cytiva
Tecan Spark plate reader	Tecan
Zeba Spin column	Thermo Fisher
General laboratory equipment (not shown)	

Software, tools and databases

Table 5: Software, tools and databases.

Software/Tool/Database	Source
Adobe Illustrator	Adobe
ApE	(Davis & Jorgensen, 2022)
UCSF Chimera	(Pettersen et al., 2004)
Expasy-ProtParam	SIB, Swis
Fiji	(Schindelin et al., 2012)
OligoCalc	(Kibbe, 2007)
OriginPro	OriginLab Corporation
PDB	RSCB
SnapGene	Insightful science
TrackMate	(Tinevez et al., 2017)
Uniprot	EMBL-EBI

Bacterial strains and insect cell lines

Table 6: Bacterial strains and insect cell lines.

Bacterial strain/Insect cell line	Antibiotic resistance	Source
E. coli XL10 Gold	/	Stratagene (regrown in-house)
E. coli BL21 (DE3)	/	EMBL Protein Expression Facility
E. coli BL21 (DE3) RIL	Cam	EMBL Protein Expression Facility
E. coli Rosetta (DE3)	Cam	Novagen #70954
E. coli Star pRare pACYC	Cam, Gent	EMBL Protein Expression Facility
Spodoptera frugiperda Sf-9	/	A. Mussachio, MPI Dortmund

Trichoplusia ni BTI-*Tnao*38	/	A. Mussachio, MPI Dortmund

Cell culture media

Table 7: Cell culture media.

Medium	Composition
LB	10 g/L bacto tryptone, 5 g/L bacto yeast extract, 10 g/l NaCl
TB	12 g/L tryptone, 24 g/L yeast extract, 2.31 g/L KH_2PO_4, 12.54 g/L K_2HPO_4, 4 mL Glycerin
SOC	20 g/L tryptone, 5 g/L yeast extract, 0.58 g/l NaCl, 0.19 g/L KCl, 2.03 g/L $MgCl_2$ x 6 H2O, 2.46 g/L $MgSO_4$ x 7 H_2O, 960 mL H_2O, 40 mL sterilized 50 % glucose (w/w)
Sf-900 II SFM	Commercially available from Gibco

Recombinant DNA constructs

Table 8: Recombinant DNA constructs.

Construct	Antibiotic resistance	Source
pET28-6xHis-Thrombin-GGTase1β	Kan	K. Gavriljuk
pETM11-6xHis-SenP2	Kan	EMBL Protein Expression Facility
pETM60-6xHis-NusA-TEV-GGGGG-2xpTPR-ArhGAP29$_{cat}$	Kan	this work
pETM60-6xHis-NusA-TEV-GGGGG-2xpTPR-ITSN$_{cat}$	Kan	this work
pETM60-6xHis-NusA-TEV-GGGGG-2xrREM-Abr$_{cat}$	Kan	this work
pETM60-6xHis-NusA-TEV-GGGGG-2xwCRIB	Kan	this work
pETM60-6xHis-NusA-TEV-GGGGG-2xwCRIB-Tiam1$_{cat}$	Kan	this work
pETM60-6xHis-NusA-TEV-GGGGG-p2CRIB-ArhGAP29$_{cat}$	Kan	this work
pETM60-6xHis-NusA-TEV-GGGGG-pTPR	Kan	this work
pETM60-6xHis-NusA-TEV-GGGGG-pTPR-ArhGAP29$_{cat}$	Kan	this work
pETM60-6xHis-NusA-TEV-GGGGG-pTPR-ITSN$_{cat}$	Kan	this work
pETM60-6xHis-NusA-TEV-GGGGG-rREM-Abr$_{cat}$	Kan	this work
pETM60-6xHis-NusA-TEV-GGGGG-wCRIB	Kan	this work
pETM60-6xHis-NusA-TEV-GGGGG-wCRIB-Tiam1$_{cat}$	Kan	this work
pETM66-NusA-His-TEV-SortaseA(delta59)	Kan	M. Armstrong
pETMSumo3-10xHis-TEV-Sumo3-GGGGG-OPHN1$_{cat}$	Kan	P. Bieling
pETMSumo3-10xHis-TEV-Sumo3-GGGGG-PLCδ(PH)-ITSN$_{cat}$	Kan	P. Bieling

pETMSumo3-6xHis-TEV-Sumo3-GGGGG-PLCδ(PH)	Kan	S. Hansen
pETMz2-6xHis-zTag-TEV-Cdc42(wt)	Kan	P. Bieling
pETMz2-6xHis-zTag-TEV-Cys-RhoGDI1(BT,wt)	Kan	P. Bieling
pETMz2-6xHis-zTag-TEV-Rac1(Q61L)	Kan	P. Bieling
pETMz2-6xHis-zTag-TEV-Rac1(wt)	Kan	P. Bieling
pETMz2-6xHis-zTag-TEV-RhoA(Q63L)	Kan	P. Bieling
pETMz2-6xHis-zTag-TEV-RhoA(wt)	Kan	P. Bieling
pFastBac1-6xHis-MBP-10xAsn-TEV-GGGG-PI4P5K	Amp	S. Hansen
pFB-6xHis-TEV-NWASP	Amp	A. Roy
pGATEV-6xHis-GST-RabGGTaseβ	Amp	K. Gavriljuk
pGATEV-6xHis-GST-TEV-GGTase2β	Amp	K. Gavriljuk
pMal-C2-MBP-TEV(site)-6xHis-TEV(Protein, S129V)-6xArg	Amp	S. Hansen
pMPB-6xHis-MBP-10xAsn-TEV-GGGG-DrrA-GGGG-OCRL	Kan	S. Hansen

Methods

Expression and purification of recombinant proteins

From *E. coli*

TEV protease

Coding sequence for the catalytic domain (aa: 2038-2273) of the nuclear-inclusion-a endopeptidase from tobacco etch virus (Uniprot: P04517) with a S2256V mutation (numbering according to uniprot entry), decreasing its autoproteolytic activity (Kapust et al., 2001), was extended by an N-terminal 6xHis-tag to allow for affinity chromatography for the purification. Additionally, the coding sequence was extended by a C-terminal 5xarginine-tag to allow for separation of the truncated versions of the protein during purification if necessary. The coding sequence was cloned into a pMal-C2 vector, creating a maltose-binding protein (MBP) fusion to increase protein yield (Kapust & Waugh, 1999). Chemically competent BL21 (DE3) RIL *E. coli* cells were transformed with the construct. 50 mL lysogeny broth (LB), supplemented with antibiotics (see Materials: Bacterial strains and insect cell lines, Recombinant DNA constructs), were inoculated with a positive clone and cultured overnight at 30 °C. The culture was expanded on the next day to a total volume of 6-12 L with terrific broth (TB) supplemented with the respective antibiotics and kept at 37 °C. After achieving an OD_{600} of 0.8-1.2 the culture was cooled down to 30 °C, subsequently induced with 1 mM IPTG and incubated at 30 °C for 4 h. Cell harvesting was accomplished by centrifugation at 3500 x g for 20 min at 4 °C. Pellets were snap-frozen in liquid nitrogen and stored at -80 °C.

For purification, frozen pellets were thawed for 10 min at RT, put immediately back on ice and resuspended in a 3x volume of lysis buffer (75 mM KPi pH 7.7, 350 mM NaCl, 10% (v/v) glycerol, 0.4 mM β-mercaptoethanol, 1 mM PMSF, ~10 µg/mL DNAseI). Cell suspension was homogenized by 7-10 cycles in a dounce homogenizer on ice and lysis was completed with a high-pressure homogenizer at 4 °C. Lysate was centrifuged at 142,000 x g for 1 h at 4 °C and further clarified by filtering the supernatant through a 0.45 µm syringe filter. Following clarification of the lysate, affinity purification on a 5 mL HiTrap Chelating HP column loaded with 200 mM $CoCl_2$, washed with water and equilibrated with equilibration buffer (75 mM KPi pH 7.7, 350 mM NaCl, 10% (v/v) glycerol, 0.4 mM β-mercaptoethanol) was performed. The filtrate was recirculated over the equilibrated column for 2-3 h at 4 °C. After washing the column with equilibration

buffer, the protein was eluted over a linear gradient (6 column volumes (CV)) of equilibration buffer containing 500 mM imidazole. Peak fractions of the eluate were pooled, concentrated using Vivaspin concentrators with a molecular weight cut-off of 10 kDa and gel filtered in storage buffer (50 mM KPi pH 7.7, 250 mM NaCl, 20% (v/v) glycerol, 0.5 mM TCEP) over a Superdex 200 26/60 column. Peak fractions were pooled and concentrated as before. The protein was snap-frozen in liquid nitrogen and stored at -80 °C.

SenP2

Coding sequence for the catalytic domain (aa: 364-589) of human SenP2 (Uniprot: Q9HC62-1) was cloned into a pETM11 vector, creating a TEV cleavable 6xHis fusion to allow for affinity chromatography for the purification. Chemically competent BL21 (DE3) *E. coli* cells were transformed with the construct. 50 mL lysogeny broth (LB), supplemented with antibiotics (see Materials: Bacterial strains and insect cell lines, Recombinant DNA constructs), were inoculated with a positive clone and cultured overnight at 30 °C. The culture was expanded on the next day to a total volume of 6-12 L with terrific broth (TB) supplemented with the respective antibiotics and kept at 37 °C. After achieving an OD_{600} of 0.8-1.2 the culture was cooled down to 30 °C, subsequently induced with 100 µM IPTG and incubated at 30 °C for 6 h. Cell harvesting was accomplished by centrifugation at 3500 x g for 20 min at 4 °C. Pellets were snap-frozen in liquid nitrogen and stored at -80 °C.

For purification, frozen pellets were thawed for 10 min at RT, put immediately back on ice and resuspended in a 3x volume of lysis buffer (50 mM KPO_4 pH 7.5, 400 mM NaCl, 0.4 mM β-mercaptoethanol, 15 µg/mL Benzamidine, 1 mM PMSF, ~10 µg/mL DNAseI). Cell suspension was homogenized by 7-10 cycles in a dounce homogenizer on ice and lysis was completed with a high-pressure homogenizer at 4 °C. Lysate was centrifuged at 142,000 x g for 1 h at 4 °C and further clarified by filtering the supernatant through a 0.45 µm syringe filter. Following clarification of the lysate, affinity purification on a 5 mL HiTrap Chelating HP column loaded with 200 mM $CoCl_2$, washed with water and equilibrated with equilibration buffer (50 mM KPO_4 pH 7.5, 400 mM NaCl, 0.4 mM β-mercaptoethanol, 15 µg/mL Benzamidine) was performed. The filtrate was recirculated over the equilibrated column for 2-3 h at 4 °C. After washing the column with equilibration buffer, the protein was eluted over a linear gradient (6 column volumes (CV)) of

equilibration buffer containing 500 mM imidazole. Peak fractions of the eluate were pooled and dialyzed in storage buffer (20 mM HEPES pH 7.5, 300 mM KCl, 20% (v/v) glycerol, 0.5 mM TCEP) at 4 °C overnight. The protein was concentrated using Vivaspin concentrators with a molecular weight cut-off of 10 kDa, snap-frozen in liquid nitrogen and stored at -80 °C.

Sortase

Coding sequence for the catalytic domain (aa: 60-206) of a sortase from *Staphylococcus aureus* (Uniprot: Q2FV99) was cloned into a pETM66 vector, creating a TEV cleavable NusA-6xHis fusion to increase protein yield and allow for affinity chromatography for the purification. Chemically competent BL21 (DE3) *E. coli* cells were transformed with the construct. 50 mL lysogeny broth (LB), supplemented with antibiotics (see Materials: Bacterial strains and insect cell lines, Recombinant DNA constructs), were inoculated with a positive clone and cultured overnight at 30 °C. The culture was expanded on the next day to a total volume of 6-12 L with terrific broth (TB) supplemented with the respective antibiotics and kept at 37 °C. After achieving an OD_{600} of 0.8-1.2 the culture was cooled down to 18 °C, subsequently induced with 250 µM IPTG and incubated at 18 °C overnight. Cell harvesting was accomplished by centrifugation at 3500 x g for 20 min at 4 °C. Pellets were snap-frozen in liquid nitrogen and stored at -80 °C.

For purification, frozen pellets were thawed for 10 min at RT, put immediately back on ice and resuspended in a 3x volume of lysis buffer (50 mM KPO_4 pH 7.5, 400 mM NaCl, 0.4 mM β-mercaptoethanol, 15 µg/mL Benzamidine, 1 mM PMSF, ~10 µg/mL DNAseI). Cell suspension was homogenized by 7-10 cycles in a dounce homogenizer on ice and lysis was completed with a high-pressure homogenizer at 4 °C. Lysate was centrifuged at 142,000 x g for 1 h at 4 °C and further clarified by filtering the supernatant through a 0.45 µm syringe filter. Following clarification of the lysate, affinity purification on a 5 mL HiTrap Chelating HP column loaded with 200 mM $CoCl_2$, washed with water and equilibrated with equilibration buffer (50 mM KPO_4 pH 7.5, 400 mM NaCl, 0.4 mM β-mercaptoethanol and 15 µg/mL Benzamidine) was performed. The filtrate was recirculated over the equilibrated column for 2-3 h at 4 °C. After washing the column with equilibration buffer, the protein was eluted over a linear gradient (6 column volumes (CV)) of equilibration buffer containing 500 mM imidazole. Peak fractions of the eluate were pooled, concentrated using Vivaspin concentrators with a molecular weight cut-off of 10 kDa and

gel filtered in storage buffer (20 mM HEPES pH 7.5, 150 mM KCl, 10% (v/v) glycerol, 0.5 mM DTT) over a Superdex 200 26/60 column. Peak fractions were pooled, concentrated as before and glycerol was added to a total of 20%. Proteins were snap-frozen in liquid nitrogen and stored at -80 °C.

GGTaseI and RabGGTase β

The subunits GGTaseI α (Uniprot: Q04631) and GGTaseI β (Uniprot: P53610) of GGTaseI from *R. norvegicus* were coexpressed in BL21 (DE3) RIL *E. coli* cells and afterwards copurified by nickel affinity chromatography followed by a subsequent gel filtration step as previously described (Gavriljuk et al., 2013).
RabGGTase β from *R. norvegicus* (Uniprot: Q08603) was also expressed in BL21 (DE3) RIL *E. coli* cells afterwards purified by nickel affinity chromatography followed by a subsequent gel filtration step as previously described (Gavriljuk et al., 2013).

Human Rho GTPases – Cdc42, Rac1 and RhoA

Coding sequences for human Cdc42 (Uniprot: A0A494C1M1), human Rac1 (Uniprot: P63000) and human RhoA (Uniprot: P61586) were extended by a N-terminal 5xglycine-tag to allow for protein labelling by Sortase-mediated peptide ligation. To optimize protein translation in bacteria, coding sequences were codon optimized for *E. coli* expression prior to DNA synthesis (GeneStrand from Eurofins). The synthesized coding sequence was cloned into a pETMz2 vector containing a TEV cleavable 6xHis-z-tag. Chemically competent BL21 (DE3) *E. coli* cells were transformed with the respective construct. 50 mL lysogeny broth (LB), supplemented with antibiotics (see Materials: Bacterial strains and insect cell lines, Recombinant DNA constructs), were inoculated with a positive clone and cultured overnight at 30 °C. The culture was expanded on the next day to a total volume of 2-6 L with terrific broth (TB) supplemented with the respective antibiotics and kept at 37 °C. After achieving an OD_{600} of 0.8-1.2 the culture was induced with 1 mM IPTG and incubated at 37°C for 4 h. Cell harvesting was accomplished by centrifugation at 3500 x g for 20 min at 4 °C. Pellets were snap-frozen in liquid nitrogen and stored at -80 °C.
For purification, frozen pellets were thawed for 10 min at RT, put immediately back on ice and resuspended in a 3x volume of lysis buffer (100 mM KPi pH 7.4, 400 mM NaCl, 5 mM $MgCl_2$, 0.1 mM GDP, 0.5 mM β-mercaptoethanol, 1 mM PMSF, ~10 µg/mL DNAseI). Cell suspension was homogenized by 7-10 cycles in a dounce homogenizer on ice and lysis was

completed with a high-pressure homogenizer at 4 °C. Lysate was centrifuged at 142,000 x g for 1 h at 4 °C and further clarified by filtering the supernatant through a 0.45 µm syringe filter. Following clarification of the lysate, affinity purification on a 5 mL HiTrap Chelating HP column loaded with 200 mM $CoCl_2$, washed with water and equilibrated with equilibration buffer (100 mM KPi pH 7.4, 400 mM NaCl, 5 mM $MgCl_2$, 0.1 mM GDP, 0.5 mM β-mercaptoethanol) was performed. The filtrate was recirculated over the equilibrated column for 2-3 h at 4 °C. After washing the column with equilibration buffer, the protein was eluted over a linear gradient (6 column volumes (CV)) of equilibration buffer containing 500 mM imidazole. Peak fractions of the eluate were pooled and the 6xHis-z-tag was removed by TEV cleavage (His-TEV, molar ratio 1:30) at 4 °C overnight. Removal of imidazole from the cleaved protein was performed with a HiPrep 26/10 Desalting column equilibrated with equilibration buffer at 4 °C. To remove His-TEV and the cleaved 6xHis-z-tag, the buffer exchanged and cleaved protein was recirculated over a 5 ml HiTrap Chelating HP equilibrated with equilibration buffer for 1-2 h at 4 °C. The flow-through was collected, concentrated using Vivaspin concentrators with a molecular weight cut-off of 10 kDa and gel filtered in storage buffer (50 mM HEPES pH 7.5, 50 mM NaCl, 2 mM $MgCl_2$, 2 mM DTT, 10% (v/v) glycerol) over a Superdex 75 16/60 column. Peak fractions were pooled, concentrated as before and glycerol was added to a total of 20%. Proteins were snap-frozen in liquid nitrogen and stored at -80 °C.

RhoGDI1

Bovine RhoGDI1 (Uniprot: P19803) was expressed in Rosetta (DE3) *E. coli* cells and afterwards purified by GST-affinity chromatography followed by a subsequent gel filtration step as previously described (Golding et al., 2019).

PLCδ(PH)-ITSN$_{cat}$ and PLCδ(PH)

Coding sequence of the catalytic GEF module consisting of the tandem DH-PH domains (aa:1229-1577) of human Intersectin (Uniprot: Q15811) fused via a 6xGS linker to the PI(4,5)P_2-binding domain (PH domain, aa: 12-140) of human phospholipase C delta 1 (Uniprot: P51178) at the C-terminus or the coding sequence of the isolated PI(4,5)P_2-binding domain (PH domain, aa:12-140) were extended by a N-terminal 5xglycine-tag to allow for protein labelling by Sortase-mediated peptide ligation. To optimize protein translation in bacteria, coding sequences were codon optimized for *E. coli* expression

prior to DNA synthesis (GeneStrand from Eurofins). The synthesized coding sequence was cloned into a pETMSumo3 vector containing a SenP2 cleavable 10xHis-Sumo-tag. Chemically competent Rosetta (DE3) *E. coli* cells were transformed with the respective construct. 50 mL lysogeny broth (LB), supplemented with antibiotics (see Materials: Bacterial strains and insect cell lines, Recombinant DNA constructs), were inoculated with a positive clone and cultured overnight at 30 °C. The culture was expanded on the next day to a total volume of 2-6 L with terrific broth (TB) supplemented with the respective antibiotics and kept at 37 °C. After achieving an OD_{600} of 0.8-1.2 the culture was cooled down to 18 °C, subsequently induced with 250 µM IPTG and incubated at 18 °C overnight. Cell harvesting was accomplished by centrifugation at 3500 x g for 20 min at 4 °C. Pellets were snap-frozen in liquid nitrogen and stored at -80 °C.

For purification, frozen pellets were thawed for 10 min at RT, put immediately back on ice and resuspended in a 3x volume of lysis buffer (50 mM KPi pH 7.5, 400 mM NaCl, 0.5 mM β-mercaptoethanol, 15 µg/mL Benzamidine, 1 mM PMSF, ~10 µg/mL DNAseI). Cell suspension was homogenized by 7-10 cycles in a dounce homogenizer on ice and lysis was completed with a high-pressure homogenizer at 4 °C. Lysate was centrifuged at 142,000 x g for 1 h at 4 °C and further clarified by filtering the supernatant through a 0.45 µm syringe filter. Following clarification of the lysate, affinity purification on a 5 mL HiTrap Chelating HP column loaded with 200 mM $CoCl_2$, washed with water and equilibrated with equilibration buffer (50 mM KPi pH 7.5, 400 mM NaCl, 0.5 mM β-mercaptoethanol, 15 µg/mL Benzamidine) was performed. The filtrate was recirculated over the equilibrated column for 2-3 h at 4 °C. After washing the column with equilibration buffer, the protein was eluted over a linear gradient (6 column volumes (CV), up to 45%) of equilibration buffer containing 500 mM imidazole. Peak fractions of the eluate were pooled and the 10xHis-Sumo-tag was removed by SenP2 cleavage (His-SenP2, molar ratio 1:50) at 4 °C overnight. Removal of imidazole from the cleaved protein was performed with a HiPrep 26/10 Desalting column equilibrated with equilibration buffer at 4 °C. To remove His-SenP2 and the cleaved 10xHis-Sumo-tag, the buffer exchanged and cleaved protein was recirculated over a 5 ml HiTrap Chelating HP for 1-2 h at 4 °C. The flow-through was collected, concentrated using Vivaspin concentrators with a molecular weight cut-off of 10 kDa and gel filtered in storage buffer (20 mM HEPES pH 7.5, 150 mM NaCl, 0.5 mM TCEP) over a Superdex 200 16/60 column. Peak fractions were pooled,

concentrated as before and glycerol was added to a total of 20%. Proteins were snap-frozen in liquid nitrogen and stored at -80 °C.

OPHN1$_{cat}$

Coding sequence for the catalytic domain (aa:375-583) of murine Oligophrenin-1 (Uniprot: Q99J31) was extended by a N-terminal 5xglycine-tag to allow for protein labelling by Sortase-mediated peptide ligation. To optimize protein translation in bacteria, coding sequence was codon optimized for *E. coli* expression prior to DNA synthesis (GeneStrand from Eurofins). The synthesized coding sequence was cloned into a pETMSumo3 vector containing a SenP2 cleavable 10xHis-Sumo-tag. Chemically competent Rosetta (DE3) *E. coli* cells were transformed with the respective construct. 50 mL lysogeny broth (LB), supplemented with antibiotics (see Materials: Bacterial strains and insect cell lines, Recombinant DNA constructs), were inoculated with a positive clone and cultured overnight at 30 °C. The culture was expanded on the next day to a total volume of 2-6 L with terrific broth (TB) supplemented with the respective antibiotics and kept at 37 °C. After achieving an OD_{600} of 0.8-1.2 the culture was cooled down to 18 °C, subsequently induced with 250 µM IPTG and incubated at 18 °C overnight. Cell harvesting was accomplished by centrifugation at 3500 x g for 20 min at 4 °C. Pellets were snap-frozen in liquid nitrogen and stored at -80 °C.

For purification, frozen pellets were thawed for 10 min at RT, put immediately back on ice and resuspended in a 3x volume of lysis buffer (100 mM KPi pH 7.5, 400 mM NaCl, 5 mM $MgCl_2$, 0.5 mM β-mercaptoethanol, 1 mM PMSF, ~10 µg/mL DNAseI). Cell suspension was homogenized by 7-10 cycles in a dounce homogenizer on ice and lysis was completed with a high-pressure homogenizer at 4 °C. Lysate was centrifuged at 142,000 x g for 1 h at 4 °C and further clarified by filtering the supernatant through a 0.45 µm syringe filter. Following clarification of the lysate, affinity purification on a 5 mL HiTrap Chelating HP column loaded with 200 mM $CoCl_2$, washed with water and equilibrated with equilibration buffer (100 mM KPi pH 7.5, 400 mM NaCl, 5 mM $MgCl_2$, 0.5 mM β-mercaptoethanol) was performed. The filtrate was recirculated over the equilibrated column for 2-3 h at 4 °C. After washing the column with equilibration buffer, the protein was eluted over a linear gradient (6 column volumes (CV)) of equilibration buffer containing 500 mM imidazole. Peak fractions of the eluate were pooled and the 10xHis-Sumo-tag was removed by SenP2 cleavage (His-SenP2, molar ratio 1:50) at 4 °C overnight.

Removal of imidazole from the cleaved protein was performed with a HiPrep 26/10 Desalting column equilibrated with equilibration buffer at 4 °C. To remove His-SenP2 and the cleaved 10xHis-Sumo-tag, the buffer exchanged and cleaved protein was recirculated over a 5 ml HiTrap Chelating HP for 1-2 h at 4 °C. The flow-through was collected, concentrated using Vivaspin concentrators with a molecular weight cut-off of 10 kDa and gel filtered in storage buffer (50 mM HEPES pH 7.5, 50 mM NaCl, 5 mM $MgCl_2$, 2 mM DTT, 10% (v/v) glycerol) over a Superdex 200 16/60 column. Peak fractions were pooled, concentrated as before and glycerol was added to a total of 20%. The protein was snap-frozen in liquid nitrogen and stored at -80 °C.

wCRIB, 2xwCRIB and pTPR

Coding sequences for the isolated CRIB domain (aa: 201-268) of human WASP (Uniprot: P42768), the coding sequence of the corresponding tandem CRIB domain separated by a GAPSGGGATAGAGGGGPAG linker or the coding sequence of the three TPR domains (aa: 1-203) of human p67phox (Uniprot: P19878) were extended by a N-terminal 5xglycine-tag to allow for protein labelling by Sortase-mediated peptide ligation. To optimize protein translation in bacteria, coding sequences were codon optimized for *E. coli* expression prior to DNA synthesis (GeneStrand from Eurofins). The synthesized coding sequence was cloned into a pETM60 vector containing a TEV cleavable N-terminal NusA-tag. Chemically competent Star pRare pACYC *E. coli* cells were transformed with the respective construct. 50 mL lysogeny broth (LB), supplemented with antibiotics (see Materials: Bacterial strains and insect cell lines, Recombinant DNA constructs), were inoculated with a positive clone and cultured overnight at 30 °C. The culture was expanded on the next day to a total volume of 2-6 L with terrific broth (TB) supplemented with the respective antibiotics and kept at 37 °C. After achieving an OD_{600} of 0.8-1.2 the culture was cooled down to 15 °C, subsequently induced with 50 µM IPTG and incubated at 15 °C overnight. Cell harvesting was accomplished by centrifugation at 3500 x g for 20 min at 4 °C. Pellets were snap-frozen in liquid nitrogen and stored at -80 °C.

For purification, frozen pellets were thawed for 10 min at RT, put immediately back on ice and resuspended in a 5x volume of lysis buffer (50 mM HEPES pH 7.5, 100 mM NaCl, 50 mM arginine, 50 mM glutamic acid, 0.4 mM β-mercaptoethanol, 15 µg/mL Benzamidine, 10% (v/v) glycerol, 1 mM PMSF, ~10 µg/mL DNAse1, 1 EDTA free protease inhibitor tablet/100 mL). Cell suspension was homogenized by 7-10 cycles in a dounce

homogenizer on ice and lysis was completed with a high-pressure homogenizer at 4 °C. Lysate was centrifuged at 142,000 x g for 1 h at 4 °C and further clarified by filtering the supernatant through a 0.45 µm syringe filter. Following clarification of the lysate, affinity purification on a 5 mL HiTrap Chelating HP column loaded with 200 mM $CoCl_2$, washed with water and equilibrated with equilibration buffer (50 mM HEPES pH 7.5, 100 mM NaCl, 50 mM Arginine, 50 mM Glutamic acid, 0.4 mM β-mercaptoethanol, 15 µg/mL Benzamidine, 10% (v/v) glycerol) was performed. The filtrate was recirculated over the equilibrated column for 2-3 h at 4 °C. After washing the column with equilibration buffer, the protein was eluted over a linear gradient (6 column volumes (CV)) of equilibration buffer containing 500 mM imidazole. Peak fractions of the eluate were pooled and the NusA-tag was removed by TEV cleavage (His-TEV, molar ratio 1:30) at 4 °C overnight. Removal of imidazole from the cleaved protein and general desalting was performed with a HiPrep 26/10 Desalting column equilibrated with MonoS low salt buffer (5 mM HEPES pH 7.5, 10 mM NaCl, 7.5 mM arginine, 7.5 mM glutamic acid, 0.4 mM β-mercaptoethanol, 10% (v/v) glycerol). Desalted protein was subjected to cation exchange chromatography using a MonoS 15/50 GL column (GE Healthcare) and eluted over a 30 CV linear gradient of MonoS high salt buffer (5 mM HEPES pH 7.5, 750 mM NaCl, 7.5 mM arginine, 7.5 mM glutamic acid, 0.4 mM βME, 10% (v/v) glycerol). Peak fractions were pooled and gel filtered in storage buffer (50 mM HEPES pH 7.5, 100 mM NaCl, 50 mM Arginine, 50 mM Glutamic acid, 1 mM TCEP, 10% (v/v) glycerol) over a Superdex 75 16/600 column. Peak fractions were pooled, concentrated as before and glycerol was added to a total of 20%. Proteins were snap-frozen in liquid nitrogen and stored at -80 °C.

(2x)GBD-GAP/GEF chimeras

Chimeras were designed by fusing a GTPase binding domain (GBD) or the corresponding tandem GBD separated by a GAPSGGGATAGAGGGGPAG linker to either the catalytic domain of a GAP or a GEF again separated by a GAPSGGGATAGAGGGGPAG linker. The following constructs and their 2xGBD variants were designed: (2x)rREM-Abr where the REM domain (aa: 1-89) of mouse Rhotekin (Uniprot: Q8C6B2, Isoform 2) was fused to the catalytic domain (aa: 627-859) of human Abr (Uniprot: Q12979, Isoform Long), (2x)pTPR-ArhGAP29 where the three TPR domains (1-203) of human p67phox (Uniprot: P19878, Isoform 1) were fused to the catalytic domain (aa: 658-898) of human ArhGAP29 (Uniprot: Q52LW3), p2CRIB-ArhGAP29 where the CRIB domain (35-149) of human PAK2

(Uniprot: Q13177) was fused to the catalytic domain (aa: 658-898) of human ArhGAP29 (Uniprot: Q52LW3, Isoform 1), (2x)pTPR-ITSN where the three TPR domains (1-203) of human p67phox (Uniprot: P19878, Isoform 1) were fused to the catalytic domain (aa:1229-1449, K1367R) of human Intersectin (Uniprot: Q15811, Isoform 1) and (2x)wCRIB-Tiam1 where the CRIB domain (aa: 201-268) of human WASP (Uniprot: P42768) was fused to the catalytic domain (aa: 1033-1265) of human Tiam1 (Uniprot: Q13009, Isoform 1). Coding sequences for the chimeras were extended by a N-terminal 5xglycine-tag to allow for protein labelling by Sortase-mediated peptide ligation. To optimize protein translation in bacteria, coding sequences were codon optimized for *E. coli* expression prior to DNA synthesis (GeneStrand from Eurofins). The synthesized coding sequence was cloned into a pETM60 vector containing a TEV cleavable N-terminal NusA-tag. Chemically competent Star pRare pACYC *E. coli* cells were transformed with the respective construct. 50 mL lysogeny broth (LB), supplemented with antibiotics (see Materials: Bacterial strains and insect cell lines, Recombinant DNA constructs), were inoculated with a positive clone and cultured overnight at 30 °C. The culture was expanded on the next day to a total volume of 2-6 L with terrific broth (TB) supplemented with the respective antibiotics and kept at 37 °C. After achieving an OD_{600} of 0.8-1.2 the culture was cooled down to 15 °C, subsequently induced with 50 µM IPTG and incubated at 15 °C overnight. Cell harvesting was accomplished by centrifugation at 3500 x g for 20 min at 4 °C. Pellets were snap-frozen in liquid nitrogen and stored at -80 °C.

For purification, frozen pellets were thawed for 10 min at RT, put immediately back on ice and resuspended in a 5x volume of lysis buffer (50 mM HEPES pH 7.0, 100 mM NaCl, 50 mM arginine, 50 mM glutamic acid, 0.4 mM β-mercaptoethanol, 15 µg/mL Benzamidine, 10% (v/v) glycerol, 1 mM PMSF, ~10 µg/mL DNAse1, 1 EDTA free protease inhibitor tablet/100 mL). Cell suspension was homogenized by 7-10 cycles in a dounce homogenizer on ice and lysis was completed with a high-pressure homogenizer at 4 °C. Lysate was centrifuged at 142,000 x g for 1 h at 4 °C and further clarified by filtering the supernatant through a 0.45 µm syringe filter. Following clarification of the lysate, affinity purification on a 5 mL HiTrap Chelating HP column loaded with 200 mM $CoCl_2$, washed with water and equilibrated with equilibration buffer (50 mM HEPES pH 7.0, 100 mM NaCl, 50 mM Arginine, 50 mM Glutamic acid, 0.4 mM β-mercaptoethanol, 15 µg/mL Benzamidine, 10% (v/v) glycerol) was performed. The filtrate was recirculated over the equilibrated column for 2-3 h at 4 °C. After washing the column with equilibration buffer,

the protein was eluted over a linear gradient (6 column volumes (CV)) of equilibration buffer containing 500 mM imidazole. Peak fractions of the eluate were pooled and the NusA-tag was removed by TEV cleavage (His-TEV, molar ratio 1:30) at 4 °C overnight. Removal of imidazole from the cleaved protein was performed with a HiPrep 26/10 Desalting column equilibrated with equilibration buffer at 4 °C. To remove His-TEV and the cleaved NusA-tag, the buffer exchanged and cleaved protein was recirculated over a 5 ml HiTrap Chelating HP equilibrated with equilibration buffer for 1-2 h at 4 °C. The flow-through was collected, concentrated using Vivaspin concentrators with a molecular weight cut-off of 10 kDa and gel filtered in storage buffer (50 mM HEPES pH 7.5, 100 mM NaCl, 50 mM Arginine, 50 mM Glutamic acid, 1 mM TCEP, 10% (v/v) glycerol) over a Superdex 200 16/60 column. Peak fractions were pooled, concentrated as before and glycerol was added to a total of 20%. Proteins were snap-frozen in liquid nitrogen and stored at -80 °C.

DrrA-OCRL

The chimeric 5'phosphatase consists of the PI(4)P-binding domain (aa: 544-647) of DrrA/SidM from *L. pneumophila* (Uniprot: Q29ST3) fused via a GSGGGGGTS linker to the catalytic 5'phosphatase domain (aa: 234-539) of phosphoinositide 5-phosphatase OCRL (Uniprot: A0A2R8YG38). The coding sequence was cloned into a modified pET expression vector containing an N-terminal 6xHis-MBP-Asn_{10}-TEV-Gly_5-tag.
The protein was expressed in BL21 (DE3) *E. coli* cells and afterwards purified by cobalt affinity chromatography followed by a subsequent gel filtration step as previously described (Hansen et al., 2019)

From insect cells

Full length N-WASP

Full length human N-WASP (Uniprot: O00401) was cloned from a cDNA clone into a modified pLib vector (Weissmann et al., 2016) containing a TEV-cleavable 6xHis-tag and transformed into DH10Bac-competent *E. coli* (Thermo Fisher). A positive clone was selected by blue-white screening and used to generate Bacmid DNA. Sf-9 insect cells (1 $x10^6$ cells) were transfected with the purified bacmid DNA together with FuGene6 transfection reagent and incubated for 5 days at 27 °C. After two passages, the cell suspension was spun down at 100 x g for 10 min at RT, the supernatant was filtered, 10 %

FBS added and stored at 4 °C. TnaO38 suspension culture (c = 1x10^6 cells/mL) was infected with virus, incubated for 4 days and pelleted by centrifugation at 868 x g for 20 min at 18 °C.

For purification, frozen pellets were thawed for 10 min at RT, put immediately back on ice and resuspended in a 3x volume of lysis buffer (25 mM Tris pH 7.5, 150 mM NaCl, 0.5 mM EDTA, 5 mM β-mercaptoethanol, 15 µg/mL Benzamidine, 10% (v/v) glycerol, ~10 µg/mL DNAse1, 1 EDTA-free cOmplete protease inhibitor tablets/50 mL). Cell suspension was homogenized by 7-10 cycles in a dounce homogenizer on ice and lysis was completed with a high-pressure homogenizer at 4 °C. Lysate was centrifuged at 142,000 x g for 1 h at 4 °C and further clarified by filtering the supernatant through a 0.45 µm syringe filter. Following clarification of the lysate, affinity purification on a HisTrap excel column equilibrated with equilibration buffer (25 mM Tris pH 7.5, 150 mM NaCl, 0.5 mM EDTA, 5 mM β-mercaptoethanol, 15 µg/mL Benzamidine, 10% (v/v) glycerol) was performed. The filtrate was recirculated over the equilibrated column for 2-3 h at 4 °C. After washing the column with equilibration buffer, the protein was eluted over a linear gradient (6 column volumes (CV)) of equilibration buffer containing 500 mM imidazole. Peak fractions of the eluate were pooled and the 6xHis-tag was removed by TEV cleavage (His-TEV, molar ratio 1:30) at 4 °C overnight. Cleaved protein was gel filtered in storage buffer (25 mM Tris pH 7.5, 150 mM NaCl, 1 mM TCEP, 20% (v/v) glycerol) over a HiLoad Superdex 200 16/600 column.

The protein was passed through a HiPrep 26/10 Desalting column (GE-Healthcare) equilibrated with MonoS low salt buffer (5 mM HEPES pH 7.5, 10 mM NaCl, 7.5 mM arginine, 7.5 mM glutamic acid, 0.4 mM β-mercaptoethanol, 10% (v/v) glycerol). Desalted protein was subjected to cation exchange chromatography using a MonoS 15/50 GL column (GE Healthcare) and eluted over a 30 CV linear gradient of MonoS high salt buffer (5 mM HEPES pH 7.5, 750 mM NaCl, 7.5 mM arginine, 7.5 mM glutamic acid, 0.4 mM β-mercaptoethanol, 10% (v/v) glycerol). Peak fractions were pooled and buffer exchanged via Nap5 columns equilibrated with storage buffer prior to maleimide labeling.

PIP5K

The kinase domain (aa: 1-421) of human Phosphatidylinositol 4-phosphate 5-kinase type-1 beta (Uniprot: O14986-3) in frame with a N-terminal his6-MBP-(Asn)10 -TEV-GGGGG fusion. The coding sequence was cloned into a FastBac1 vector to generate Bacmid DNA

for insect cell expression. The protein was expressed in TnaO38 insect cells and afterwards purified by nickel affinity chromatography followed by cation exchange chromatography and a subsequent gel filtration step as previously described (Hansen et al., 2019).

Protein labeling, prenylation and complex formation

Protein modifications

Prenylation

For the *in vitro* prenylation of Cdc42 a reaction mix was prepared in prenylation reaction buffer (50 mM HEPES pH 7.5, 50 mM NaCl, 2 mM $MgCl_2$, 2% w/v CHAPS, 2 mM DTT). The different components of the reaction mix were pipetted in the following order: 10 µM $ZnSO_4$, 10% (v/v) glycerol, 58.8 µM Cdc42, 9.2 µM GGTase1, 148 µM geranylgeranyl pyrophosphate (GGPP). The reaction mix was protected from light and rotated on a disc rotator at 4 °C overnight. Prenylated Cdc42 was concentrated using Vivaspin concentrators with a molecular weight cut-off of 10 kDa and gel filtered in prenylation buffer (50 mM HEPES pH 7.5, 50 mM NaCl, 2 mM $MgCl_2$, 0.5% w/v CHAPS, 2 mM DTT) over a Superdex 200 16/60 column. Peak fractions were pooled, concentrated as before and protein concentration was determined. If prenylated and labeled Cdc42 was required sortase-mediated peptide ligation (see Methods: Sortase-mediated labeling) was performed before complex formation with RhoGDI1 or RabGGtase β (see Methods: GTPase:RhoGDI1 and GTPase:RabGGtase β).

Sortase-mediated labeling

For sortase-mediated labeling, respective NHS-Dyes were first conjugated to LPETGG peptides (Genscript). A reaction mix of 40 mM NHS-Dye, 20 mM peptide and 30 mM triethylamine in DMSO was incubated overnight shielded from light in a mixing heat block at 42 °C and 750 rpm. The reaction was quenched by the addition of Tris-Cl (pH 8.0) to a final concentration of 100 mM followed by an incubation period of 12 h at room temperature. Final dye-LPETGG conjugates were then stored at -20 °C.

Sortase-mediated labeling reactions of proteins containing the N-terminal penta-glycine motif were started by mixing a > 250 µM of the substrate protein, 4x - 7x molar excess of dye-LPETGG and the sortase at $1/3^{rd}$ of the substrate protein concentration in labelling buffer (150 mM KCl, 0.5 mM TCEP). Furthermore, $CaCl_2$ and Tris-HCl (pH = 8) were added

at a final concentration of 6 mM and 150 mM respectively. The reaction mix was incubated overnight at 16 °C while spinning at 16000 x g. To remove excess dye-LPETGG conjugate and sortase, proteins were passed through a HiLoad Superdex 75 10/300 equilibrated with storage buffer (buffer as described in Methods: protein purification). Peak fractions were pooled, concentrated, final glycerol concentration increased to 20% and labelling efficiency determined. Labeled proteins were snap-frozen in liquid nitrogen and stored at -80 °C or carried forward to complex formation.

Maleimide labeling

Full length N-WASP was mixed in maleimide labeling buffer buffer (50 mM HEPES pH 7.5, 50 mM NaCl and 2 mM $MgCl_2$) with a 7x molar excess of Atto488-maleimide and incubated overnight on ice. To quench the reaction DTT was added to a final concentration of 5 mM and the reaction mix was incubated for 10 min on ice. To remove excess Atto488-maleimid, proteins were passed through a HiLoad Superdex 200 10/300 equilibrated with storage buffer (25 mM Tris pH 7.5, 150 mM NaCl, 1 mM TCEP, 20% glycerol). Peak fractions were pooled, concentrated, final glycerol concentration increased to 20% and labelling efficiency determined. Labeled full length N-WASP was snap-frozen in liquid nitrogen and stored at -80 °C.

Complex formation

Nucleotide exchange

For the nucleotide exchange of Rho GTPases, a reaction mix was prepared in nucleotide exchange buffer (50 mM HEPES pH 7.5, 50 mM NaCl, 10 mM β-mercaptoethanol). The different components of the reaction mix were pipetted in the following order: 100 μM Rho GTPase, 500 μM nucleotide (mant-GDP, mant-GppNHp, Cy3-GTP or TAMRA-GTP), 2 mM EDTA. To destabilize the native nucleotide the reaction mix was incubated for 30 min at 4 °C protected from light. Simultaneously, two Zeba Spin Desalting columns (Thermo Fisher) were placed in a 2 mL Eppendorf tube each and spun at 1500 x g for 1 min at 4 °C to remove the column storage buffer. Columns were washed by adding 300 μL of nucleotide exchange buffer to the columns followed by a centrifugation step as above and the subsequent discarding of the flow through. This wash step was repeated an additional two times. To passivate the column, 300 uL of nucleotide exchange buffer supplemented with 1 mg/mL β-casein were added to the columns and incubated at room

temperature for 2 min. Buffer was removed by centrifugation of the columns at 1500 x g for 2 min at 4 °C and the flow through was discarded. The wash step with nucleotide exchange buffer as described above was repeated three times and the columns were transferred to a new 1.5 mL low-protein-binding Eppendorf tube. 100 uL of the reaction mix were added to one of the columns and incubated at room temperature in the dark for 2 min. Columns were then spun at 1500 x g for 2 min at 4 °C and the flow-through was collected. The flow-through was then passed over the second desalting column prepared as described above. Glycerol was added to the flow-through to a final concentration of 20%. The nucleotide exchanged Rho GTPases were snap-frozen in liquid nitrogen and stored at -80 °C.

GTPase:RhoGDI1 and GTPase:RabGGtase β

To form a stoichiometric complex, equimolar ratios of prenylated, labeled Cdc42 were mixed with RhoGDI1 and incubated on ice for 10 min. The complex was then gel filtered in gel filtration buffer (50 mM HEPES pH 7.5, 50 mM NaCl, 2 mM $MgCl_2$, and 2 mM DTT) over a Superdex 75 10/300 column. Peak fractions were pooled and concentrated. To remove residual detergent, a detergent removal kit (Pierce) was used. Two columns were placed in a 2 mL Eppendorf tube each and spun at 1500 x g for 1 min at 4 °C to remove the column storage buffer. Columns were washed by adding 300 μL of gel filtration buffer followed by a centrifugation step as above and the subsequent discarding of the flow through. This wash step was repeated an additional two times. To passivate the column, 300 uL of gel filtration buffer supplemented with 1 mg/mL β-casein were added to the column and incubated at room temperature for 2 min. Buffer was removed by centrifugation of the columns at 1500 x g for 2 min at 4 °C and the flow through was discarded. The wash step with gel filtration buffer as described above was repeated three times and the columns were transferred to a new 1.5 mL low-protein-binding Eppendorf tube. 100 uL of the Cdc42:RhoGDI1 complex were added to one of the columns and incubated at room temperature in the dark for 2 min. Columns were then spun for 2 min at 1500 x g at 4 °C and the flow-through was collected. The flow-through was then passed over the second detergent removal column prepared as described above. Glycerol was added to the flow-through to a final concentration of 20%. The formed Cdc42:RhoGDI1 was snap-frozen in liquid nitrogen and stored at -80 °C.

Complex formation with RabGGtase β is performed similarly except for the 1.2x molar excess of RabGGtase β used over prenylated Cdc42 for complex formation and the exchange of the gel filtration step with simple desalting of the Cdc42:RabGGtase β complex via Nap 5 columns equilibrated with gel filtration buffer.

Preparation of supported lipid bilayers (SLBs)

Glassware cleaning

All glassware involved in the preparation of lipids was washed similarly. First, the glassware was submerged in 5% Hellmanex III for 45 min at 60 °C in a dry oven. The cleaning solution was discarded and the glassware was rinsed five times with ultrapure water. Glassware was submerged in a solution of 50% 2-propanol:50% ultrapure water, sealed with Parafilm and sonicated for 30 min. After sonication, glassware was again rinsed five times with ultrapure water and placed back in the dry oven at 60 °C to completely dry overnight.

Round-bottom flasks were washed as described above, however, after the final rinsing, both the flasks and stoppers were submerged in piranha solution (5 parts sulfuric acid to 3 parts hydrogen peroxide (30%)) for ≥90 min. The flasks were rinsed with ultrapure water as above and placed in a clean beaker in the 60 °C dry oven to dry overnight.

Preparation of SUVs

A total amount of 1 mM of the desired lipid species (26.5% DOPC, 26.5% DOPE, 22.5% DOPS, 2% PI(4)P, 2% PI(4,5)P_2, 0.5% PEG5000, 20% cholesterol) were mixed from their stock solutions in a total volume of 1 ml of chloroform in round-bottom flask and attached to a rotary evaporator. Lipids were dried to a thin film under vacuum rotating at 110 rpm in a 35 °C water bath. Once the solvent completely evaporated, the flasks were placed in a desiccator under vacuum for 30 min. Dried lipids were resuspended to a final concentration of 1 mM in PBS by gentle vortexing for 2 min. SUVs were prepared by extruding the resuspended lipid mixture with a 30 nm filter 11 times. SUVs were stored in brown glass vials at 4 °C for up to 3 days.

SLB formation

Coverslips (Coverslips for sticky-Slides 1.5H Glass, Ibidi) were incubated in 5% Hellmanex III at 60 °C in the dry oven for 45 min. They were then rinsed 5 times with ultrapure water

and submerged in piranha solution (5 parts sulfuric acid to 3 parts hydrogen peroxide (30%)) overnight. Coverslips were rinsed with ultrapure water and dried with an argon line. Sticky slides VI (Ibidi) were plasma cleaned for 3 min and stuck to the coverslips. These "chambers" were placed on a pre-heated metal block at 45 °C for 2.5 min, lipid mixture was added and incubated for additional 2.5 min. At this point, moving the chambers from the heat block was omitted as it would interfere with the SLB formation. To burst SUVs, NaCl (500 mM final concentration) was flushed into the chamber and pipetted gently from each end to ensure proper mixing. Chambers were then incubated for 30 min at 45 °C. Following incubation, chambers were washed, each with 5 mL of PBS followed by 1 mL of kinase buffer (20 mM HEPES pH 8.0, 150 mM NaCl, 5 mM $MgCl_2$, 0.5 mM EGTA). The heat block was switched off and allowed to cool to RT over several hours only then chambers were removed from the heat block.

Flow chamber assembly

Counter slides were plasma cleaned for 3 min and small pieces of double-sided tape were attached, while leaving space in between each piece to create flow chambers. Coverslips were gently attached to the counter slides and flow chambers were passivated with either β-casein or PLL-PEG for 3 min at room temperature. Afterwards flow chambers were washed with 150 µL of MilliQ water.

Biochemical assays

GAP assays

Nucleotide hydrolysis assays were set up by diluting Cy3-GTP:RhoA or TAMRA-GTP:Cdc42 (or Rac1) to 100 nM in hydrolysis buffer (50 mM Tris-HCl pH 7.5, 10 mM K_2HPO_4/KH_2PO_4, $MgCl_2$, 10 mM β-mercaptoethanol, 100 µg/mL β-casein). The GAP chimera (rREM-Abr_{cat} or p2CRIB-$ArhGAP29_{cat}$) was pre-diluted in hydrolysis buffer. The diluted Rho GTPase was transferred to a quartz cuvette with a pathlength of 10 mm. After acquiring an initial baseline for 150 s, the GAP chimera was added to achieve the respective concentration as stated in the specific figures and imaging was continued under constant stirring at room temperature. Fluorescence intensities were measured at 1 s intervals by exciting at 520 nm and measuring emission at 575 nm for Cy3-GTP or by exciting at 535 nm and measuring emission at 583 nm for TAMRA-GTP via a QuantaMaster Fluorometer (PTI).

GEF assays

Nucleotide exchange reactions were set up by separately preparing multiple 2xGEF chimera mixes and a 2xGTPase mix. For the 2xGEF chimera mixes, a serial dilution of the respective GEF chimeras (pTPR-ITSN$_{cat}$ or wCRIB-Tiam1$_{cat}$) was prepared by diluting samples of the serial dilution to 2x working concentration as stated in the specific figures in GEF buffer (50 mM Tris-HCl pH 7.5, 10 mM K_2HPO_4/KH_2PO_4, 0.2 mM GTP, 10 mM β-mercaptoethanol, 100 µg/mL β-casein). For the 2xGTPase mix, nucleotide exchanged Rho GTPases (mant-GDP:Cdc42 or mant-GDP:Rac1) were diluted to 200 nM in GEF buffer without GTP. The reaction was then immediately initiated by mixing equal volumes of the 2xGEF chimera mix (multiple samples of the serial dilution) with the 2xGTPase mix in a 96-well plate. Fluorescence intensities were measured at 10 s intervals by exciting at 365 nm and measuring emission at 450 nm via a Tecan Spark fluorescence plate reader.

Binding assays

Bead assays

Activated thiol Sepharose 4B beads (100 uL) were resuspended in 1 mL of MilliQ water followed by centrifugation at 1000 x g for 1 min at 4 °C. Supernatant was discarded and the wash step repeated once more with 1 mL of MilliQ water and twice with 1 mL of coupling buffer (1xPBS, 1 mM $MgCl_2$, 0.1 mM GDP, 0.1 mM TCEP). Washed thiol beads were resuspended in 1 mL of coupling buffer and 150 uL of this bead slurry were mixed with 0.2 mg of the respective protein used for coating (RhoAQ63L or dCherry). The bead-protein mixture was incubated while rotating for 1 h at 4 °C. The protein coated beads were washed thrice with kinase buffer (20 mM HEPES pH 7.0, 150 mM NaCl, 5 mM $MgCl_2$, 0.1 mM GTP, 20 mM β-mercaptoethanol, 200 µg/mL β-casein) as described above and resuspended in a final volume of 100 uL of kinase buffer. The protein-coated bead slurry was mixed with 100 µL of the respective ligand (rREM-Abr$_{cat}$) diluted to 800 nM in kinase buffer and incubated for 3 min at room temperature. Flow chambers were prepared as described before (see Methods: Flow chamber assembly) and 20 uL of the final protein-coated bead slurry was added to the flow chambers. Beads were imaged using a widefield microscope with 20 ms exposure.

Microscale thermophoresis

A serial dilution (80 µM to ~2.4 nM) of the ligand (pTPR) was prepared in MST buffer (20 mM HEPES pH 7.5, 150 mM NaCl, 0.1% Triton X-100, 10 mM β-mercaptoethanol). To account for the carry-over of glycerol by the ligand stock solution, each dilution sample was adjusted to a final glycerol concentration of 2%. For a 2xGTPase mix, A647-Rac1Q61L was diluted in MST buffer to a final concentration of 400 nM. Each glycerol-adjusted ligand sample of the dilution series was mixed with equal volumes of the 2xGTPase mix and Monolith Nt. 115 Premium Capillaries were filled with the resulting mix by capillary forces. Capillaries were placed in the respective holder of the Monolith Nt. 115 and the 'Binding affinity' routine of the NT Analysis software from NanoTemper was initiated at 25 °C.

Nucleotide dissociation inhibition assays

Nucleotide dissociation inhibition assays were set up by separately preparing multiple 2xGEF chimera mixes and a 2xGTPase mix. For the 2xGEF chimera mixes, a serial dilution of the respective GEF chimera (wCRIB-Tiam1$_{cat}$) was prepared by diluting samples of the serial dilution to 2x working concentration as stated in the specific figures in GEF buffer (50 mM Tris-HCl pH 7.45, 10 mM K_2HPO_4/KH_2PO_4, 0.2 mM GppNHp, 10 mM β-mercaptoethanol, 100 µg/mL β-casein). For the 2xGTPase mix, nucleotide exchanged Rho GTPases (mant-GppNHp:Cdc42) were diluted to 200 nM in GEF buffer without GppNHp. The reaction was then immediately initiated by mixing equal volumes of the 2xGEF chimera mix (multiple samples of the serial dilution) with the 2xGTPase mix in a 96-well plate. Fluorescence intensities were measured at 10 s intervals by exciting at 365 nm and measuring emission at 450 nm via a Tecan Spark fluorescence plate reader.

TIRF microscopy-based assays

Membrane fluidity

To assess membrane fluidity of the SLBs made with the PM-Mix of lipids, Fluorescence recovery after photobleaching (FRAP) experiments were conducted. Supported lipid bilayers were prepared as described above with a lipid composition of 26.49% DOPC, 26.5% DOPE, 22.5% DOPS, 2% PI(4)P, 2% PI(4,5)P_2, 0.5% PEG5000, 20% cholesterol and 0.01% 18:1 Lissamine rhodamine-PE (molar fraction). TIRF images of the bilayer were captured at 1-second time intervals for 5 s to acquire a baseline. SLBs were photobleached

for 3 s in a defined area at 100% laser power using the Visitron system (Visitron systems). Imaging was continued as above for a total of 2 min.

Lipid pattern formation and visualization

Following supported lipid bilayer preparation (see Methods: Preparation of supported lipid bilayers (SLBs)), chambers were washed with 1 mL imaging buffer (20 mM HEPES pH 8.0, 150 mM NaCl, 5 mM $MgCl_2$, 0.5 mM EGTA, 1 mM GTP, 1 mM ATP, 20 mM β-mercaptoethanol, 200 µg/mL β-casein, 1.25 mg/mL glucose oxidase, 0.2 mg/mL catalase and 400 mg/mL glucose).

For lipid pattern formation, 20 nM PIP5K and 6 nM DrrA-OCRL diluted in imaging buffer were added to the flow chamber, if not stated otherwise in the figure legend.

To visualize the developing lipid pattern, additionally 2 nM A488-DrrA and 2 nM A647-PH diluted in imaging buffer were included in the protein mix that was added to the flow chamber to observe PI(4)P and PI(4,5)P_2 respectively. Bilayers were imaged in TIRFM for 40 min with 100 ms exposure at 10-second time intervals.

GEF localization and densities

Following supported lipid bilayer preparation (see Methods: Preparation of supported lipid bilayers (SLBs)), chambers were washed with 1 mL imaging buffer (20 mM HEPES pH 8.0, 150 mM NaCl, 5 mM $MgCl_2$, 0.5 mM EGTA, 1 mM GTP, 1 mM ATP, 20 mM β-mercaptoethanol, 200 µg/mL β-casein, 1.25 mg/mL glucose oxidase, 0.2 mg/mL catalase and 400 mg/mL glucose).

Lipid patterns were formed and allowed to stabilize for 10 - 15 min in the presence of "base mix" (2 nM A647-PH, 20 nM PIP5K and 6 nM Drra-OCRL) in fresh imaging buffer. TIRF images of the bilayer were captured at 10-second time intervals for 3 min at 100 ms exposure to acquire a baseline. Imaging was paused, "Base mix" with 1 nM A488-$ITSN_{cat}$-PH in fresh imaging buffer was then flushed into the chamber and imaging was resumed for a total of 10 min.

For GEF density measurements microscope settings were adjusted to an exposure of 22 ms. Additionally, the labeled fraction of (A488-)$ITSN_{cat}$-PH was reduced (5-, 10- , 20- or 50-fold) to reach single molecule regime.

Membrane-templated Rho GTPase patterns (bulk and single molecule)

Following supported lipid bilayer preparation (see Methods: Preparation of supported lipid bilayers (SLBs)), chambers were washed with 1 mL imaging buffer (20 mM HEPES pH 8.0, 150 mM NaCl, 5 mM $MgCl_2$, 0.5 mM EGTA, 1 mM GTP, 1 mM ATP, 20 mM β-mercaptoethanol, 200 μg/mL β-casein, 1.25 mg/mL glucose oxidase, 0.2 mg/mL catalase and 400 mg/mL glucose).

Lipid patterns were formed and allowed to stabilize for 10-15 min in the presence of supplemented "base mix" (20 nM PIP5K, 6 nM DrrA-OCRL, 2 nM Cy3-PLCδ(PH)) in fresh imaging buffer. The supplements varied with experiments and are detailed in figure legends where appropriate. Supplements used were: 1) Cdc42; provided either alone (5.5 nM) or in 1:1 complex with RhoGDI1 (600 nM) (formed *in situ*). 2) An activity readout (either 40 nM A488-wCRIB, 20 nM A488-2xwCRIB or 40 nM Atto488-N-WASP). 3) A soluble GAP (20 nM $OPHN1_{cat}$). TIRF images of the bilayer were captured at 10-second time intervals for 3 min at 100 ms exposure to acquire a baseline. Imaging was paused, supplemented "base mix" with 1 nM $ITSN_{cat}$-PH in fresh imaging buffer was then flushed into the chamber and imaging was resumed for a total of 10 min.

For single molecule experiments of Cdc42 on patterned SLBs, the labeled fraction of (A647-) Cdc42 was reduced (100-fold) to reach single molecule regime. Membrane-templated Cdc42 patterns were allowed to form for 5 min (as described above). Next, single molecule TIRFM movies were captured at 22 ms exposure and continuous illumination for 1 min.

Cdc42 dwell time measurements

Following supported lipid bilayer preparation (see Methods: Preparation of supported lipid bilayers (SLBs)), chambers were washed with 1 mL imaging buffer (20 mM HEPES pH 8.0, 150 mM NaCl, 5 mM $MgCl_2$, 0.5 mM EGTA, 1 mM GTP, 1 mM ATP, 20 mM β-mercaptoethanol, 200 μg/mL β-casein, 1.25 mg/mL glucose oxidase, 0.2 mg/mL catalase and 400 mg/mL glucose).

Lipid patterns were formed and allowed to stabilize for 10-15 min in the presence of supplemented "base mix" (20 nM PIP5K, 6 nM DrrA-OCRL, 2 nM Cy3-PLCδ(PH)) in fresh imaging buffer. Fixed supplements were 1) Cdc42; provided alone (5.5 nM). 2) A soluble GAP (20 nM $OPHN1_{cat}$). Some supplements varied with experiments and are detailed in figure legends where appropriate. Varying supplements were the activity readout (either

40 nM A488-wCRIB or 20 nM A488-2xwCRIB). After flushing in fresh supplemented “base mix” with 1 nM $ITSN_{cat}$-PH in fresh imaging buffer, membrane templated Cdc42 patterns were allowed to form for 5-10 min. Next, TIRF images were acquired every 5 s with 100 ms exposure for 70 s to establish a baseline. A flow of supplemented “base mix” in fresh imaging buffer without Cdc42 but with 22 nM GDI was initiated (5 μL/s) via a syringe pump whilst continuing to image as above for a minimum of 200 s total.

Data analysis

Membrane fluidity

Time traces of the normalized fluorescence intensity in FRAP regions were measured with Fiji (Schindelin et al., 2012) and were fitted with a mono exponential function in Origin (OriginLab Corporation).

Segmentation of Cdc42 patterns

The lipid patterns visualized by the A647-PH marker were segmented using custom scripts written in house by Dr. Ankit Roy. The scripts execute denoising, equalization, and pattern segmentation (autoSegmentation_dice-N-splice_LipidPatch.py and autoSegmentation_LipidPatch.py). Initially, the A647-PH channel time series underwent denoising using a Non-Local Means algorithm from Scikit-Image's restoration module. Post-denoising, histogram equalization was implemented to uniformly readjust contrast levels across all image sections. An adaptive Histogram Equalization method (CLAHE) from OpenCV was employed for this purpose. Lastly, the histogram-equalized image timeseries was segmented through application of a Random Walker Segmentation algorithm, featuring two distinct labels: one for lipid pattern regions and another for areas exterior to the pattern. Preliminary markers for these regions were designated by assigning markers based on the histogram's splitting points above (inside the pattern) and below (outside the pattern) the 50th percentile. Following segmentation, regions underwent expansion from their initial markers, subsequently removing any errant pixels via execution of five iterations of binary closing and binary opening using Scipy's ndimage module. Segmentation scripts are publicly accessible through our GitHub repository.

Calculation of the patterning index

Using the segmentation map generated from the lipid channel, an "inside" (high $PI(4,5)P_2$) and "outside" (high PI(4)P) region was designated for each frame. Images were analyzed in Fiji (Schindelin et al., 2012) with a custom Macro (see Source Code). Briefly, mean intensity values of both regions were measured and the values from "inside" were divided by the values from "outside" for both total- and active-Cdc42. The resulting ratio was termed "patterning index (PI)".

Single molecule tracking of total Cdc42

Following segmentation, A647-Cdc42 was tracked using the Fiji plugin Trackmate (Tinevez et al., 2017). Individual spots were detected, and corresponding tracks generated, with spot statistics provided in an output file for both "inside" and "outside" regions. Statistics for Cdc42 tracks were used as an input for our custom scripts, StepSize-distribution.R and MSD-distribution.py to determine metrics such as step size and MSD distributions. The source codes for these scripts are hosted publicly on GitHub.

Calculation of GEF density for single molecule TIRFM assays

A488-$ITSN_{cat}$-PH spots were counted with the Fiji plugin Trackmate (Tinevez et al., 2017). Assuming a linear relationship between the spot number and labeling ratio of A488-$ITSN_{cat}$-PH, GEF densities were calculated inside $PI(4,5)P_2$-rich regions by plotting spot number vs labeled $ITSN_{cat}$-PH concentration and fitting the data with a linear function in Origin (OriginLab Corporation).

GAP and GEF assays

Observed rate constants were obtained by fitting the titration data from GAP and GEF assays with a mono exponential function in Origin (OriginLab Corporation). Observed rate constants were plotted as a function of chimera concentration and catalytic efficiencies were acquired by fitting the data with a linear function in Origin (OriginLab Corporation).

Binding assays

Bead assays

Widefield microscopy images of bead assays were analyzed with Fiji (Schindelin et al., 2012). After background subtraction, individual beads were detected using Fiji's 'Analyze Particles' function and average intensities were measured.

Microscale thermophoresis

MST data were analyzed with the NT Analysis software from NanoTemper using the 'Binding affinity' routine following the manufacturer's instructions. Affinity values were acquired by fitting the binding curves of the titration experiment with the K_d-fit function of the NT Analysis software.

Nucleotide dissociation inhibition assays

Observed rate constants were obtained by fitting the titration data from the nucleotide dissociation inhibition assay with a mono exponential function in Origin (OriginLab Corporation). Observed rate constants were plotted as a function of chimera concentration affinity values were acquired by fitting the data with the following hyperbolic function in Origin (OriginLab Corporation).

$$k_{obs} = \frac{k_{-1}}{(1 + \mathrm{x}/\mathrm{K}_D)}$$

Microscopy

TIRF microscopy

TIRFM experiments were conducted at room temperature using a customized Nikon TIRF Ti2 microscope (Nikon Instruments), operated through the Nikon NIS – Elements software (Nikon Instruments). Images were captured using dual EM CCD Andor iXon cooled cameras (Cairn Research). Imaging was performed through an Apo TIRF 60x oil DIC N2 objective using a custom multi-laser launch system with 488, 532, 561 and 639 nm lasers (AcalBFi LC). Single molecule experiments were performed with continuous illumination, which resulted in a 22 ms exposure time. Bulk experiment movies were captured with a range of exposures between 20 – 100 ms with interleaved imaging.

FRAP-TIRF microscopy

FRAP-TIRFM experiments were conducted at room temperature using a Nikon Ti1 microscope (Nikon Instruments), operated through the Visiview software (Visitron Systems). Images were captured using Evolve Delta cameras (Teledyne Photometrics). A circular ROI was drawn in the Visiview software on the bilayer at which photobleaching took place. 100% laser power was applied for 3 seconds using the FRAP module within the Visitron software (Visitron systems). Following FRAP, TIRF images were captured at 1-second time intervals for a total of 2 min.

Widefield microscopy

Widefield microscopy experiments were conducted at 37 °C using a Cell^R microscope (Olympus), operated through the cellSens software (Olympus). Images were captured using the ORCA-Quest qCMOS camera (Hamamatsu). Imaging was performed through an UPlanSApo 10x or 20x air objective using MT20 fluorescence lamp with excitation (575/25) and emission (641/75) filter in place. Bead assay experiments were captured at 20 ms exposure time.

References

Adams, A. E., Johnson, D. I., Longnecker, R. M., Sloat, B. F., & Pringle, J. R. (1990). CDC42 and CDC43, two additional genes involved in budding and the establishment of cell polarity in the yeast Saccharomyces cerevisiae. *The Journal of Cell Biology*, *111*(1), 131–142. https://doi.org/10.1083/jcb.111.1.131

Ahmed, S., Goh, W. I., & Bu, W. (2010). I-BAR domains, IRSp53 and filopodium formation. *Seminars in Cell & Developmental Biology*, *21*(4), 350–356. https://doi.org/10.1016/j.semcdb.2009.11.008

Alekhina, O., Burstein, E., & Billadeau, D. D. (2017). Cellular functions of WASP family proteins at a glance. *Journal of Cell Science*, *130*(14), 2235–2241. https://doi.org/10.1242/jcs.199570

Amin, E., Jaiswal, M., Derewenda, U., Reis, K., Nouri, K., Koessmeier, K. T., Aspenström, P., Somlyo, A. V., Dvorsky, R., & Ahmadian, M. R. (2016). Deciphering the Molecular and Functional Basis of RHOGAP Family Proteins. *Journal of Biological Chemistry*, *291*(39), 20353–20371. https://doi.org/10.1074/jbc.M116.736967

Anderegg, R. J., Betz, R., Carr, S. A., Crabb, J. W., & Duntze, W. (1988). Structure of Saccharomyces cerevisiae mating hormone a-factor. Identification of S-farnesyl cysteine as a structural component. *Journal of Biological Chemistry*, *263*(34), 18236–18240. https://doi.org/10.1016/S0021-9258(19)81351-0

Barbacid, M. (1987). Ras genes. *Annual Review of Biochemistry*, *56*, 779–827. https://doi.org/10.1146/annurev.bi.56.070187.004023

Baumeister, M. A., Martinu, L., Rossman, K. L., Sondek, J., Lemmon, M. A., & Chou, M. M. (2003). Loss of Phosphatidylinositol 3-Phosphate Binding by the C-terminal Tiam-1 Pleckstrin Homology Domain Prevents in Vivo Rac1 Activation without Affecting Membrane Targeting. *Journal of Biological Chemistry*, *278*(13), 11457–11464. https://doi.org/10.1074/jbc.M211901200

Bement, W. M., Benink, H. A., & Von Dassow, G. (2005). A microtubule-dependent zone of active RhoA during cleavage plane specification. *The Journal of Cell Biology*, *170*(1), 91–101. https://doi.org/10.1083/jcb.200501131

Bement, W. M., Goryachev, A. B., Miller, A. L., & Von Dassow, G. (2024). Patterning of the cell cortex by Rho GTPases. *Nature Reviews Molecular Cell Biology*, *25*(4), 290–308. https://doi.org/10.1038/s41580-023-00682-z

Bement, W. M., Leda, M., Moe, A. M., Kita, A. M., Larson, M. E., Golding, A. E., Pfeuti, C., Su, K.-C., Miller, A. L., Goryachev, A. B., & von Dassow, G. (2015). Activator–inhibitor coupling between Rho signalling and actin assembly makes the cell cortex an excitable medium. *Nature Cell Biology*, *17*(11), 1471–1483. https://doi.org/10.1038/ncb3251

Bement, W. M., Miller, A. L., & Von Dassow, G. (2006). Rho GTPase activity zones and transient contractile arrays. *BioEssays*, *28*(10), 983–993. https://doi.org/10.1002/bies.20477

Benink, H. A., & Bement, W. M. (2005). Concentric zones of active RhoA and Cdc42 around single cell wounds. *The Journal of Cell Biology*, *168*(3), 429–439. https://doi.org/10.1083/jcb.200411109

Bezeljak, U., Loya, H., Kaczmarek, B., Saunders, T. E., & Loose, M. (2020). Stochastic activation and bistability in a Rab GTPase regulatory network. *Proceedings of the National Academy of Sciences*, *117*(12), 6540–6549. https://doi.org/10.1073/pnas.1921027117

Bieling, P., & Rottner, K. (2023). From WRC to Arp2/3: Collective molecular mechanisms of branched actin network assembly. *Current Opinion in Cell Biology*, *80*, 102156. https://doi.org/10.1016/j.ceb.2023.102156

Bischof, J., Brand, C. A., Somogyi, K., Májer, I., Thome, S., Mori, M., Schwarz, U. S., & Lénárt, P. (2017). A cdk1 gradient guides surface contraction waves in oocytes. *Nature Communications*, *8*(1), 849. https://doi.org/10.1038/s41467-017-00979-6

Bishop, A. L., & Hall, A. (2000). Rho GTPases and their effector proteins. *The Biochemical Journal*, *348 Pt 2*(Pt 2), 241–255.

Blumenstein, L., & Ahmadian, M. R. (2004). Models of the Cooperative Mechanism for Rho Effector Recognition. *Journal of Biological Chemistry*, *279*(51), 53419–53426. https://doi.org/10.1074/jbc.M409551200

Bokoch, G. M., Vlahos, C. J., Wang, Y., Knaus, U. G., & Traynor-Kaplan, A. E. (1996). Rac GTPase interacts specifically with phosphatidylinositol 3-kinase. *Biochemical Journal*, *315*(3), 775–779. https://doi.org/10.1042/bj3150775

Boulter, E., Garcia-Mata, R., Guilluy, C., Dubash, A., Rossi, G., Brennwald, P. J., & Burridge, K. (2010). Regulation of Rho GTPase crosstalk, degradation and activity by RhoGDI1. *Nature Cell Biology*, *12*(5), 477–483. https://doi.org/10.1038/ncb2049

Budnar, S., Husain, K. B., Gomez, G. A., Naghibosadat, M., Varma, A., Verma, S., Hamilton, N. A., Morris, R. G., & Yap, A. S. (2019). Anillin Promotes Cell Contractility by Cyclic Resetting of RhoA Residence Kinetics. *Developmental Cell*, *49*(6), 894-906.e12. https://doi.org/10.1016/j.devcel.2019.04.031

Bugyi, B., & Carlier, M.-F. (2010). Control of Actin Filament Treadmilling in Cell Motility. *Annual Review of Biophysics*, *39*(1), 449–470. https://doi.org/10.1146/annurev-biophys-051309-103849

Butty, A.-C. (2002). A positive feedback loop stabilizes the guanine-nucleotide exchange factor Cdc24 at sites of polarization. *The EMBO Journal*, *21*(7), 1565–1576. https://doi.org/10.1093/emboj/21.7.1565

Canagarajah, B., Leskow, F. C., Ho, J. Y. S., Mischak, H., Saidi, L. F., Kazanietz, M. G., & Hurley, J. H. (2004). Structural Mechanism for Lipid Activation of the Rac-Specific GAP, β2-Chimaerin. *Cell*, *119*(3), 407–418. https://doi.org/10.1016/j.cell.2004.10.012

Caspi, Y., & Dekker, C. (2016). Mapping out Min protein patterns in fully confined fluidic chambers. *eLife*, *5*, e19271. https://doi.org/10.7554/eLife.19271

Castro-Castro, A., Ojeda, V., Barreira, M., Sauzeau, V., Navarro-Lérida, I., Muriel, O., Couceiro, J. R., Pimentel-Muíños, F. X., Del Pozo, M. A., & Bustelo, X. R. (2011). Coronin 1A promotes a cytoskeletal-based feedback loop that facilitates Rac1 translocation

and activation: Coro1A favours Rac1 translocation and activation. *The EMBO Journal*, *30*(19), 3913–3927. https://doi.org/10.1038/emboj.2011.310

Chen, Z., Medina, F., Liu, M., Thomas, C., Sprang, S. R., & Sternweis, P. C. (2010). Activated RhoA Binds to the Pleckstrin Homology (PH) Domain of PDZ-RhoGEF, a Potential Site for Autoregulation. *Journal of Biological Chemistry*, *285*(27), 21070–21081. https://doi.org/10.1074/jbc.M110.122549

Cheng, L., Mahon, G. M., Kostenko, E. V., & Whitehead, I. P. (2004). Pleckstrin Homology Domain-mediated Activation of the Rho-specific Guanine Nucleotide Exchange Factor Dbs by Rac1. *Journal of Biological Chemistry*, *279*(13), 12786–12793. https://doi.org/10.1074/jbc.M313099200

Cheng, L., Rossman, K. L., Mahon, G. M., Worthylake, D. K., Korus, M., Sondek, J., & Whitehead, I. P. (2002). RhoGEF Specificity Mutants Implicate RhoA as a Target for Dbs Transforming Activity. *Molecular and Cellular Biology*, *22*(19), 6895–6905. https://doi.org/10.1128/MCB.22.19.6895-6905.2002

Chiou, J., Balasubramanian, M. K., & Lew, D. J. (2017). Cell Polarity in Yeast. *Annual Review of Cell and Developmental Biology*, *33*(1), 77–101. https://doi.org/10.1146/annurev-cellbio-100616-060856

Cho, H. J., Kim, J.-T., Baek, K. E., Kim, B.-Y., & Lee, H. G. (2019). Regulation of Rho GTPases by RhoGDIs in Human Cancers. *Cells*, *8*(9), 1037. https://doi.org/10.3390/cells8091037

Choy, E., Chiu, V. K., Silletti, J., Feoktistov, M., Morimoto, T., Michaelson, D., Ivanov, I. E., & Philips, M. R. (1999). Endomembrane Trafficking of Ras. *Cell*, *98*(1), 69–80. https://doi.org/10.1016/S0092-8674(00)80607-8

Colicelli, J. (2004). Human RAS superfamily proteins and related GTPases. *Science's STKE: Signal Transduction Knowledge Environment*, *2004*(250), RE13. https://doi.org/10.1126/stke.2502004re13

Collinet, C., & Lecuit, T. (2021). Programmed and self-organized flow of information during morphogenesis. *Nature Reviews Molecular Cell Biology*, *22*(4), 245–265. https://doi.org/10.1038/s41580-020-00318-6

Crespo, P., Schuebel, K. E., Ostrom, A. A., Gutkind, J. S., & Bustelo, X. R. (1997). Phosphotyrosine-dependent activation of Rac-1 GDP/GTP exchange by the vav proto-oncogene product. *Nature*, *385*(6612), 169–172. https://doi.org/10.1038/385169a0

Das, M., Drake, T., Wiley, D. J., Buchwald, P., Vavylonis, D., & Verde, F. (2012). Oscillatory Dynamics of Cdc42 GTPase in the Control of Polarized Growth. *Science*, *337*(6091), 239–243. https://doi.org/10.1126/science.1218377

Davis, M. W., & Jorgensen, E. M. (2022). ApE, A Plasmid Editor: A Freely Available DNA Manipulation and Visualization Program. *Frontiers in Bioinformatics*, *2*, 818619. https://doi.org/10.3389/fbinf.2022.818619

De Beco, S., Vaidžiulytė, K., Manzi, J., Dalier, F., Di Federico, F., Cornilleau, G., Dahan, M., & Coppey, M. (2018). Optogenetic dissection of Rac1 and Cdc42 gradient shaping. *Nature Communications*, *9*(1), 4816. https://doi.org/10.1038/s41467-018-07286-8

De Boer, P. A. J., Crossley, R. E., & Rothfield, L. I. (1989). A division inhibitor and a topological specificity factor coded for by the minicell locus determine proper placement of the division septum in E. coli. *Cell*, *56*(4), 641–649. https://doi.org/10.1016/0092-8674(89)90586-2

De Seze, J., Bongaerts, M., Boulevard, B., & Coppey, M. (2023). *Optogenetic control of a GEF of RhoA uncovers a signaling switch from retraction to protrusion*. https://doi.org/10.7554/eLife.93180.1

DerMardirossian, C., Schnelzer, A., & Bokoch, G. M. (2004). Phosphorylation of RhoGDI by Pak1 Mediates Dissociation of Rac GTPase. *Molecular Cell*, *15*(1), 117–127. https://doi.org/10.1016/j.molcel.2004.05.019

Diez, S., Gerisch, G., Anderson, K., Müller-Taubenberger, A., & Bretschneider, T. (2005). Subsecond reorganization of the actin network in cell motility and chemotaxis. *Proceedings of the National Academy of Sciences*, *102*(21), 7601–7606. https://doi.org/10.1073/pnas.0408546102

Downward, J. (2003). Targeting RAS signalling pathways in cancer therapy. *Nature Reviews Cancer*, *3*(1), 11–22. https://doi.org/10.1038/nrc969

Driever, W., & Nüsslein-Volhard, C. (1988). A gradient of bicoid protein in Drosophila embryos. *Cell*, *54*(1), 83–93. https://doi.org/10.1016/0092-8674(88)90182-1

Eberth, A., Dvorsky, R., Becker, C. F. W., Beste, A., Goody, R. S., & Ahmadian, M. R. (2005). Monitoring the real-time kinetics of the hydrolysis reaction of guanine nucleotide-binding proteins. *Biological Chemistry*, *386*(11). https://doi.org/10.1515/BC.2005.127

Endris, V., Haussmann, L., Buss, E., Bacon, C., Bartsch, D., & Rappold, G. (2011). SrGAP3 interacts with lamellipodin at the cell membrane and regulates Rac-dependent cellular protrusions. *Journal of Cell Science*, *124*(23), 3941–3955. https://doi.org/10.1242/jcs.077081

Etienne-Manneville, S., & Hall, A. (2002). Rho GTPases in cell biology. *Nature*, *420*(6916), 629–635. https://doi.org/10.1038/nature01148

Fäßler, F., Dimchev, G., Hodirnau, V.-V., Wan, W., & Schur, F. K. M. (2020). Cryo-electron tomography structure of Arp2/3 complex in cells reveals new insights into the branch junction. *Nature Communications*, *11*(1), 6437. https://doi.org/10.1038/s41467-020-20286-x

Fauré, J., Vignais, P. V., & Dagher, M. (1999). Phosphoinositide-dependent activation of Rho A involves partial opening of the RhoA/Rho-GDI complex. *European Journal of Biochemistry*, *262*(3), 879–889. https://doi.org/10.1046/j.1432-1327.1999.00458.x

Ferguson, K. M., Lemmon, M. A., Schlessinger, J., & Sigler, P. B. (1995). Structure of the high affinity complex of inositol trisphosphate with a phospholipase C pleckstrin homology domain. *Cell*, *83*(6), 1037–1046. https://doi.org/10.1016/0092-8674(95)90219-8

Ferrell, J. E. (1996). Tripping the switch fantastic: How a protein kinase cascade can convert graded inputs into switch-like outputs. *Trends in Biochemical Sciences*, *21*(12), 460–466. https://doi.org/10.1016/S0968-0004(96)20026-X

Fidyk, N. J., & Cerione, R. A. (2002). Understanding the Catalytic Mechanism of GTPase-Activating Proteins: Demonstration of the Importance of Switch Domain Stabilization in the Stimulation of GTP Hydrolysis. *Biochemistry*, *41*(52), 15644–15653. https://doi.org/10.1021/bi026413p

Finkielstein, C. V., Overduin, M., & Capelluto, D. G. S. (2006). Cell Migration and Signaling Specificity Is Determined by the Phosphatidylserine Recognition Motif of Rac1. *Journal of Biological Chemistry*, *281*(37), 27317–27326. https://doi.org/10.1074/jbc.M605560200

Fish, K. N. (2009). Total Internal Reflection Fluorescence (TIRF) Microscopy. *Current Protocols in Cytometry*, *50*(1). https://doi.org/10.1002/0471142956.cy1218s50

Fleming, I. N., Elliott, C. M., & Exton, J. H. (1996). Differential Translocation of Rho Family GTPases by Lysophosphatidic Acid, Endothelin-1, and Platelet-derived Growth Factor. *Journal of Biological Chemistry*, *271*(51), 33067–33073. https://doi.org/10.1074/jbc.271.51.33067

Freisinger, T., Klünder, B., Johnson, J., Müller, N., Pichler, G., Beck, G., Costanzo, M., Boone, C., Cerione, R. A., Frey, E., & Wedlich-Söldner, R. (2013). Establishment of a robust single axis of cell polarity by coupling multiple positive feedback loops. *Nature Communications*, *4*(1), 1807. https://doi.org/10.1038/ncomms2795

Fukata, M., Kuroda, S., Fujii, K., Nakamura, T., Shoji, I., Matsuura, Y., Okawa, K., Iwamatsu, A., Kikuchi, A., & Kaibuchi, K. (1997). Regulation of Cross-linking of Actin Filament by IQGAP1, a Target for Cdc42. *Journal of Biological Chemistry*, *272*(47), 29579–29583. https://doi.org/10.1074/jbc.272.47.29579

Garcia-Mata, R., Boulter, E., & Burridge, K. (2011). The "invisible hand": Regulation of RHO GTPases by RHOGDIs. *Nature Reviews Molecular Cell Biology*, *12*(8), 493–504. https://doi.org/10.1038/nrm3153

Garcia-Parajo, M. F., & Mayor, S. (2024). The ubiquitous nanocluster: A molecular scale organizing principle that governs cellular information flow. *Current Opinion in Cell Biology*, *86*, 102285. https://doi.org/10.1016/j.ceb.2023.102285

Gautreau, A. M., Fregoso, F. E., Simanov, G., & Dominguez, R. (2022). Nucleation, stabilization, and disassembly of branched actin networks. *Trends in Cell Biology*, *32*(5), 421–432. https://doi.org/10.1016/j.tcb.2021.10.006

Gavriljuk, K., Itzen, A., Goody, R. S., Gerwert, K., & Kötting, C. (2013). Membrane extraction of Rab proteins by GDP dissociation inhibitor characterized using attenuated total reflection infrared spectroscopy. *Proceedings of the National Academy of Sciences of the United States of America*, *110*(33), 13380–13385. https://doi.org/10.1073/pnas.1307655110

Gibbs, J. B., Sigal, I. S., Poe, M., & Scolnick, E. M. (1984). Intrinsic GTPase activity distinguishes normal and oncogenic ras p21 molecules. *Proceedings of the National Academy of Sciences*, *81*(18), 5704–5708. https://doi.org/10.1073/pnas.81.18.5704

Golding, A. E., Visco, I., Bieling, P., & Bement, W. M. (2019). Extraction of active RhoGTPases by RhoGDI regulates spatiotemporal patterning of RhoGTPases. *eLife*, *8*, e50471. https://doi.org/10.7554/eLife.50471

Goryachev, A. B., & Leda, M. (2017). Many roads to symmetry breaking: Molecular mechanisms and theoretical models of yeast cell polarity. *Molecular Biology of the Cell*, *28*(3), 370–380. https://doi.org/10.1091/mbc.e16-10-0739

Goryachev, A. B., & Pokhilko, A. V. (2008). Dynamics of Cdc42 network embodies a Turing-type mechanism of yeast cell polarity. *FEBS Letters*, *582*(10), 1437–1443. https://doi.org/10.1016/j.febslet.2008.03.029

Graessl, M., Koch, J., Calderon, A., Kamps, D., Banerjee, S., Mazel, T., Schulze, N., Jungkurth, J. K., Patwardhan, R., Solouk, D., Hampe, N., Hoffmann, B., Dehmelt, L., & Nalbant, P. (2017). An excitable Rho GTPase signaling network generates dynamic subcellular contraction patterns. *Journal of Cell Biology*, *216*(12), 4271–4285. https://doi.org/10.1083/jcb.201706052

Gray, J. L., Von Delft, F., & Brennan, P. E. (2020). Targeting the Small GTPase Superfamily through Their Regulatory Proteins. *Angewandte Chemie International Edition*, *59*(16), 6342–6366. https://doi.org/10.1002/anie.201900585

Graziano, B. R., & Weiner, O. D. (2014). Self-organization of protrusions and polarity during eukaryotic chemotaxis. *Current Opinion in Cell Biology*, *30*, 60–67. https://doi.org/10.1016/j.ceb.2014.06.007

Gregor, T., Tank, D. W., Wieschaus, E. F., & Bialek, W. (2007). Probing the Limits to Positional Information. *Cell*, *130*(1), 153–164. https://doi.org/10.1016/j.cell.2007.05.025

Hakoshima, T. (2003). Structural Basis of the Rho GTPase Signaling. *Journal of Biochemistry*, *134*(3), 327–331. https://doi.org/10.1093/jb/mvg149

Hale, C. A., Meinhardt, H., & de Boer, P. A. (2001). Dynamic localization cycle of the cell division regulator MinE in Escherichia coli. *The EMBO Journal*, *20*(7), 1563–1572. https://doi.org/10.1093/emboj/20.7.1563

Hansen, S. D., Huang, W. Y. C., Lee, Y. K., Bieling, P., Christensen, S. M., & Groves, J. T. (2019). Stochastic geometry sensing and polarization in a lipid kinase–phosphatase competitive reaction. *Proceedings of the National Academy of Sciences*, *116*(30), 15013–15022. https://doi.org/10.1073/pnas.1901744116

Harvey, J. J. (1964). An Unidentified Virus which causes the Rapid Production of Tumours in Mice. *Nature*, *204*(4963), 1104–1105. https://doi.org/10.1038/2041104b0

Heasman, S. J., & Ridley, A. J. (2008). Mammalian Rho GTPases: New insights into their functions from in vivo studies. *Nature Reviews Molecular Cell Biology*, *9*(9), 690–701. https://doi.org/10.1038/nrm2476

Heath, R. J. W., & Insall, R. H. (2008). F-BAR domains: Multifunctional regulators of membrane curvature. *Journal of Cell Science*, *121*(12), 1951–1954. https://doi.org/10.1242/jcs.023895

Herrmann, C., Martin, G. A., & Wittinghofer, A. (1995). Quantitative Analysis of the Complex between p21 and the Ras-binding Domain of the Human Raf-1 Protein Kinase. *Journal of Biological Chemistry*, *270*(7), 2901–2905. https://doi.org/10.1074/jbc.270.7.2901

Higgs, H. (2001). Getting down to basics with actin. *Nature Cell Biology*, *3*(8), E189–E189. https://doi.org/10.1038/35087135

Hodge, R. G., & Ridley, A. J. (2016). Regulating Rho GTPases and their regulators. *Nature Reviews Molecular Cell Biology*, *17*(8), 496–510. https://doi.org/10.1038/nrm.2016.67

Hodgson, L., Spiering, D., Sabouri-Ghomi, M., Dagliyan, O., DerMardirossian, C., Danuser, G., & Hahn, K. M. (2016). FRET binding antenna reports spatiotemporal dynamics of GDI-Cdc42 GTPase interactions. *Nature Chemical Biology*, *12*(10), 802–809. https://doi.org/10.1038/nchembio.2145

Hoffman, G. R., Nassar, N., & Cerione, R. A. (2000). Structure of the Rho Family GTP-Binding Protein Cdc42 in Complex with the Multifunctional Regulator RhoGDI. *Cell*, *100*(3), 345–356. https://doi.org/10.1016/S0092-8674(00)80670-4

Howell, A. S., Savage, N. S., Johnson, S. A., Bose, I., Wagner, A. W., Zyla, T. R., Nijhout, H. F., Reed, M. C., Goryachev, A. B., & Lew, D. J. (2009). Singularity in Polarization: Rewiring Yeast Cells to Make Two Buds. *Cell*, *139*(4), 731–743. https://doi.org/10.1016/j.cell.2009.10.024

Hu, Z., & Lutkenhaus, J. (1999). Topological regulation of cell division in *Escherichia coli* involves rapid pole to pole oscillation of the division inhibitor MinC under the control of MinD and MinE. *Molecular Microbiology*, *34*(1), 82–90. https://doi.org/10.1046/j.1365-2958.1999.01575.x

Hurley, J. B., Simon, M. I., Teplow, D. B., Robishaw, J. D., & Gilman, A. G. (1984). Homologies Between Signal Transducing G Proteins and *ras* Gene Products. *Science*, *226*(4676), 860–862. https://doi.org/10.1126/science.6436980

Hussain, N. K., Jenna, S., Glogauer, M., Quinn, C. C., Wasiak, S., Guipponi, M., Antonarakis, S. E., Kay, B. K., Stossel, T. P., Lamarche-Vane, N., & McPherson, P. S. (2001). Endocytic protein intersectin-l regulates actin assembly via Cdc42 and N-WASP. *Nature Cell Biology*, *3*(10), 927–932. https://doi.org/10.1038/ncb1001-927

Jilkine, A., Marée, A. F. M., & Edelstein-Keshet, L. (2007). Mathematical Model for Spatial Segregation of the Rho-Family GTPases Based on Inhibitory Crosstalk. *Bulletin of Mathematical Biology*, *69*(6), 1943–1978. https://doi.org/10.1007/s11538-007-9200-6

John, J., Sohmen, R., Feuerstein, J., Linke, R., Wittinghofer, A., & Goody, R. S. (1990). Kinetics of interaction of nucleotides with nucleotide-free H-ras p21. *Biochemistry*, *29*(25), 6058–6065. https://doi.org/10.1021/bi00477a025

Johnson, J. L., Erickson, J. W., & Cerione, R. A. (2009). New Insights into How the Rho Guanine Nucleotide Dissociation Inhibitor Regulates the Interaction of Cdc42 with Membranes. *Journal of Biological Chemistry*, *284*(35), 23860–23871. https://doi.org/10.1074/jbc.M109.031815

Kabsch, W., Gast, W. H., Schulz, G. E., & Leberman, R. (1977). Low resolution structure of partially trypsin-degraded polypeptide elongation factor, EF-Tu, from Escherichia coli. *Journal of Molecular Biology*, *117*(4), 999–1012. https://doi.org/10.1016/S0022-2836(77)80009-0

Kamata, T., & Feramisco, J. R. (1984). Epidermal growth factor stimulates guanine nucleotide binding activity and phosphorylation of ras oncogene proteins. *Nature*, *310*(5973), 147–150. https://doi.org/10.1038/310147a0

Kammerer, R. A. (1997). α-Helical coiled-coil oligomerization domains in extracellular proteins. *Matrix Biology*, *15*(8–9), 555–565. https://doi.org/10.1016/S0945-053X(97)90031-7

Kapust, R. B., Tözsér, J., Fox, J. D., Anderson, D. E., Cherry, S., Copeland, T. D., & Waugh, D. S. (2001). Tobacco etch virus protease: Mechanism of autolysis and rational design of stable mutants with wild-type catalytic proficiency. *Protein Engineering, Design and Selection*, *14*(12), 993–1000. https://doi.org/10.1093/protein/14.12.993

Kapust, R. B., & Waugh, D. S. (1999). *Escherichia coli* maltose-binding protein is uncommonly effective at promoting the solubility of polypeptides to which it is fused. *Protein Science*, *8*(8), 1668–1674. https://doi.org/10.1110/ps.8.8.1668

Karnoub, A. E., & Weinberg, R. A. (2008). Ras oncogenes: Split personalities. *Nature Reviews Molecular Cell Biology*, *9*(7), 517–531. https://doi.org/10.1038/nrm2438

Kibbe, W. A. (2007). OligoCalc: An online oligonucleotide properties calculator. *Nucleic Acids Research*, *35*(Web Server issue), W43-46. https://doi.org/10.1093/nar/gkm234

Kirsten, W. H., & Mayer, L. A. (1967). Morphologic responses to a murine erythroblastosis virus. *Journal of the National Cancer Institute*, *39*(2), 311–335.

Kondo, S., & Miura, T. (2010). Reaction-Diffusion Model as a Framework for Understanding Biological Pattern Formation. *Science*, *329*(5999), 1616–1620. https://doi.org/10.1126/science.1179047

Koonin, E. V., Wolf, Y. I., & Aravind, L. (2000). Protein fold recognition using sequence profiles and its application in structural genomics. In *Advances in Protein Chemistry* (Vol. 54, pp. 245–275). Elsevier. https://doi.org/10.1016/S0065-3233(00)54008-X

Korn, E. D., Carlier, M.-F., & Pantaloni, D. (1987). Actin Polymerization and ATP Hydrolysis. *Science*, *238*(4827), 638–644. https://doi.org/10.1126/science.3672117

Kozma, R., Ahmed, S., Best, A., & Lim, L. (1995). The Ras-Related Protein Cdc42Hs and Bradykinin Promote Formation of Peripheral Actin Microspikes and Filopodia in Swiss 3T3 Fibroblasts. *Molecular and Cellular Biology*, *15*(4), 1942–1952. https://doi.org/10.1128/MCB.15.4.1942

Kukimoto-Niino, M., Ihara, K., Murayama, K., & Shirouzu, M. (2021). Structural insights into the small GTPase specificity of the DOCK guanine nucleotide exchange factors. *Current Opinion in Structural Biology*, *71*, 249–258. https://doi.org/10.1016/j.sbi.2021.08.001

Landge, A. N., Jordan, B. M., Diego, X., & Müller, P. (2020). Pattern formation mechanisms of self-organizing reaction-diffusion systems. *Developmental Biology*, *460*(1), 2–11. https://doi.org/10.1016/j.ydbio.2019.10.031

Lang, C. F., & Munro, E. (2017). The PAR proteins: From molecular circuits to dynamic self-stabilizing cell polarity. *Development*, *144*(19), 3405–3416. https://doi.org/10.1242/dev.139063

Lapouge, K., Smith, S. J. M., Walker, P. A., Gamblin, S. J., Smerdon, S. J., & Rittinger, K. (2000). Structure of the TPR Domain of p67phox in Complex with Rac·GTP. *Molecular Cell*, *6*(4), 899–907. https://doi.org/10.1016/S1097-2765(05)00091-2

Leipe, D. D., Wolf, Y. I., Koonin, E. V., & Aravind, L. (2002). Classification and evolution of P-loop GTPases and related ATPases. *Journal of Molecular Biology*, *317*(1), 41–72. https://doi.org/10.1006/jmbi.2001.5378

Leung, T., Chen, X.-Q., Manser, E., & Lim, L. (1996). The p160 RhoA-Binding Kinase ROKα Is a Member of a Kinase Family and Is Involved in the Reorganization of the Cytoskeleton. *Molecular and Cellular Biology*, *16*(10), 5313–5327. https://doi.org/10.1128/MCB.16.10.5313

Lin, Q., Yang, W., Baird, D., Feng, Q., & Cerione, R. A. (2006). Identification of a DOCK180-related Guanine Nucleotide Exchange Factor That Is Capable of Mediating a Positive Feedback Activation of Cdc42. *Journal of Biological Chemistry*, *281*(46), 35253–35262. https://doi.org/10.1074/jbc.M606248200

Lo, W.-C., Park, H.-O., & Chou, C.-S. (2014). Mathematical Analysis of Spontaneous Emergence of Cell Polarity. *Bulletin of Mathematical Biology*, *76*(8), 1835–1865. https://doi.org/10.1007/s11538-014-9982-2

Loose, M., Fischer-Friedrich, E., Ries, J., Kruse, K., & Schwille, P. (2008). Spatial Regulators for Bacterial Cell Division Self-Organize into Surface Waves in Vitro. *Science*, *320*(5877), 789–792. https://doi.org/10.1126/science.1154413

Lorent, J. H., Levental, K. R., Ganesan, L., Rivera-Longsworth, G., Sezgin, E., Doktorova, M., Lyman, E., & Levental, I. (2020). Plasma membranes are asymmetric in lipid unsaturation, packing and protein shape. *Nature Chemical Biology*, *16*(6), 644–652. https://doi.org/10.1038/s41589-020-0529-6

Lu, S., Jang, H., Gu, S., Zhang, J., & Nussinov, R. (2016). Drugging Ras GTPase: A comprehensive mechanistic and signaling structural view. *Chemical Society Reviews*, *45*(18), 4929–4952. https://doi.org/10.1039/C5CS00911A

Lutkenhaus, J. (2007). Assembly Dynamics of the Bacterial MinCDE System and Spatial Regulation of the Z Ring. *Annual Review of Biochemistry*, *76*(1), 539–562. https://doi.org/10.1146/annurev.biochem.75.103004.142652

Machacek, M., Hodgson, L., Welch, C., Elliott, H., Pertz, O., Nalbant, P., Abell, A., Johnson, G. L., Hahn, K. M., & Danuser, G. (2009). Coordination of Rho GTPase activities during cell protrusion. *Nature*, *461*(7260), 99–103. https://doi.org/10.1038/nature08242

Madaule, P., & Axel, R. (1985). A novel ras-related gene family. *Cell*, *41*(1), 31–40. https://doi.org/10.1016/0092-8674(85)90058-3

Mahlandt, E. K., Arts, J. J. G., Van Der Meer, W. J., Van Der Linden, F. H., Tol, S., Van Buul, J. D., Gadella, T. W. J., & Goedhart, J. (2021). Visualizing endogenous Rho activity with an improved localization-based, genetically encoded biosensor. *Journal of Cell Science*, *134*(17), jcs258823. https://doi.org/10.1242/jcs.258823

Malumbres, M., & Barbacid, M. (2003). RAS oncogenes: The first 30 years. *Nature Reviews Cancer*, *3*(6), 459–465. https://doi.org/10.1038/nrc1097

McGrath, J. P., Capon, D. J., Goeddel, D. V., & Levinson, A. D. (1984). Comparative biochemical properties of normal and activated human ras p21 protein. *Nature*, *310*(5979), 644–649. https://doi.org/10.1038/310644a0

Meca, J., Massoni-Laporte, A., Martinez, D., Sartorel, E., Loquet, A., Habenstein, B., & McCusker, D. (2019). Avidity-driven polarity establishment via multivalent lipid–GTP ase module interactions. *The EMBO Journal*, *38*(3), e99652. https://doi.org/10.15252/embj.201899652

Medina, F., Carter, A. M., Dada, O., Gutowski, S., Hadas, J., Chen, Z., & Sternweis, P. C. (2013). Activated RhoA is a positive feedback regulator of the Lbc family of Rho guanine nucleotide exchange factor proteins. *The Journal of Biological Chemistry*, *288*(16), 11325–11333. https://doi.org/10.1074/jbc.M113.450056

Medina Gomez, S., Visco, I., Merino, F., Bieling, P., & Linser, R. (2024). Transient Structural Properties of the Rho GDP-Dissociation Inhibitor. *Angewandte Chemie International Edition*, *63*(34), e202403941. https://doi.org/10.1002/anie.202403941

Meinhardt, H., & de Boer, P. A. (2001). Pattern formation in Escherichia coli: A model for the pole-to-pole oscillations of Min proteins and the localization of the division site. *Proceedings of the National Academy of Sciences of the United States of America*, *98*(25), 14202–14207. https://doi.org/10.1073/pnas.251216598

Meinhardt, H., & Gierer, A. (2000). Pattern formation by local self-activation and lateral inhibition. *BioEssays*, *22*(8), 753–760. https://doi.org/10.1002/1521-1878(200008)22:8<753::AID-BIES9>3.0.CO;2-Z

Meinhardt, H., & Klingler, M. (1987). A model for pattern formation on the shells of molluscs. *Journal of Theoretical Biology*, *126*(1), 63–89. https://doi.org/10.1016/S0022-5193(87)80101-7

Michaelson, D., Silletti, J., Murphy, G., D'Eustachio, P., Rush, M., & Philips, M. R. (2001). Differential Localization of Rho Gtpases in Live Cells. *The Journal of Cell Biology*, *152*(1), 111–126. https://doi.org/10.1083/jcb.152.1.111

Michaux, J. B., Robin, F. B., McFadden, W. M., & Munro, E. M. (2018). Excitable RhoA dynamics drive pulsed contractions in the early *C. elegans* embryo. *Journal of Cell Biology*, *217*(12), 4230–4252. https://doi.org/10.1083/jcb.201806161

Milburn, M. V., Tong, L., deVos, A. M., Brünger, A., Yamaizumi, Z., Nishimura, S., & Kim, S.-H. (1990). Molecular Switch for Signal Transduction: Structural Differences Between Active and Inactive Forms of Protooncogenic *ras* Proteins. *Science*, *247*(4945), 939–945. https://doi.org/10.1126/science.2406906

Minoshima, Y., Kawashima, T., Hirose, K., Tonozuka, Y., Kawajiri, A., Bao, Y. C., Deng, X., Tatsuka, M., Narumiya, S., May, W. S., Nosaka, T., Semba, K., Inoue, T., Satoh, T., Inagaki, M., & Kitamura, T. (2003). Phosphorylation by Aurora B Converts MgcRacGAP to a RhoGAP during Cytokinesis. *Developmental Cell*, *4*(4), 549–560. https://doi.org/10.1016/S1534-5807(03)00089-3

Mitchison, T. J., & Field, C. M. (2021). Self-Organization of Cellular Units. *Annual Review of Cell and Developmental Biology*, *37*(1), 23–41. https://doi.org/10.1146/annurev-cellbio-120319-025356

Moe, A., Holmes, W., Golding, A. E., Zola, J., Swider, Z. T., Edelstein-Keshet, L., & Bement, W. (2021). Cross-talk-dependent cortical patterning of Rho GTPases during cell repair.

Molecular Biology of the Cell, *32*(16), 1417–1432. https://doi.org/10.1091/mbc.E20-07-0481

Moissoglu, K., Slepchenko, B. M., Meller, N., Horwitz, A. F., & Schwartz, M. A. (2006). In vivo dynamics of Rac-membrane interactions. *Molecular Biology of the Cell*, *17*(6), 2770–2779. https://doi.org/10.1091/mbc.e06-01-0005

Mosaddeghzadeh, N., & Ahmadian, M. R. (2021). The RHO Family GTPases: Mechanisms of Regulation and Signaling. *Cells*, *10*(7), 1831. https://doi.org/10.3390/cells10071831

Mulcahy, L. S., Smith, M. R., & Stacey, D. W. (1985). Requirement for ras proto-oncogene function during serum-stimulated growth of NIH 3T3 cells. *Nature*, *313*(5999), 241–243. https://doi.org/10.1038/313241a0

Müller, P. M., Rademacher, J., Bagshaw, R. D., Wortmann, C., Barth, C., Van Unen, J., Alp, K. M., Giudice, G., Eccles, R. L., Heinrich, L. E., Pascual-Vargas, P., Sanchez-Castro, M., Brandenburg, L., Mbamalu, G., Tucholska, M., Spatt, L., Czajkowski, M. T., Welke, R.-W., Zhang, S., … Rocks, O. (2020). Systems analysis of RhoGEF and RhoGAP regulatory proteins reveals spatially organized RAC1 signalling from integrin adhesions. *Nature Cell Biology*, *22*(4), 498–511. https://doi.org/10.1038/s41556-020-0488-x

Nobes, C. D., & Hall, A. (1995). Rho, Rac, and Cdc42 GTPases regulate the assembly of multimolecular focal complexes associated with actin stress fibers, lamellipodia, and filopodia. *Cell*, *81*(1), 53–62. https://doi.org/10.1016/0092-8674(95)90370-4

Nobes, C. D., & Hall, A. (1999). Rho GTPases Control Polarity, Protrusion, and Adhesion during Cell Movement. *The Journal of Cell Biology*, *144*(6), 1235–1244. https://doi.org/10.1083/jcb.144.6.1235

Ohta, Y., Hartwig, J. H., & Stossel, T. P. (2006). FilGAP, a Rho- and ROCK-regulated GAP for Rac binds filamin A to control actin remodelling. *Nature Cell Biology*, *8*(8), 803–814. https://doi.org/10.1038/ncb1437

Okabe, T., Nakamura, T., Nishimura, Y. N., Kohu, K., Ohwada, S., Morishita, Y., & Akiyama, T. (2003). RICS, a Novel GTPase-activating Protein for Cdc42 and Rac1, Is Involved in the β-Catenin-N-cadherin andN-Methyl-d-aspartate Receptor Signaling. *Journal of Biological Chemistry*, *278*(11), 9920–9927. https://doi.org/10.1074/jbc.M208872200

Ozbudak, E. M., Becskei, A., & Van Oudenaarden, A. (2005). A System of Counteracting Feedback Loops Regulates Cdc42p Activity during Spontaneous Cell Polarization. *Developmental Cell*, *9*(4), 565–571. https://doi.org/10.1016/j.devcel.2005.08.014

Padrick, S. B., Cheng, H.-C., Ismail, A. M., Panchal, S. C., Doolittle, L. K., Kim, S., Skehan, B. M., Umetani, J., Brautigam, C. A., Leong, J. M., & Rosen, M. K. (2008). Hierarchical regulation of WASP/WAVE proteins. *Molecular Cell*, *32*(3), 426–438. https://doi.org/10.1016/j.molcel.2008.10.012

Parks, W. P., & Scolnick, E. M. (1977). In vitro translation of Harvey murine sarcoma virus RNA. *Journal of Virology*, *22*(3), 711–719. https://doi.org/10.1128/jvi.22.3.711-719.1977

Patterson, G. H., & Lippincott-Schwartz, J. (2002). A Photoactivatable GFP for Selective Photolabeling of Proteins and Cells. *Science*, *297*(5588), 1873–1877. https://doi.org/10.1126/science.1074952

Pettersen, E. F., Goddard, T. D., Huang, C. C., Couch, G. S., Greenblatt, D. M., Meng, E. C., & Ferrin, T. E. (2004). UCSF Chimera—A visualization system for exploratory research and analysis. *Journal of Computational Chemistry*, *25*(13), 1605–1612. https://doi.org/10.1002/jcc.20084

Philips, M. R., Pillinger, M. H., Staud, R., Volker, C., Rosenfeld, M. G., Weissmann, G., & Stock, J. B. (1993). Carboxyl Methylation of Ras-Related Proteins During Signal Transduction in Neutrophils. *Science*, *259*(5097), 977–980. https://doi.org/10.1126/science.8438158

Piekny, A. J., & Glotzer, M. (2008). Anillin Is a Scaffold Protein That Links RhoA, Actin, and Myosin during Cytokinesis. *Current Biology*, *18*(1), 30–36. https://doi.org/10.1016/j.cub.2007.11.068

Pollard, T. D. (2007). Regulation of Actin Filament Assembly by Arp2/3 Complex and Formins. *Annual Review of Biophysics and Biomolecular Structure*, *36*(1), 451–477. https://doi.org/10.1146/annurev.biophys.35.040405.101936

Pollard, T. D., & Cooper, J. A. (2009). Actin, a Central Player in Cell Shape and Movement. *Science*, *326*(5957), 1208–1212. https://doi.org/10.1126/science.1175862

Pruyne, D., & Bretscher, A. (2000). Polarization of cell growth in yeast: I. Establishment and maintenance of polarity states. *Journal of Cell Science*, *113*(3), 365–375. https://doi.org/10.1242/jcs.113.3.365

Randazzo, P. A., Nie, Z., Miura, K., & Hsu, V. W. (2000). Molecular Aspects of the Cellular Activities of ADP-Ribosylation Factors. *Science's STKE*, *2000*(59). https://doi.org/10.1126/stke.2000.59.re1

Rao, C. V., Wolf, D. M., & Arkin, A. P. (2002). Control, exploitation and tolerance of intracellular noise. *Nature*, *420*(6912), 231–237. https://doi.org/10.1038/nature01258

Rappel, W.-J., & Edelstein-Keshet, L. (2017). Mechanisms of cell polarization. *Current Opinion in Systems Biology*, *3*, 43–53. https://doi.org/10.1016/j.coisb.2017.03.005

Raskin, D. M., & De Boer, P. A. J. (1999). Rapid pole-to-pole oscillation of a protein required for directing division to the middle of *Escherichia coli*. *Proceedings of the National Academy of Sciences*, *96*(9), 4971–4976. https://doi.org/10.1073/pnas.96.9.4971

Remorino, A., De Beco, S., Cayrac, F., Di Federico, F., Cornilleau, G., Gautreau, A., Parrini, M. C., Masson, J.-B., Dahan, M., & Coppey, M. (2017). Gradients of Rac1 Nanoclusters Support Spatial Patterns of Rac1 Signaling. *Cell Reports*, *21*(7), 1922–1935. https://doi.org/10.1016/j.celrep.2017.10.069

Ridley, A. J. (2001). Rho family proteins: Coordinating cell responses. *Trends in Cell Biology*, *11*(12), 471–477. https://doi.org/10.1016/S0962-8924(01)02153-5

Ridley, A. J., & Hall, A. (1992). The small GTP-binding protein rho regulates the assembly of focal adhesions and actin stress fibers in response to growth factors. *Cell*, *70*(3), 389–399. https://doi.org/10.1016/0092-8674(92)90163-7

Ridley, A. J., Paterson, H. F., Johnston, C. L., Diekmann, D., & Hall, A. (1992). The small GTP-binding protein rac regulates growth factor-induced membrane ruffling. *Cell*, *70*(3), 401–410. https://doi.org/10.1016/0092-8674(92)90164-8

Ridley, A. J., Schwartz, M. A., Burridge, K., Firtel, R. A., Ginsberg, M. H., Borisy, G., Parsons, J. T., & Horwitz, A. R. (2003). Cell Migration: Integrating Signals from Front to Back. *Science*, *302*(5651), 1704–1709. https://doi.org/10.1126/science.1092053

Riento, K., & Ridley, A. J. (2003). ROCKs: Multifunctional kinases in cell behaviour. *Nature Reviews Molecular Cell Biology*, *4*(6), 446–456. https://doi.org/10.1038/nrm1128

Robbe, K., Otto-Bruc, A., Chardin, P., & Antonny, B. (2003). Dissociation of GDP Dissociation Inhibitor and Membrane Translocation Are Required for Efficient Activation of Rac by the Dbl Homology-Pleckstrin Homology Region of Tiam. *Journal of Biological Chemistry*, *278*(7), 4756–4762. https://doi.org/10.1074/jbc.M210412200

Rossman, K. L., & Campbell, S. L. (2000). Bacterial expressed DH and DH/PH domains. In *Methods in Enzymology* (Vol. 325, pp. 25–38). Elsevier. https://doi.org/10.1016/S0076-6879(00)25428-1

Rossman, K. L., Der, C. J., & Sondek, J. (2005). GEF means go: Turning on RHO GTPases with guanine nucleotide-exchange factors. *Nature Reviews Molecular Cell Biology*, *6*(2), 167–180. https://doi.org/10.1038/nrm1587

Rottner, K., Stradal, T. E. B., & Chen, B. (2021). WAVE regulatory complex. *Current Biology: CB*, *31*(10), R512–R517. https://doi.org/10.1016/j.cub.2021.01.086

Rudolph, M. G., Bayer, P., Abo, A., Kuhlmann, J., Vetter, I. R., & Wittinghofer, A. (1998). The Cdc42/Rac Interactive Binding Region Motif of the Wiskott Aldrich Syndrome Protein (WASP) Is Necessary but Not Sufficient for Tight Binding to Cdc42 and Structure Formation. *Journal of Biological Chemistry*, *273*(29), 18067–18076. https://doi.org/10.1074/jbc.273.29.18067

Saras, J., Franzén, P., Aspenström, P., Hellman, U., Gonez, L. J., & Heldin, C.-H. (1997). A Novel GTPase-activating Protein for Rho Interacts with a PDZ Domain of the Protein-tyrosine Phosphatase PTPL1. *Journal of Biological Chemistry*, *272*(39), 24333–24338. https://doi.org/10.1074/jbc.272.39.24333

Saraste, M., Sibbald, P. R., & Wittinghofer, A. (1990). The P-loop—A common motif in ATP- and GTP-binding proteins. *Trends in Biochemical Sciences*, *15*(11), 430–434. https://doi.org/10.1016/0968-0004(90)90281-F

Schafer, W. R., Kim, R., Sterne, R., Thorner, J., Kim, S.-H., & Rine, J. (1989). Genetic and Pharmacological Suppression of Oncogenic Mutations in *RAS* Genes of Yeast and Humans. *Science*, *245*(4916), 379–385. https://doi.org/10.1126/science.2569235

Schafer, W. R., Trueblood, C. E., Yang, C.-C., Mayer, M. P., Rosenberg, S., Poulter, C. D., Kim, S.-H., & Rine, J. (1990). Enzymatic Coupling of Cholesterol Intermediates to a Mating Pheromone Precursor and to the Ras Protein. *Science*, *249*(4973), 1133–1139. https://doi.org/10.1126/science.2204115

Schindelin, J., Arganda-Carreras, I., Frise, E., Kaynig, V., Longair, M., Pietzsch, T., Preibisch, S., Rueden, C., Saalfeld, S., Schmid, B., Tinevez, J.-Y., White, D. J., Hartenstein, V., Eliceiri, K., Tomancak, P., & Cardona, A. (2012). Fiji: An open-source platform for

biological-image analysis. *Nature Methods*, *9*(7), 676–682. https://doi.org/10.1038/nmeth.2019

Schmidt, A., & Hall, A. (2002). Guanine nucleotide exchange factors for Rho GTPases: Turning on the switch. *Genes & Development*, *16*(13), 1587–1609. https://doi.org/10.1101/gad.1003302

Scolnick, E. M., Papageorge, A. G., & Shih, T. Y. (1979). Guanine nucleotide-binding activity as an assay for *src* protein of rat-derived murine sarcoma viruses. *Proceedings of the National Academy of Sciences*, *76*(10), 5355–5359. https://doi.org/10.1073/pnas.76.10.5355

Segal, D., Zaritsky, A., Schejter, E. D., & Shilo, B.-Z. (2018). Feedback inhibition of actin on Rho mediates content release from large secretory vesicles. *Journal of Cell Biology*, *217*(5), 1815–1826. https://doi.org/10.1083/jcb.201711006

Self, A. J., & Hall, A. (1995). [8] Measurement of intrinsic nucleotide exchange and GTP hydrolysis rates. In *Methods in Enzymology* (Vol. 256, pp. 67–76). Elsevier. https://doi.org/10.1016/0076-6879(95)56010-6

Shih, T. Y., Papageorge, A. G., Stokes, P. E., Weeks, M. O., & Scolnick, E. M. (1980). Guanine nucleotide-binding and autophosphorylating activities associated with the p21src protein of Harvey murine sarcoma virus. *Nature*, *287*(5784), 686–691. https://doi.org/10.1038/287686a0

Shih, T. Y., Weeks, M. O., Young, H. A., & Scolnick, E. M. (1979). P21 of Kirsten murine sarcoma virus is thermolabile in a viral mutant temperature sensitive for the maintenance of transformation. *Journal of Virology*, *31*(2), 546–546. https://doi.org/10.1128/jvi.31.2.546-546.1979

Shimizu, K., Goldfarb, M., Perucho, M., & Wigler, M. (1983). Isolation and preliminary characterization of the transforming gene of a human neuroblastoma cell line. *Proceedings of the National Academy of Sciences*, *80*(2), 383–387. https://doi.org/10.1073/pnas.80.2.383

Smith, M. R., DeGudicibus, S. J., & Stacey, D. W. (1986). Requirement for c-ras proteins during viral oncogene transformation. *Nature*, *320*(6062), 540–543. https://doi.org/10.1038/320540a0

Stam, J. C., Sander, E. E., Michiels, F., Van Leeuwen, F. N., Kain, H. E. T., Van Der Kammen, R. A., & Collard, J. G. (1997). Targeting of Tiam1 to the Plasma Membrane Requires the Cooperative Function of the N-terminal Pleckstrin Homology Domain and an Adjacent Protein Interaction Domain. *Journal of Biological Chemistry*, *272*(45), 28447–28454. https://doi.org/10.1074/jbc.272.45.28447

Straub, F. B., & Feuer, G. (1950). Adenosinetriphosphate the functional group of actin. *Biochimica et Biophysica Acta*, *4*, 455–470. https://doi.org/10.1016/0006-3002(50)90052-7

Sun, Y., Leong, N. T., Jiang, T., Tangara, A., Darzacq, X., & Drubin, D. G. (2017). Switch-like Arp2/3 activation upon WASP and WIP recruitment to an apparent threshold level by multivalent linker proteins in vivo. *eLife*, *6*, e29140. https://doi.org/10.7554/eLife.29140

Tcherkezian, J., & Lamarche-Vane, N. (2007). Current knowledge of the large RhoGAP family of proteins. *Biology of the Cell*, *99*(2), 67–86. https://doi.org/10.1042/BC20060086

Tinevez, J.-Y., Perry, N., Schindelin, J., Hoopes, G. M., Reynolds, G. D., Laplantine, E., Bednarek, S. Y., Shorte, S. L., & Eliceiri, K. W. (2017). TrackMate: An open and extensible platform for single-particle tracking. *Methods (San Diego, Calif.)*, *115*, 80–90. https://doi.org/10.1016/j.ymeth.2016.09.016

Tojkander, S., Gateva, G., Husain, A., Krishnan, R., & Lappalainen, P. (2015). Generation of contractile actomyosin bundles depends on mechanosensitive actin filament assembly and disassembly. *eLife*, *4*, e06126. https://doi.org/10.7554/eLife.06126

Traut, T. W. (1994). Physiological concentrations of purines and pyrimidines. *Molecular and Cellular Biochemistry*, *140*(1), 1–22. https://doi.org/10.1007/BF00928361

Turing, A. (1952). The chemical basis of morphogenesis. *Philosophical Transactions of the Royal Society of London. Series B, Biological Sciences*, *237*(641), 37–72. https://doi.org/10.1098/rstb.1952.0012

Ueda, T., Kikuchi, A., Ohga, N., Yamamoto, J., & Takai, Y. (1990). Purification and characterization from bovine brain cytosol of a novel regulatory protein inhibiting the dissociation of GDP from and the subsequent binding of GTP to rhoB p20, a ras p21-like GTP-binding protein. *Journal of Biological Chemistry*, *265*(16), 9373–9380. https://doi.org/10.1016/S0021-9258(19)38859-3

Ugolev, Y., Berdichevsky, Y., Weinbaum, C., & Pick, E. (2008). Dissociation of Rac1(GDP).RhoGDI complexes by the cooperative action of anionic liposomes containing phosphatidylinositol 3,4,5-trisphosphate, Rac guanine nucleotide exchange factor, and GTP. *The Journal of Biological Chemistry*, *283*(32), 22257–22271. https://doi.org/10.1074/jbc.M800734200

Van Meer, G., Voelker, D. R., & Feigenson, G. W. (2008). Membrane lipids: Where they are and how they behave. *Nature Reviews Molecular Cell Biology*, *9*(2), 112–124. https://doi.org/10.1038/nrm2330

Vaughan, E. M., Miller, A. L., Yu, H.-Y. E., & Bement, W. M. (2011). Control of Local Rho GTPase Crosstalk by Abr. *Current Biology*, *21*(4), 270–277. https://doi.org/10.1016/j.cub.2011.01.014

Vaughan, E. M., You, J.-S., Elsie Yu, H.-Y., Lasek, A., Vitale, N., Hornberger, T. A., & Bement, W. M. (2014). Lipid domain–dependent regulation of single-cell wound repair. *Molecular Biology of the Cell*, *25*(12), 1867–1876. https://doi.org/10.1091/mbc.e14-03-0839

Vendel, K. J. A., Tschirpke, S., Shamsi, F., Dogterom, M., & Laan, L. (2019). Minimal *in vitro* systems shed light on cell polarity. *Journal of Cell Science*, *132*(4), jcs217554. https://doi.org/10.1242/jcs.217554

Vetter, I. R., & Wittinghofer, A. (2001). The Guanine Nucleotide-Binding Switch in Three Dimensions. *Science*, *294*(5545), 1299–1304. https://doi.org/10.1126/science.1062023

Walker, J. E., Saraste, M., Runswick, M. J., & Gay, N. J. (1982). Distantly related sequences in the alpha- and beta-subunits of ATP synthase, myosin, kinases and other ATP-

requiring enzymes and a common nucleotide binding fold. *The EMBO Journal*, *1*(8), 945–951. https://doi.org/10.1002/j.1460-2075.1982.tb01276.x

Weiner, O. D., Marganski, W. A., Wu, L. F., Altschuler, S. J., & Kirschner, M. W. (2007). An Actin-Based Wave Generator Organizes Cell Motility. *PLoS Biology*, *5*(9), e221. https://doi.org/10.1371/journal.pbio.0050221

Weis, K. (2003). Regulating Access to the Genome. *Cell*, *112*(4), 441–451. https://doi.org/10.1016/S0092-8674(03)00082-5

Weiß, Y. (2021). A synthetic polarizing GTPase system. Master thesis, TU Dortmund.

Weissmann, F., Petzold, G., VanderLinden, R., Huis In 'T Veld, P. J., Brown, N. G., Lampert, F., Westermann, S., Stark, H., Schulman, B. A., & Peters, J.-M. (2016). biGBac enables rapid gene assembly for the expression of large multisubunit protein complexes. *Proceedings of the National Academy of Sciences*, *113*(19). https://doi.org/10.1073/pnas.1604935113

Wennerberg, K., & Der, C. J. (2004). Rho-family GTPases: It's not only Rac and Rho (and I like it). *Journal of Cell Science*, *117*(8), 1301–1312. https://doi.org/10.1242/jcs.01118

Wennerberg, K., Rossman, K. L., & Der, C. J. (2005). The Ras superfamily at a glance. *Journal of Cell Science*, *118*(5), 843–846. https://doi.org/10.1242/jcs.01660

White, C. D., Erdemir, H. H., & Sacks, D. B. (2012). IQGAP1 and its binding proteins control diverse biological functions. *Cellular Signalling*, *24*(4), 826–834. https://doi.org/10.1016/j.cellsig.2011.12.005

Willingham, M. C., Pastan, I., Shih, T. Y., & Scolnick, E. M. (1980). Localization of the src gene product of the Harvey strain of MSV to plasma membrane of transformed cells by electron microscopic immunocytochemistry. *Cell*, *19*(4), 1005–1014. https://doi.org/10.1016/0092-8674(80)90091-4

Willumsen, B. M., Christensen, A., Hubbert, N. L., Papageorge, A. G., & Lowy, D. R. (1984). The p21 ras C-terminus is required for transformation and membrane association. *Nature*, *310*(5978), 583–586. https://doi.org/10.1038/310583a0

Wittinghofer, A., & Vetter, I. R. (2011). Structure-Function Relationships of the G Domain, a Canonical Switch Motif. *Annual Review of Biochemistry*, *80*(1), 943–971. https://doi.org/10.1146/annurev-biochem-062708-134043

Worthylake, D. K., Rossman, K. L., & Sondek, J. (2000). Crystal structure of Rac1 in complex with the guanine nucleotide exchange region of Tiam1. *Nature*, *408*(6813), 682–688. https://doi.org/10.1038/35047014

Zerial, M., & McBride, H. (2001). Rab proteins as membrane organizers. *Nature Reviews Molecular Cell Biology*, *2*(2), 107–117. https://doi.org/10.1038/35052055

Zimmermann, G., Papke, B., Ismail, S., Vartak, N., Chandra, A., Hoffmann, M., Hahn, S. A., Triola, G., Wittinghofer, A., Bastiaens, P. I. H., & Waldmann, H. (2013). Small molecule inhibition of the KRAS–PDEδ interaction impairs oncogenic KRAS signalling. *Nature*, *497*(7451), 638–642. https://doi.org/10.1038/nature12205

List of Figures

List of Tables

Abbreviations

(N-)WASP	(Neural) Wiskott-Aldrich syndrome protein
5'-PPtase	5'-Phosphatase
A	activator
a.u.	arbitrary units
A488	Alexa488
A647	Alexa647
aa	amino acid
Abr_{cat}	catalytic domain of active breakpoint cluster region-related protein
$ArhGAP29_{cat}$	catalytic domain of Rho GTPase activating protein 29
Arp2/3	actin related protein 2/3 complex
ATP	adenosine triphosphate
ATPase	adenosine nucleoside-triphosphatase
BFP	blue fluorescent protein
c	concentration
CAAX	C= Cysteine, A = aliphatic aa, X =terminal aa
Cdc42	cell division control protein 42 homolog
CHAPS	3-((3-cholamidopropyl) dimethylammonio)-1-propanesulfonate
Cy3	Cyanine3
Dbl	diffuse B-cell lymphoma
dCherry	dark Cherry
DH	Dbl homology domain
DOPC	1,2-dioleoyl-sn-glycero-3-phosphocholine
DOPE	1,2-dioleoyl-sn-glycero-3-phosphoethanolamine
DOPS	1,2-dioleoyl-sn-glycero-3-phospho-L-serine
DrrA	lipid binding domain of DrrA
DTT	1,4-Dithiothreitol
EDTA	ethylenediaminetetraacetic acid
eGFP	enhanced GFP
EGTA	Ethylene glycol-bis(β-aminoethyl ether)-N,N,N0,N0-tetraacetic acid
F-actin	filamentous actin
FBS	fetal bovine serum
FRAP	fluorescence recovery after photobleaching
FRAP	fluorescence recovery after photobleaching
FRET	förster resonance energy transfer
FtsZ	Filamenting temperature-sensing mutant Z
G	glycin
GAP	GTPase activating protein

GBD	GTPase binding domain
GDP	guanosine diphosphate
GEF	guanine nucleotide exchange factor
GFP	green fluorescent protein
GGPP	geranylgeranyl pyrophosphate
Gly	glycine
GppNHp	guanosine-5'-[(β,γ)-imido]triphosphate
GST	glutathione-S-transferase
GTP	guanosine triphosphate
GTPase	guanine nucleoside-triphosphatase
HeLa	Henrietta Lacks
HEPES	4-(2-hydroxyethyl)-1-piperazineethanesulfonic acid
His	histidine
I	inhibitor
I_{In}	intensity inside GEF-enriched areas
I_{Out}	intensity outside GEF-enriched areas
IPTG	isopropyl-β-D-thiogalactosid
IT-Cdc42	internally tagged Cdc42
$ITSN_{cat}$	catalytic domain of Intersectin-1
k_{cat}/K_M	catalytic efficiency
K_D	equilibrium dissociation constant
kDa	kilodalton
k_{obs}	Observed reactions rates
L	leucine
LB	lysogeny broth
mant	2'/3'-O-(N-Methyl-anthraniloyl)
MBP	maltose binding protein
mCherry	monomeric Cherry
MLC	myosin light chain
mRFP	monomeric red fluorescent protein
mRNA	messenger RNA
NPF	nucleation promoting factor
NTPase	Nucleoside-triphosphatase
NusA	N-utilization substance protein A
OCRL	phosphoinositide 5-phosphatase
OD600	optical density (absorbance) at 600 nm
$OPHN1_{cat}$	catalytic domain of Oligophrenin-1
P	Pre-zone
PA	photoactivatable

PE-PEG5000	1,2-dioleoyl-sn-glycero-3-phosphoethanolamine- N-[methoxy(polyethylene glycol)-5000]
PH	pleckstrin homology domain
pH	Power of Hydrogen
PI	patterning index
PI(4)P	phosphatidylinositol 4-phosphate
PI(4,5)P_2	phosphatidylinositol 4,5-bisphosphate
PIP	phosphatidylinositol phosphate
PIP5K	phosphatidylinositol-4-phosphate 5-kinase
PLCδ	phospholipase C-delta
PM	plasma membrane
PMSF	phenylmethylsulfonyl fluoride
PTM	post translational modifications
pTPR	GTPase binding domain of p67phox
Q	glutamine
Rac1	ras-related C3 botulinum toxin substrate 1
rGBD	GTPase binding domain of Rhotekin
RhoA	ras homolog family member A
Rhodamine-PE	1,2-dioleoyl-sn-glycero-3-phosphoethanolamine-N-(lissamine rhodamine B sulfonyl)
RhoGDI	Rho-specific nucleotide dissociation inhibitor
ROCK	Rho kinase
rREM	GTPase binding domain of Rhotekin (different boundaries)
SD	standard deviation
SH3	src homology 3
SLB	supported lipid bilayer
SM	single molecule
SOC	super optimal broth with catabolite repression
SUV	Small unilamellar vesicles
sw1	switch 1
sw2	switch 2
t	Time
$t_{1/2}$	half-time
TAMRA	2´(3´)-O-(N-ethylcarbamoyl-(5´´-carboxytetramethylrhodamine)amide)
TB	terrific broth
Thr	threonine
$Tiam1_{cat}$	catalytic GEF domain of T-cell lymphoma invasion and metastasis-inducing protein 1
TIRF	total internal reflection fluorescence
TIRFM	total internal reflection fluorescence microscopy
Tris	tris(hydroxymethyl)aminomethane

Tris-Cl	tris(hydroxymethyl)aminomethane with HCl
Utr	Utrophin
V	Valine
VCA	verprolin, cofilin, acidic
W	Wound
WAVE	WASP family Verprolin-homologous protein
wCRIB	GTPase binding domain of WASP
wGBD	GTPase binding domain of WASP
WRC	WAVE regulatory complex
Z	Zone

Source Code

Custom scripts to generate segmentation maps from the lipid pattern channel and to analyze single molecule data were written in house by Dr. Ankit Roy and are made available to the public in the following GitHub repository: https://github.com/iamankitroy/GTPase-Patterning

The generated segmentation maps together with the following macro for Fiji were used to analyze the TIRF-based assays of templated Rho GTPase activity patterns. The macro has average intensities of the activity channel and of the channel of total Rho GTPase amounts inside and outside GEF-enriched areas as an output.

```
////Cropping with ROI and saving the tiff in parent folder
waitForUser("Create ROI of choice, select segmentation map and hit OK");
originalName = getTitle();
path = getDirectory("image");
outputdir = File.getDirectory(path);
originalNameWithoutExt = replace(originalName, ".tif", "");
run("Duplicate...", "duplicate");
roiManager("Select", 0);
run("Crop");
cropName = originalNameWithoutExt + "_75%";
saveAs("Tiff", outputdir + cropName);
rename(cropName);
run("Duplicate...", "duplicate");

////Generating inside mask
selectImage(cropName);;
run("32-bit");
setThreshold(255.0000, 255.0000);
run("NaN Background", "stack");
run("Divide...", "value=255.000 stack");
insMask = cropName + "_inside_Mask";
saveAs("Tiff", outputdir + insMask);
rename(insMask);

////Generating outside mask
selectImage(cropName + "-1");
run("32-bit");
setThreshold(0.0000, 0.0000);
run("NaN Background", "stack");
run("Add...", "value=1 stack");
outMask = cropName + "_outside_Mask";
saveAs("Tiff", outputdir + outMask);
rename(outMask);

////Multiplying inside with Active channel
waitForUser("Select Active channel and hit OK");
roiManager("Select", 0);
run("Crop");
```

```
activeChannel = getTitle();
imageCalculator("Multiply create stack", insMask, activeChannel);
saveAs("Tiff", outputdir + insMask + "_Active");
rename(insMask + "_Active");

////Measuring average intensity inside
run("Clear Results");
String.resetBuffer;
// Measure Stack: This macro measures all the slices in a stack.
for (i=1; i<=nSlices; i++)
   {setSlice(i);
   run("Measure");}
// Copies the entire Mean column into the clipboard
for (i=0; i<nResults; i++)
String.append(getResult("Mean", i) + "\n");
String.copy(String.buffer);
waitForUser("Copy average intensity: Inside, Active");
close(insMask + "_Active");

////Multiplying outside with Active channel
imageCalculator("Multiply create stack", outMask, activeChannel);
saveAs("Tiff", outputdir + outMask + "_Active");
rename(outMask + "_Active");

////Measuring average intensity inside
run("Clear Results");
String.resetBuffer;
// Measure Stack: This macro measures all the slices in a stack.
for (i=1; i<=nSlices; i++)
   {setSlice(i);
   run("Measure");}
// Copies the entire Mean column into the clipboard
for (i=0; i<nResults; i++)
String.append(getResult("Mean", i) + "\n");
String.copy(String.buffer);
waitForUser("Copy average intensity: Outside, Active");
close(outMask + "_Active");
close(activeChannel)

////Multiplying with Total channel
waitForUser("Select Total channel and hit OK");
roiManager("Select", 0);
run("Crop");
totalChannel = getTitle();
imageCalculator("Multiply create stack", insMask, totalChannel);
saveAs("Tiff", outputdir + insMask + "_Total");
rename(insMask + "_Total");

////Measuring average intensity inside
run("Clear Results");
String.resetBuffer;
// Measure Stack: This macro measures all the slices in a stack.
for (i=1; i<=nSlices; i++)
   {setSlice(i);
   run("Measure");}
// Copies the entire Mean column into the clipboard
for (i=0; i<nResults; i++)
```

```
96  String.append(getResult("Mean", i) + "\n");
97  String.copy(String.buffer);
98  waitForUser("Copy average intensity: Inside, Total");
99  close(insMask + "_Total");
100
101 ////Multiplying outside with Total channel
102 imageCalculator("Multiply create stack", outMask, totalChannel);
103 saveAs("Tiff", outputdir + outMask + "_Total");
104 rename(outMask + "_Total");
105
106 ////Measuring average intensity inside
107 run("Clear Results");
108 String.resetBuffer;
109 // Measure Stack: This macro measures all the slices in a stack.
110 for (i=1; i<=nSlices; i++)
111    {setSlice(i);
112    run("Measure");}
113 // Copies the entire Mean column into the clipboard
114 for (i=0; i<nResults; i++)
115 String.append(getResult("Mean", i) + "\n");
116 String.copy(String.buffer);
117 waitForUser("Copy average intensity: Outside, Total");
118 run("Close All");
```

Appendix

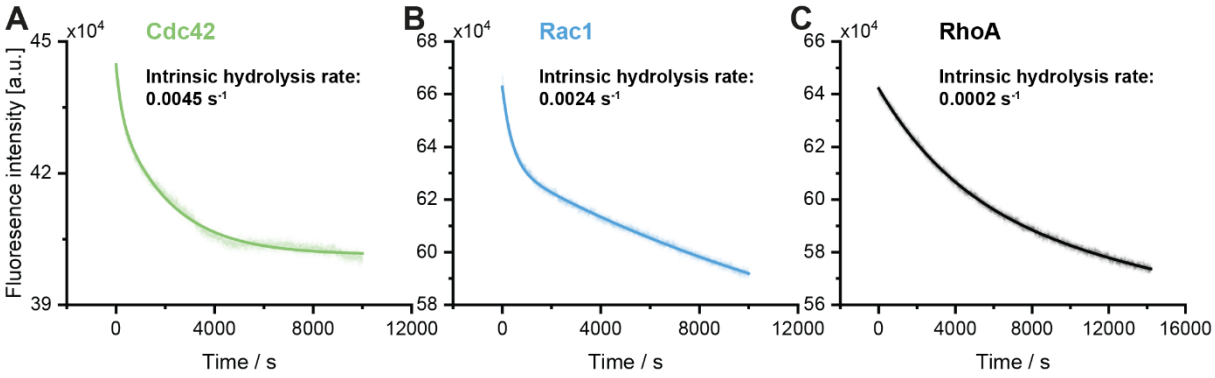

Supplementary figure 1: Intrinsic hydrolysis rates of Cdc42, Rac1, RhoA. Rho GTPase activity assay of (**A**) Cdc42, (**B**) Rac1 and (**C**) RhoA. Rho GTPases were loaded with either TAMRA-GTP (Cdc42, Rac1) or Cy3-GTP (RhoA). Normalized intensities of TAMRA-GTP:Cdc42 (green, 100 nM), TAMRA-GTP:Rac1 (blue, 100 nM) or Cy3-GTP:RhoA (black, 100 nM) as a function of time. Observed rate constants were obtained by biexponential fits of the data (Faster rate). Raw data for the characterization of the intrinsic hydrolysis rate of Rho GTPases (Weiß, Master thesis, TU Dortmund, 2021) was reanalyzed.

Publications

This thesis partially contains work which was submitted on the 17th of September 2024 to 'The EMBO journal' with the title 'Mechanistic principles of Rho GTPase patterning' and is currently under revision.

Figures and figure legends were modified and rewritten if necessary to fit the format of a thesis and improve the overall reading flow. Especially, the numbering of figures and figure panels as well as the size of some figures were altered in that regard.

Additionally, methods were adapted in a way to include more specific information about individual procedures.

Acknowledgements

I would like to thank Dr. Peter Bieling for giving me the opportunity to pursue my PhD in his research group. I still recall our initial project discussion, where we also spoke about alternative options since he considered it a “high risk” project. I am very grateful to him that I was able to work on such an exciting and ambitious project, which can’t be taken for granted. There were moments when I felt overwhelmed, but Peter provided guidance and support every step of the way within *just a moment*. His seemingly endless knowledge of all things protein made this project possible.

This gratitude extends to all the previous and current members of the group I was part of. Johanna and especially Lena showed me every trick there is around the lab. Ilaria is the reason I found my way into this amazing group, since her circumstances opened the door for my initial role as a research assistant. Mike was the one who introduced me to the GTPase business and never failed to lift the lab’s spirits with his endless repertoire of Dad jokes and sitcom trivia. Svenja was the backbone of our lab - without her, everything would have fallen apart, *pinky promise*. And then there’s Ankit - I don’t even know where to begin, and if I did, I probably wouldn’t know when to stop. He was my coworker, fellow PhD student, and roommate, which meant I saw him all day every day. The fact that we’re still friends is proof that we always had something exciting to talk about. It was truly a joy working with each and every one of you, and for that, I am deeply thankful.

I would like to thank Prof. Dr. Philippe Bastiaens for creating such an engaging environment where unconventional ideas are heard and more often than not provided the solution to the scientific problems at hand.

It goes without saying that such an environment relies on the people within it. With that in mind, I would like to thank everyone in department II, who helped me in more ways than I can count.

Speaking out every random thought that comes to mind is just part of who I am, and Michelle, Sina and Max can definitely attest to that. This habit often sparked some rather

unusual, often misleading conversations – for which I take full responsibility – but they stuck around and made every lunch break that much more enjoyable.

My deepest gratitude goes to Julia, who constantly kept me grounded and offered comforting words in these past few stressful months. Without you, this period would have been far more challenging. I genuinely mean it when I say that I couldn't have been luckier to have met you during this PhD journey.

I would not be the person that I am today without my family, they always supported me without hesitation, no matter how unconventional my decisions were. I am especially grateful to my parents, who have given me every opportunity in life and continue to do so. Dad, I can't wait for us to travel to every island around the world once you have your pilot's license.

I want to dedicate these final words to my mum. You always believed in me and wished nothing but the best for me. I wish you could be here to celebrate this moment. Thank you from the bottom of my heart.

In loving memory of my mum.